END ZONE DESIGN FOR ALABAMA

DEEP PRESTRESSED GIRDERS

by

DAVID ISAAC BURKHALTER

SRIRAM AALETI, COMMITTEE CO-CHAIR
WEI SONG, COMMITTEE CO-CHAIR
JAMES RICHARDSON
MARK BARKEY

A THESIS

Submitted in partial fulfillment of the requirements
for the degree of Master of Science
in the Department of Civil, Construction, and Environmental Engineering
in the Graduate School of
The University of Alabama

TUSCALOOSA, ALABAMA

2016

ABSTRACT

Deep prestressed concrete bridge girders are becoming increasingly popular due to their ability to span longer distances and reduce the total cost of bridge projects. However, these girders have frequently been subject to end zone cracking during the transfer of prestress forces despite being designed to current AASHTO specifications. Previously, the Alabama Department of Transportation (ALDOT) has designed deep prestressed girders which can span up to 165 ft. During the fabrication of these girders, crack formations in the end zone were typically noticed. To address this concern, longitudinal reinforcement was added to the end zones. This solution controlled cracking to some extent but could not completely eliminate cracking.

An experimental study was conducted to find a practical engineering solution to the problem of end zone cracking, as well as to develop a 78 in. deep prestressed bulb-tee girder design to reach a span length of 180 ft. 3D finite element modeling was used to find three practical alternative end zone modifications to the standard design. The modified designs included a lowered draping angle, partial debonding of the strands, and a combination of the two.

Four 54 ft. long specimens, including three with end zone modifications, were fabricated at Hanson Pipe & Precast in Pelham, Alabama, and monitored during the detensioning process. The end zones were instrumented with steel and concrete strain gauges to better understand the complex behavior of girder end zones. External DEMEC instrumentation was also included at the girder ends to measure the transfer length of the strands in each specimen. The specimens were then load tested at the UA Large Scale Structures Laboratory (LSSL) to determine the effects of

the modified end zone details on the girder capacity. Based on the study, modified girder end zone details are recommended to ALDOT for implementation.

DEDICATION

This thesis is dedicated to my loving family: to my mom, who taught me how to write; my dad, who taught me how to solve problems; and my grandfathers, who taught me how to build. Finally, this thesis is dedicated to my fiancée, who makes me a better person every day. Any success I have is because of you all.

LIST OF ABBREVIATIONS AND SYMBOLS

AASHTO	American Association of State Highway and Transportation Officials
ACI	American Concrete Institute
ALDOT	Alabama Department of Transportation
AMS	Average Maximum Strain
BT-78	Bulb-tee girder, 78 in. deep
DEMEC	Demountable, mechanical (targets and gauges)
FDOT	Florida Department of Transportation
FEM	Finite Element Modeling
LRFD	Load and Resistance Factor Design
LSSL	UA's Large Scale Structures Laboratory
SCC	Self-Consolidating Concrete
WisDOT	Wisconsin Department of Transportation
VDOT	Virginia Department of Transportation

ACKNOWLEDGEMENTS

I would like to thank all of the members of my thesis committee who made this research opportunity possible for me and through whose continued efforts I gleaned knowledge and wisdom that I will cherish throughout my career. Dr. Sriram Aaleti's technical knowledge and enthusiasm for engineering served an irreplaceable role throughout the entire development of this thesis. Dr. Wei Song provided me with much insight and vision through both the experimental and writing stages. I would also like to thank Vidya Sagar Ronanki whose guidance and willingness to help throughout the project made the process not only possible, but enjoyable.

I also owe gratitude to the following graduate and undergraduate students for donating their time to help me reach this goal: Luan Rocha Dominguez, Drew Landsell, Saeid Hayati, Shanglian Zhou, Qi Kuang, Kobir Hossain, Shane Crawford, and Daniel Bridi Valentim. Collin Sewell, the LSSL's Research Engineer, provided me with a great amount of practical advice in the lab, for which I am very appreciative.

This research was only possible through the generous funding from the Alabama Department of Transportation, to whom our entire team is very grateful. Also, many thanks go to the team at Hanson Pipe & Precast in Pelham, Alabama who worked with us through the fabrication process. We would also like to thank Steve Koch at Sumiden wire for donating prestressing strand and making it possible to construct the test girders in two phases.

Finally, I would like to thank God, my family, and my friends who provided me with the support and encouragement that I needed to accomplish this goal.

CONTENTS

LIST OF TABLES

LIST OF FIGURES

Chapter 1 Introduction

1.1. Background

1.1.1. Overview of Prestressed Concrete

Since the decades following World War II, precast/prestressed concrete products have become increasingly popular in the United States. Prestressed concrete members can be commonly found in structural elements such as bridge girders, beams, floor slabs, foundations and columns. Today, precast/prestressed concrete girders are frequently chosen for bridge superstructures due to their comparative advantages over steel girders, including high durability, better cost-efficiency, and shorter construction time.

Prestressed concrete has many advantages over traditionally reinforced concrete. Due to the compressive forces in the concrete created by prestress transfer, prestressed members have an increased capacity to resist service load stresses. This increased capacity can result in the reduction or elimination of typical flexural and shear cracking. Furthermore, with proper design, prestressed members can be much smaller and lighter than reinforced concrete, which can ultimately lead to a reduction in both fabrication costs and construction time.

Prestressed concrete can be either pretensioned or post-tensioned with high-grade steel prestressing strands. Pretensioned concrete involves the tensioning of strands before the concrete is cast, as opposed to post-tensioned concrete, in which the strands are tensioned after the concrete is cast. In the fabrication of pretensioned concrete members, prestressing strands are stretched above the casting bed between two stationary abutments and formwork is set in place around the

bed. The concrete is then cast within the formwork and allowed to bond directly with the strands. Once the concrete has reached a prescribed compressive strength, the formwork is removed and each prestressing strand is cut simultaneously on either end of the member. The process of cutting the prestressing strands is referred to as prestress transfer, or detensioning.

As the prestressing force is transferred to the member, the concrete is axially loaded in compression, and the performance capacity of the concrete is drastically increased. With the advent of high-strength concrete and efficient girder shapes, pretensioned girders can be designed to contain enormous amounts of prestressing strands, which in turn allows for even greater capacity. For this reason, state departments of transportation continue to investigate and implement deep pretensioned concrete girders.

One major benefit of deep pretensioned concrete girders is their ability to span longer distances than traditionally reinforced concrete members. Several long-span prestressed concrete girders have been implemented in bridge projects across the country including: the Florida I-beam (max. span 210 ft), the Washington WF100G (max. span 220 ft), and the Nebraska NU girder (max. span 240 ft). In many situations, long-span girders are a more practical, cheaper alternative to short-span girders since long-span girders decrease the need for supporting substructure members. This can result in several cost, safety, and environmental benefits. With less piers, contractors spend less money on materials. Long-span girders on bridges spanning over bodies of water require less construction in the harsh working conditions of the water. This can benefit both the contractor, by reducing the risk of injury for workers, and the environment, by reducing the amount of hazardous material and disturbances to the surrounding ecosystems.

1.1.2. End Zone Cracking

A common problem typically observed in deep prestressed concrete girders is the development of cracks in the girder ends, where the prestress in transferred to the concrete. These cracks, known as end zone cracks or anchorage zone cracks, typically occur during or immediately after the transfer of force from the prestressing strands to the concrete. This transfer of force occurs gradually along a short distance from the girder end called the transfer length. As this force grows over a relatively small length, cracking is likely to occur in areas of congested prestressing strands with a small amount of concrete to distribute the force.

Some girder sections are more susceptible to end zone cracking than others. End zone cracking is generally known to be associated with deep, narrow-stemmed girders which contain a large amount of prestressing strands.

As shown in Figure 1-1, three characteristic crack types have been identified in girder end zones: horizontal cracks over the web depth, splitting "Y" shaped cracks at the bottom flange-web interface, and inclined cracks that run parallel to draped strands in the top of the web. The consequences of these cracks are concerning. Since the cracks naturally form near the location of prestressing strands, they open up a direct path for moisture and corrosives to reach the strands. This results in strand corrosion, concrete spalling, and eventually a reduction in the flexural and shear load resisting capacity of the member by interrupting the bond between the strands and the concrete. Excessive cracking in the end zones require the fabricators to epoxy inject the cracks or, in some severe cases, even reject the girder.

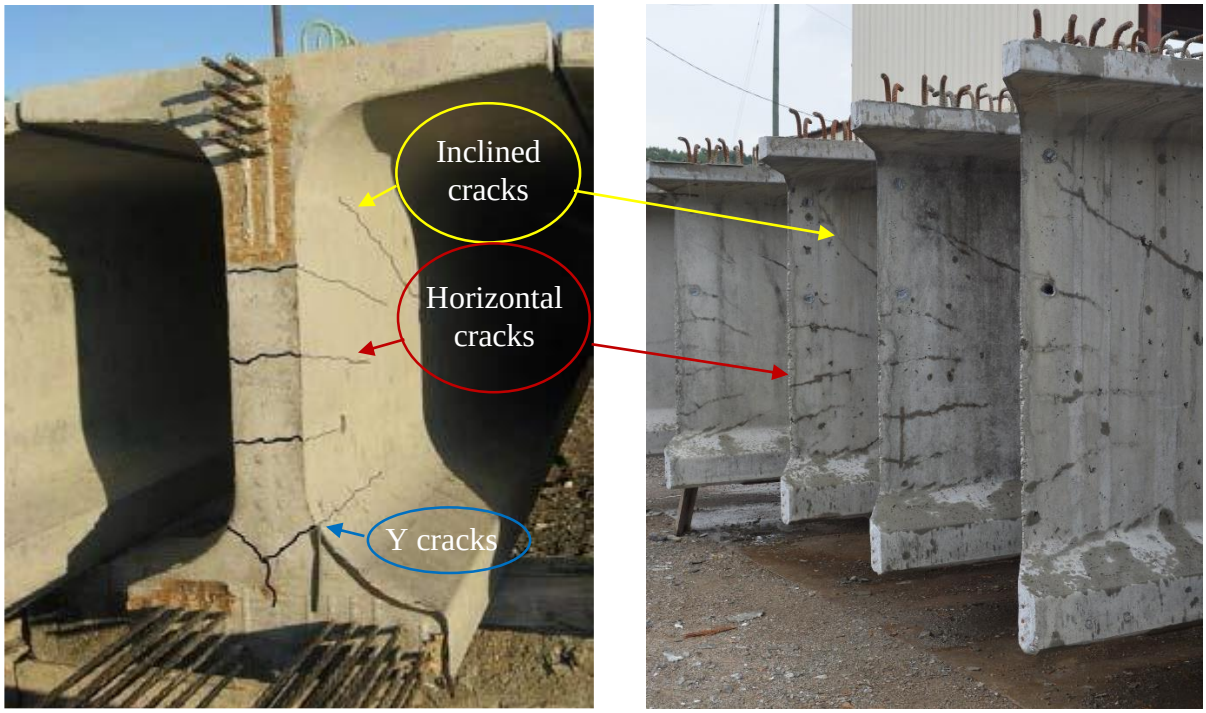

a) WisDOT 54W girder in storage yard (Oliva & Okumus, 2011)

b) ALDOT BT-72 girders in storage yard

Figure 1-1 Typical end zone cracks in pretensioned girders

1.2. Project Objectives and Scope

The main objective of the research project was to provide the ALDOT Bridge Bureau with practical and experimentally verified end zone details to minimize end zone cracking issues, prolong the service life, and improve durability of pretensioned concrete girders in Alabama. This goal was achieved by combining finite element modeling, field monitoring and experimental testing of four 78 in. deep girders specimens with different end zone designs. The specimens were fabricated at a local precast plant and the critical concrete and steel strains in the girder end zones were monitored using internal and external strain gauges. To verify the theoretical capacity of

these girders and understand the impact of the design modifications, a load test was then conducted on all specimens in the University of Alabama's Large Scale Structures Laboratory (LSSL).

1.3. Organization of Thesis

Chapter 2 includes a literature review of historical experimental and analytical studies involving end zone cracking and transfer length in deep prestressed girders. The literature review includes experimental studies from several state departments of transportation as well as current code standards from the American Concrete Institute (ACI) and the American Association of State Highway and Transportation Officials (AASHTO). Chapter 3 presents the methodology and calibration of the finite element analysis used in the design of the experimental specimens and the instrumentation plan. Chapter 4 explains the design details for the experimental specimens. The instrumentation program used to capture the behavior of the specimens and the fabrication process used in constructing the specimens is also discussed in Chapter 4. Chapter 5 includes the instrumentation plan for the laboratory load tests. Chapter 6 presents the results collected from the instrumentation during prestress release and during load testing. The data captured from the experimental specimens is analyzed and compared in this chapter. The final chapter includes conclusions from the project and recommendations for future ALDOT girder end zone designs, as well as recommendations for future research.

Chapter 2 Review of End Zone Cracking and Transfer Length in Pretensioned Girders

2.1. Introduction

In recent years, precast/prestressed concrete girder end zone cracking has become an increasing concern for designers. End zone cracking was first recognized as a problem during the pretensioned concrete boom of the 1950's and 1960's; thus, warranting an in-depth study of the causes for end zone cracking. Marshall and Mattock (1962) conducted the first reported experimental study on this issue, which resulted in the first code provisions for end zone reinforcement requirements in the 1961 AASHTO Interim Specifications (Tuan et al., 2004). These specifications, requiring a 20 ksi stress limit for vertical reinforcement bars and a splitting force equal to no less than 4 percent of the total prestressing force, were a simplified form of the recommendations of the study conducted by Marshall and Mattock. However, these recommendations were not fully successful in eliminating end zone cracking especially in modern prestressed concrete girders Following the experimental study by Marshall and Mattock, several researchers have conducted experimental studies in combination with finite element modeling to identify factors affecting end zone cracking and design end zone reinforcement more efficiently for deep prestressed concrete girders. Based on these studies, recommendations for modifying the end zone reinforcement design were proposed in the literature. The following sections include an explanation of transfer bond theory, a review of key literature focusing on end zone cracking, and a review of key expressions which have been previously used to describe transfer length in deep pretensioned girders.

2.2. Bond Theory of Pretensioned Concrete

The physics of pretensioned concrete can be explained by the application of three bond mechanisms: adhesion, friction, and mechanical resistance (Hanson and Kaar, 1959). These mechanisms explain the behavior of the system as the pretensioned strand bonds with the concrete. The transfer of stress which follows is called the transfer bond stress. These mechanisms are helpful in explaining the causes of both end zone cracking and transfer lengths.

The first mechanism, adhesion, is the process in which the prestressing strand forms a sticky bond with the concrete. This process occurs as concrete is poured around the strand and is allowed to harden. Adhesion is a particularly weak bond which is usually broken at prestress release as the strand slips within the concrete (Barnes, Grove, and Burns, 2003).

Friction, the second mechanism, plays a large role in creating transfer bond stress at the strand-concrete interface. This mechanism is a product of the Hoyer Effect. As a prestressing strand is pulled in tension the strand elongates, causing the diameter of that strand to simultaneously decrease. This principle, known as the Poisson Effect, helps explain what occurs after the strands are released from the abutments of the prestressing bed. Through the curing process, concrete hardens around the pretensioned strand. When the concrete has reached a desirable release strength, the strand is cut and tends to naturally shrink back to its original length, causing the diameter to increase. The hardened concrete inhibits the strand from returning to its original size, thus the transfer of mechanical stress from the strand to the concrete is manifested in a radial fashion around the strand. The Hoyer Effect is a key contributor to transfer bond stress as it creates frictional resistance between the concrete and the strand. The Hoyer Effect can be visualized in Figure 2-1.

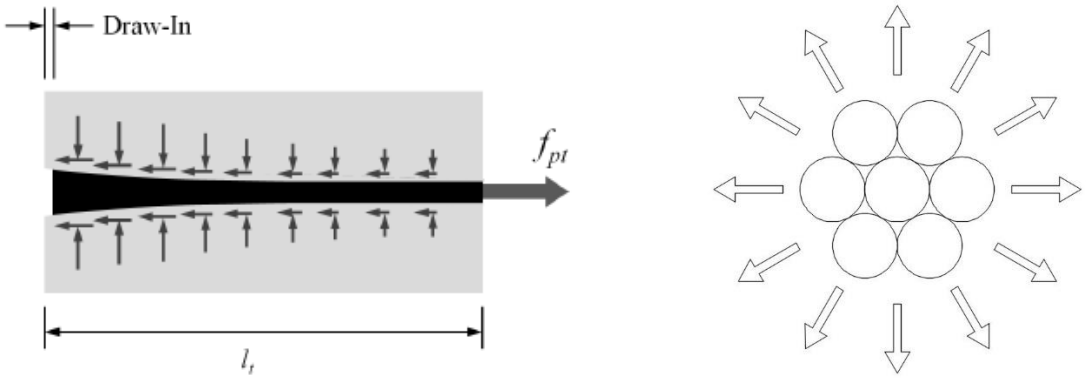

a) Strand slip (Dunham, 2011) **b) Radial stresses of seven-wire strand**

Figure 2-1 Hoyer Effect

The third transfer bond mechanism is mechanical resistance. Most prestressing strands are comprised of seven wires twisted together in a helical pattern. This allows for better bearing stress with the concrete. After the concrete is cast around the strand, small grooves are created within the concrete which increase the surface area of the strand. As a result, when the member is loaded, these grooves can create a mechanical resistance which helps the strand combat slip and can help develop larger capacity within the member (Hanson and Kaar, 1959).

The three bond mechanisms have wide implications on end zone cracking and transfer length. End zone cracking occurs as a result of the Hoyer Effect. The radial compressive stresses of the strand subject the surrounding concrete to high strains which can sometimes emerge as end zone cracks on the outside surface of the member, especially when strands are placed near the outside of the member. According to AASHTO (2015), the prestressing force is assumed to be zero at the edge of the girder and increases linearly along the transfer length of the girder. This drastic increase in stress is resisted by a limited amount of concrete near the girder end, especially in thin-webbed members, which is the cause of end zone cracking in many prestressed girders.

2.3. Review of End Zone Cracking in Pretensioned Concrete Girders

Current code specifications for end zone design and a summary of the findings from previous studies on end zone cracking are presented in this section. These studies, which occurred between 1961 and 2014, describe several methods of analysis and design for pretensioned concrete girders such as the Gergely-Sozen method (1967), the strut-and-tie method, and a variety of finite element analysis methods. As time progresses and more research is conducted, our ability to understand the complex strain distributions in the end zones of heavily pretensioned girders increases. This literature review was conducted to compile and compare the outcomes of some of the recent studies involving end zone cracking.

2.4. AASHTO Provisions for Splitting Reinforcement

Section 5.10.10 of AASHTO's *LRFD Bridge Design Specifications* (2015) specifies that the reinforcement design in the anchorage zone in the ends of pretensioned beams provide the minimum splitting resistance shown in Equation 2-1.

$$P_r = f_s A_s \quad \textbf{(2-2)}$$

Where: f_s = stress in steel not to exceed 20 ksi

A_s = total area of reinforcement located within the distance h/4 from the end of the beam (in.^{2})

h = overall dimension of precast member in the direction in which splitting resistance is being evaluated (in.)

According to AASHTO, the resistance must not be less than four percent of the total prestressing force of the beam at transfer. The AASHTO commentary explains the purpose of limiting the allowable stress in end-zone reinforcement, f_s to 20-ksi is to maintain cracks in the end zones of the members within acceptable limits.

2.5. Previous Experimental and Analytical Research Related to End Zone Cracking

2.5.1. Tuan et al. (2004)

Researchers at the University of Nebraska-Lincoln and Western Michigan University investigated the end zone cracking in twelve prestressed girder types including six NU-I girders and six NU inverted-tee girders. Based on their investigation, they then designed and tested a new girder type to minimize end zone cracking. The project was completed in two phases: (I) the evaluation of end zone vertical reinforcement immediately after prestress release in girders designed meeting AASHTO Specifications (2002); and (II) the design, testing, and analysis of new specimens with modified end zone details.

In Phase I, data was collected from twelve pretensioned concrete girders designed meeting the AASHTO specifications and fabricated at two different precast producers in Nebraska. The girders included in the Phase-I study were six NU I -girders (three NU1800 and three NU1600), and six NU inverted-tee girders (three IT600 and three IT400). Each girder was instrumented with four strain gauges, placed on vertical reinforcing bars in the end zone region (within a horizontal distance from the girder end equal to the height of the girder, *h*.) The strain gauges were used to measure the strain in the vertical reinforcement during prestress transfer. As a result of the Phase I tests, it was found that the strain in the reinforcing bars was highest at the member end and rapidly decreased as the distance from the girder end increased until total dissipation occurred at an approximate distance equal to *h*. The maximum strain values in the reinforcement occurred after the release of all strands. Among the end zone reinforcement, the stress levels varied between 0.2 and 12.9 ksi. However, all the measured steel stress values were well under the design stress of 20 ksi, as required by the AASHTO Specifications. The average splitting force of the girders tested in Phase I was roughly 2 percent of the prestressing force. Cracking was invisible in the

inverted T- girders. Cracks with lengths between 8 and 12 inches were noticed in the web regions of the NU I-girders.

Phase II involved the design of new end zone details based on information learned in Phase I. Three criteria were followed in the new design: 1) the end zone reinforcement was concentrated as close as possible to the girder end since this was the location susceptible to the highest splitting forces, 2) a working design stress of 20 ksi in vertical reinforcement was used, and 3) special vertical reinforcement was implemented within a distance of $h/8$ from the girder end, while the remainder of the vertical reinforcement was distributed as required for the critical shear section. The results of Phase II demonstrated that the new end zone reinforcement design improved the efficiency of the steel placement while reducing the quantity of steel used. The Phase II experiment confirms that in order to reduce the strain in steel and the concrete cracking it is necessary to use a large area of steel as close to the girder end as possible. The strain in the vertical bars within the Phase II I-girders followed the same trends as in Phase I. While the maximum stresses in these bars varied between 0.4 and 25.8 ksi, the strain was highest towards the girder end and decreased rapidly as the distance from the girder end increased. The variation of the maximum vertical reinforcement stress in the end zone can be seen in Figure 2-2. The measured crack widths and lengths in Phase II of the study were smaller than those in Phase I. The Gergely-Sozen (1967) method of analysis was used to predict crack locations after Phase II testing. This method proved to be an effective predictor of crack locations.

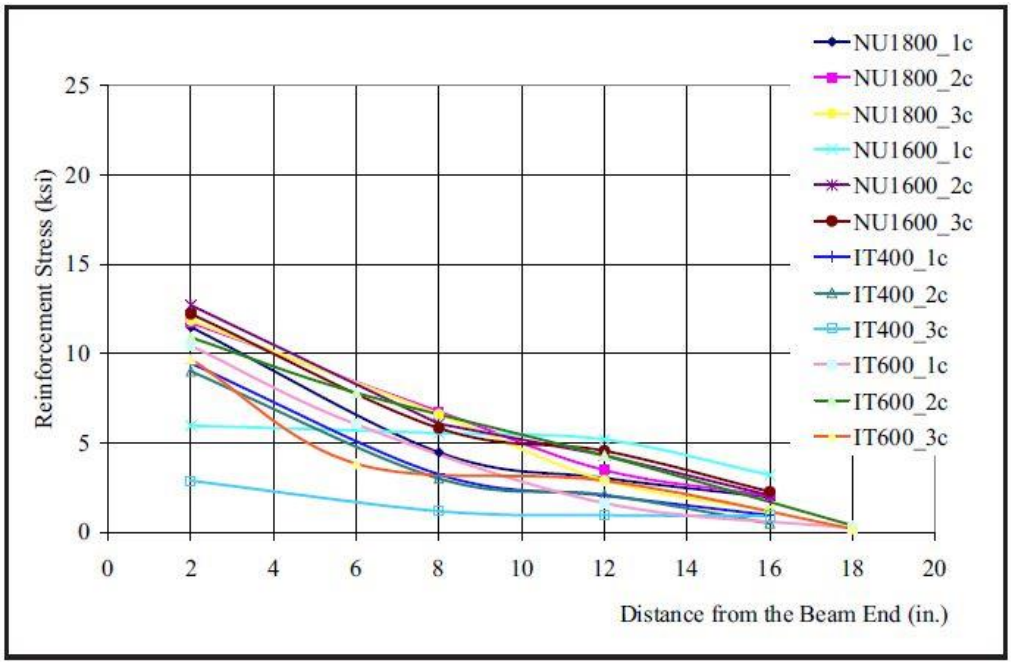

Figure 2-2 Variation of Maximum Steel Stress in the End Zone, (Tuan et al., 2004)

The ratio of the splitting force to the prestress force in Phase II testing ranged from 0.69 to 3.02 percent. The maximum measured splitting force of 3.02 was significantly under the required AASHTO standard which mandates that the splitting force be designed for 4 percent of the total prestress force. The relationships between the splitting force and the prestressing force for the girders studied in this project can be seen in Figure 2-3. Considering the data gained from the Phase II testing, the authors suggest that the current AASHTO recommendations of 4 percent splitting force could be an overly conservative estimation when the steel is concentrated very near the end of the member. Instead, the authors suggest that a pair of very large bars, designed for 2 percent of the prestress at a stress level of 20 ksi, be placed near the end of the girder to control the splitting cracks. The remaining balance of the prestressing force is recommended to be distributed across the critical shear section. The authors also proposed an alternative design of

distributing the splitting force of 4 percent along a distance of *h*/2 from the girder end with 50 percent of that force placed within a distance of *h*/8 of the girder end.

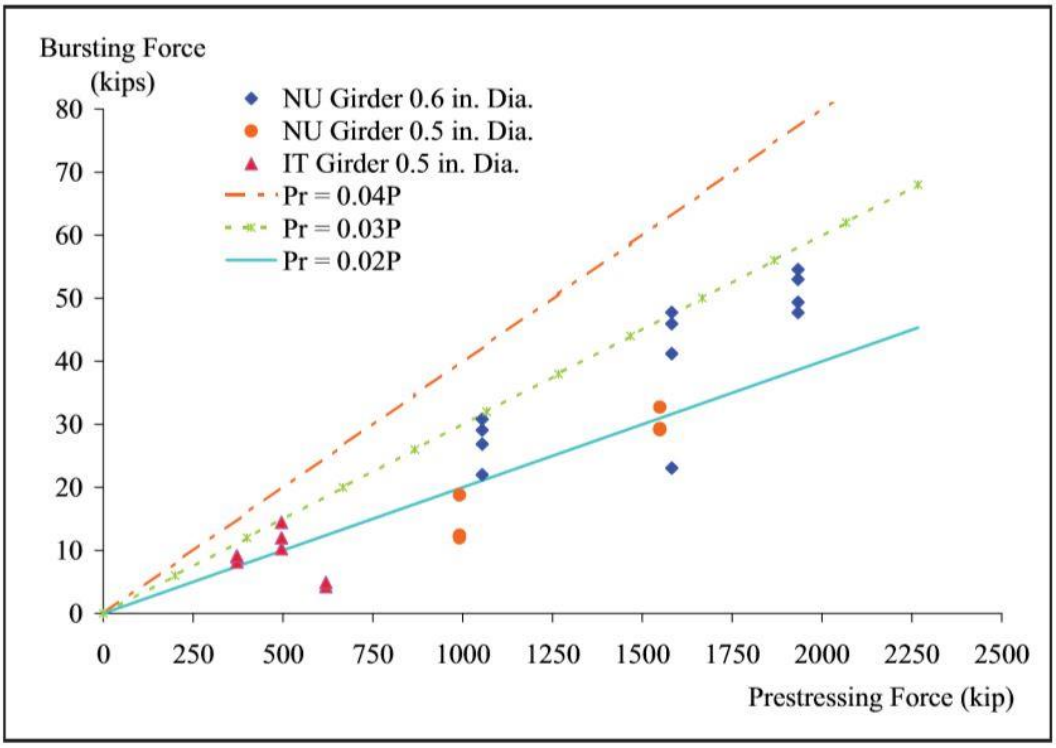

Figure 2-3 Relationship between splitting force and prestressing force, (Tuan et al., 2004)

The authors' conclusions from the experiments are summarized below:

- The Gergely-Sozen method of analysis adequately predicted cracking in full-scale specimens
- 3 percent of the prestressing force was the upper bound for the splitting force.
- The splitting force was close to 25 ksi in the reinforcement close to the girder end and quickly decreased until finally diminishing at a distance equal to the depth of the girder.

- 60 percent of the splitting force was found in the first *h*/4 of the girder while about 85 percent was found in the first *h*/2.
- The most effective reinforcement for resisting end zone cracks involves large bars that are designed for 2 percent of the prestressing force and placed at the end of the girder, however, such reinforcement may be too expensive.
- One realistic design solution is to design the splitting reinforcement for a splitting force equal to 4 percent of the total prestressing force and a uniform stress of 20 ksi. The placement of 50 percent of this reinforcement is to be within *h*/8 from the girder end, while the rest is to be contained within *h*/2 from the girder end.
- Since the recommended procedure requires the same total splitting reinforcement area, it can be seen as a validation of the current AASHTO Specifications.
- The proposed procedure may still be too conservative. More research is needed to investigate the potential of reducing the splitting reinforcement by increasing the stress limit to 30 ksi or 36 ksi.

2.5.2. Hamilton, Consolazio, & Ross (2013)

Research was conducted by the Florida Department of Transportation (FDOT) in 2012 that included a multi-component test program to evaluate the effects of web splitting, flange splitting, and lateral splitting on Florida I-beam**s**. The research also investigated the shear strength and behavior of early pretensioned girders used in retired Florida highways bridges. Four main test programs were conducted throughout the study: 1) the small beam test program, which investigated the function and effect of confinement reinforcement in twelve 28 in. deep precast-pretensioned beams, 2) the SR-72 test program, which performed ultimate tests on precast

pretensioned girders which were removed from a Florida bridge after 55 years of service, 3) the FIB-54 test program, which evaluated the effects of different end region details on girder capacity and behavior, and 4) the FIB-63 test program, which compared four detailing schemed for controlling and/or preventing web cracking. The FIB-54 and FIB-63 tests are discussed in the following section.

2.5.2.1. FIB-54 Test Program

The FIB-54 test program included the fabrication and load testing of five 54-in. deep FIB girders to evaluate the effects of different end zone detailing on girder capacity and behavior. The five girders included ten different end zones which all contained different detailing schemes. Variables in the detailing included: embedded steel bearing plate presence, confinement reinforcement quantity and configuration, strand bond patterns, strand quantity, and end zone reinforcement quantity. The specimens were loaded in a three-point bending configuration with a shear span-to-depth ratio of 2.0. Web-shear, bond-shear, and lateral-splitting were all reported failure modes of the FIB-54 tests. The end zone detailing of the ten specimens is shown in Table 2-1. The labeling scheme can be seen in Figure 2-4.

During prestress transfer, the strands were cut from the outside of the specimens to the inside. Concrete strains were collected in the bottom flange of the end of four specimens at prestress transfer. No cracks were visible on these specimens, however, strains reached up to nine times larger than the predicted rupture strain in some cases. For the instrumented specimens, these maximum strains occurred immediately after the outer strands were cut. It is believed that the cracks closed after the inner strands were cut.

Web and flange splitting cracks due to prestress were first noticed nine days after prestress transfer for girders H and V (which were cast together in Phase I) and were noticed during prestress

transfer for girders W, F, and D (which were cast together during Phase II). The cracks grew over time. The final crack properties are presented in Figure 2-5. The most severe cracking occurred in specimen FB and FN

Table 2-1 FIB-54 Specimen Detailing Variables (Hamilton et al. 2013)

Test Girder	Specimen	Bearing plate	Mild reinforcement		Strand bond pattern	Confinement reinforcement	Phase
			Vertical	Horizontal			
H	HC	Yes	FDOT	Yes	Design	FDOT	1
	HU	Yes	FDOT	Yes	Design	No	1
V	VC	Yes	Mod	No	Design	FDOT	1
	VU	Yes	Mod	No	Design	No	1
W	WN	No	FDOT	No	Web	Mod	2
	WB	Yes	FDOT	No	Web	Mod	2
F	FN	No	FDOT	No	Flange	Mod	2
	FB	Yes	FDOT	No	Flange	Mod	2
D	DC	Yes	FDOT	No	Design	FDOT	2
	DM	Yes	FDOT	No	Design	Mod	2

FDOT: Detailed per FDOT design standards
Mod: Detailed with modifications to FDOT design standards
Web: Fully bonded strands placed below web (24 fully bonded strands)
Flange: Fully bonded strands placed in outer portion of flange (24 fully bonded strands)
Design: Strand pattern based on prototype design (45 fully bonded strands)

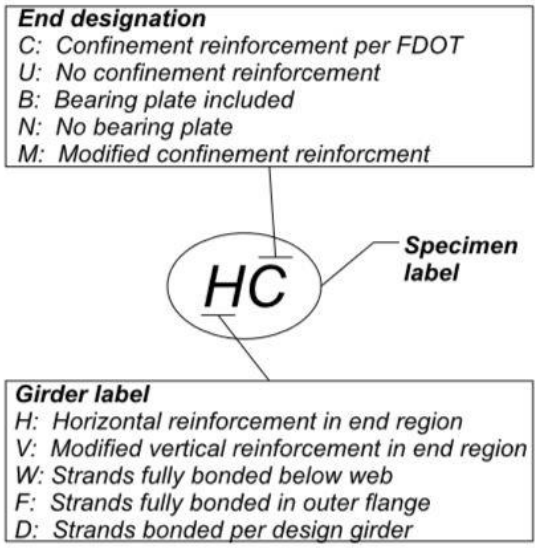

Figure 2-4 FIB-54 labeling scheme (Hamilton et al. 2013)

The length and area of the bottom flange cracks are represented in Figure 2-5. The most severe cracking occurred in specimens FB and FN. The severity of these cracks is likely due to the presence of fully bonded strands in the outer flange. The transverse tension created by these fully bonded outer strands is likely responsible for the large lengths and areas of these cracks.

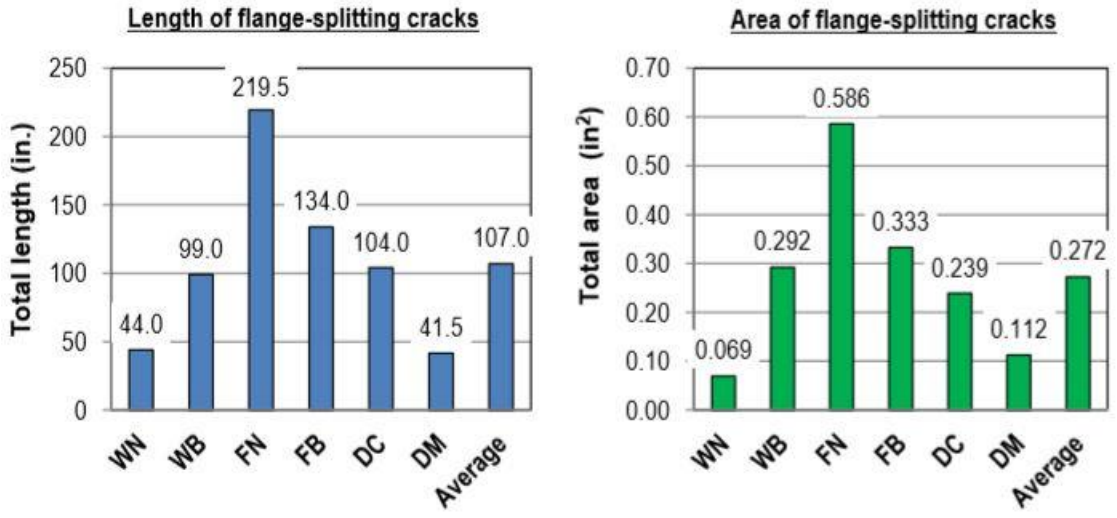

Figure 2-5 Flange splitting cracks in girders W, F, and D (Hamilton et al. 2013)

For the second portion of the FIB-54 test program, the girders were loaded to failure. Three distinct failure modes were reported during load testing: lateral splitting failure, bond-shear failure, and web-crushing failure. The highest peak shear force, at 793 kips, was observed in specimen HC, while specimen FN, at 402 kips, produced the lowest peak shear force. Bond-shear failure occurred only for the W girders which contained strands fully bonded below the web. Through the use of strain gauges during load testing, it was estimated that transverse forces of up to 100 kips were present in the bottom flange of specimens H and V. The peak shear forces and failure modes of each specimen can be seen in Figure 2-6.

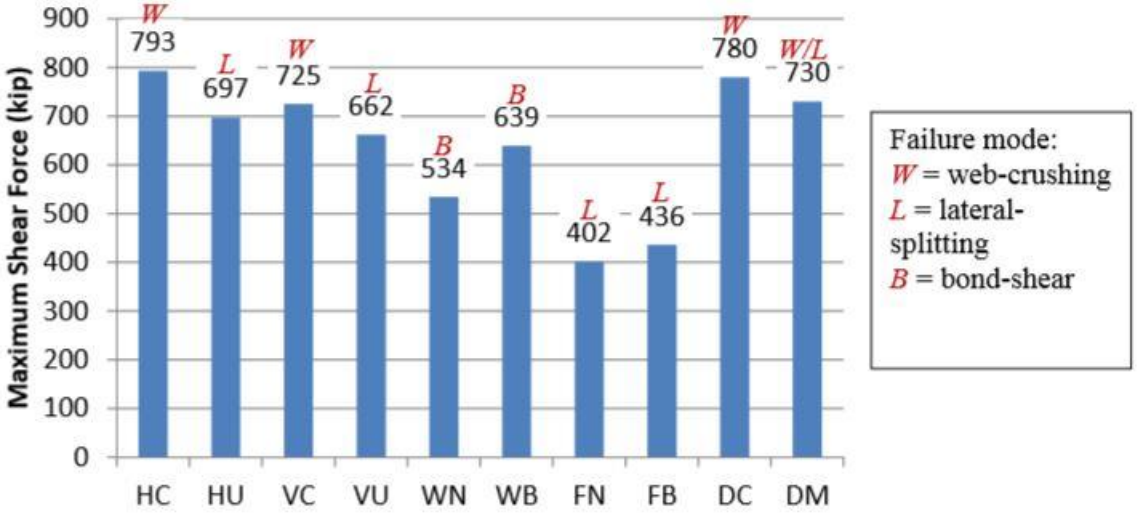

Figure 2-6 Peak shear forces and failure modes (Hamilton et al. 2013)

Relevant conclusions from the FIB-54 test study are as follows:

- Transverse tensile strains were measured during prestress release and during load testing. These strains are believed to be the cause of the flange-splitting cracks.

- Transverse tensile strains are greatest where fully bonded strands are present only in the outer portions of the bottom flange. The eccentricity of these strands causes bending and transverse tension near the end of the girder.
- The detailing schemes had a significant effect on end zone cracks, which varied in length from 75 in. to 291 in.
- The flange splitting cracks were present up to 30 in. from the specimen end. This length suggests that the AASHTO LRFD transfer length of 60 strand diameters (36 in.) is a reasonable distance to place confinement reinforcement for controlling flange splitting cracks.
- Differences in detailing had a significant effect on the end zone capacity. The maximum capacity of the different specimens ranged from 402 kips to 793 kips.

2.5.2.2. FIB-63 Test Program

The FIB-63 test program investigated end zone cracking in four FIB specimens with varying end zone designs. Two 63 inch deep girders were cast for the study and each of the four girder ends represented a different end zone design. The first design, specimen CT, was a control design which represented the current design of Florida I-beam girders and complied with AASHTO LRFD Bridge Design Specifications. The second design, specimen SL, included regular end zone reinforcement, however, 45% of the strands were shielded, or debonded, in the end zone region. Although this violated AASHTO LRFD's requirement of 25% maximum debonding, the research team chose to investigate this design to provide more information on the effectiveness of debonding with respect to end zone crack mitigation. The third specimen, PT, contained vertically post-tensioned rods in the end zone and 33% less vertical end zone reinforcement than the control specimen. The final specimen, LB, used thicker, 1 inch diameter threaded rods as vertical end

zone reinforcement. Specimen LB contained 30% less vertical end zone reinforcement than the control specimen. The BT-63 test specimen end zone designs are shown in Figure 2-7.

The girders were both fabricated at a length of 49.5 feet. The full span of girders with the same cross section are typically upwards of 125 feet. The specimens each included 52 0.6-inch diameter prestressing strands in the bottom flange and four 3/8-inch diameter tie strands in the top flange. Since the specimens would be tested to failure in a laboratory, they were fabricated without a top deck in order to reduce the load required in testing. The specimens were loaded in 3-point bending and instrumented to collect load, displacement, strain, and strand-slip data during testing.

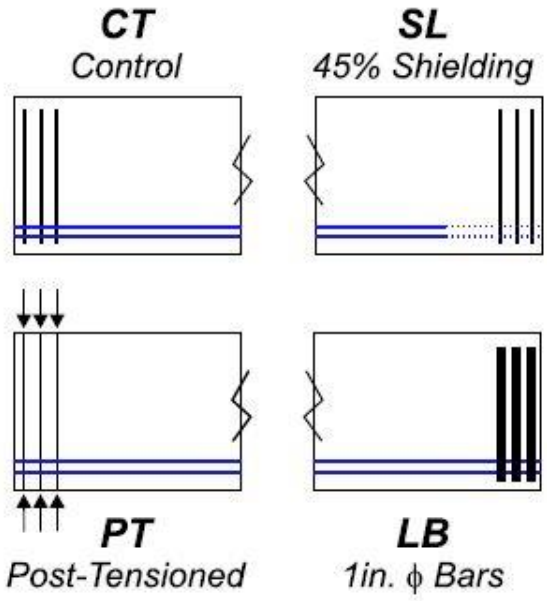

Figure 2-7 BT-63 end zone designs (Hamilton et al. 2013)

Cracking in the specimens was measured at prestress transfer and for several months after. Cracking was first observed during prestress transfer and grew in the months following. The control specimen, CT, was the least effective at controlling the end zone cracks with 28% longer cracks and 53% higher cracking area than the average of all specimens. Specimen SL produced the best results in every category except for total crack length. SL had 59% less area and 44%

smaller average width than specimen CT. The success of specimen SL is attributed to the reduction of tensile stresses, caused by partial debonding. Specimen PT was the most effective specimen in controlling web splitting crack length with 50% less length than specimen CT. Cracking on the FIB-63 specimens after prestress transfer can be seen in Figure 2-8.

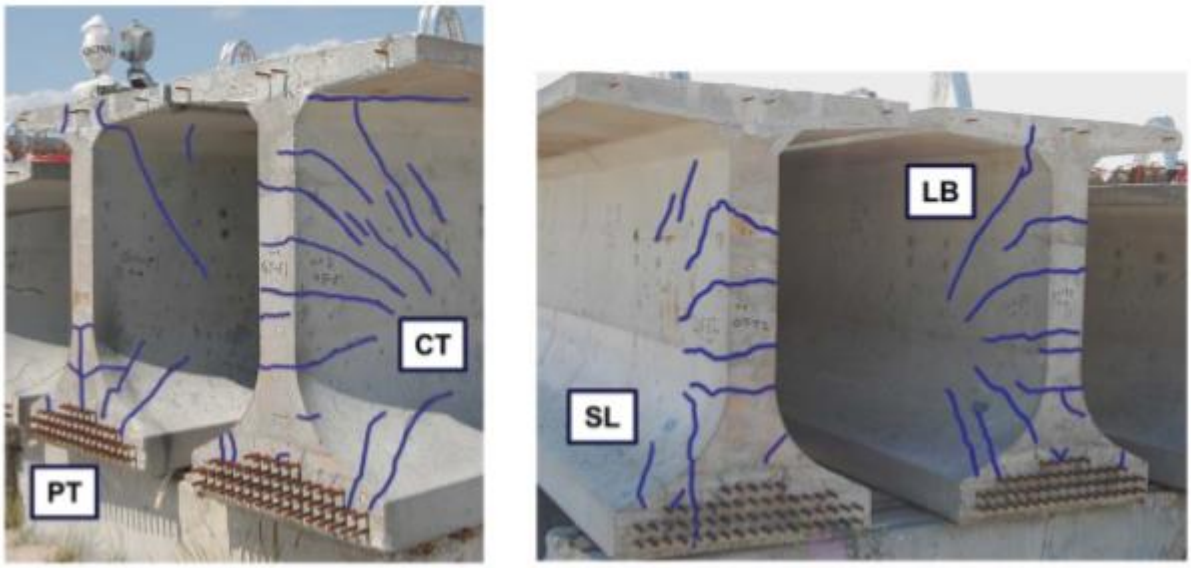

Figure 2-8 FIB-63 cracking after prestress transfer (Hamilton et al. 2013)

The high diagonal cracking in specimen PT, which can be seen in Figure 2-8, are believed by the authors to have been caused by forces introduced at the bearing plate of the vertical post-tensioning system. This crack was the greatest crack width and largest average web crack width, at 30% greater than that of specimen CT. The average and maximum crack lengths and areas were recorded for each specimen and can be seen in Figure 2-9 and Figure 2-10.

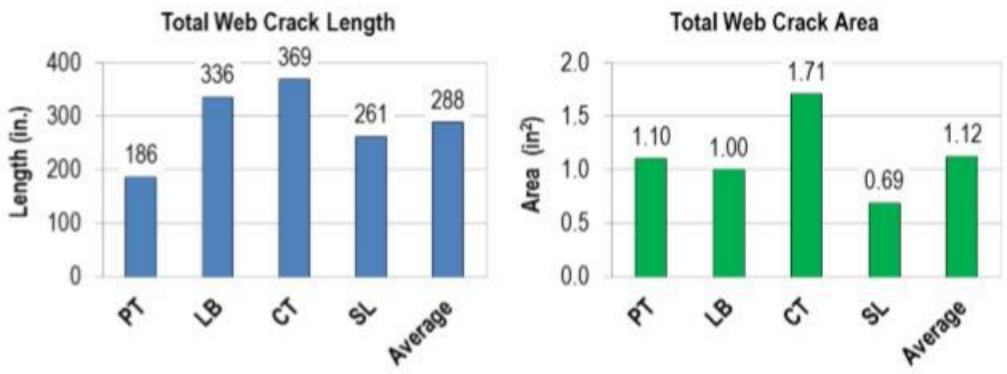

Figure 2-9 FIB 63 web splitting crack length and area (Hamilton et al. 2013)

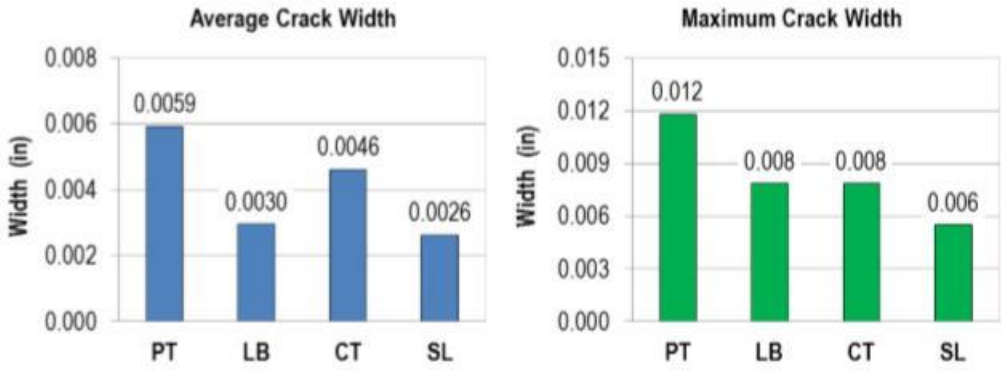

Figure 2-10 FIB 63 web splitting crack widths (Hamilton et al. 2013)

Approximately four months after prestress release, the specimens were loaded to failure in a 3-point bending test. Specimen LB reached a peak shear force of 612 kips before a punching failure through the flange occurred. This failure was due to the orientation of the load point bearing pad. Despite premature punching failure, specimen LB exceeded the calculated nominal shear capacity by roughly 20%. The pad orientation was adjusted for the subsequent tests.

The control specimen, CT, reached a maximum shear force of 791 kips before web failure. Breakout failure also occurred in the top hooks of the vertical reinforcement although it was not clear whether this failure preceded or was caused by the web failure. The control specimen exhibited a capacity approximately 50% greater than the calculated nominal capacity.

Specimen SL, which contained 45% shielding, reached a maximum shear force of 609 kips, which was the lowest measured maximum force of the four specimens. Specimen SL failed through bond-shear failure. The low amount of fully bonded strands was the reason for both the lower capacity and the failure mode, according to the authors. Specimen SL contained a little more than half of the bonded strands than the other specimens, thus, SL was more affected by cracks interrupting the strand development length.

Specimen PT reached a maximum shear force of 800 kips. The capacity of the specimen exceeded the capacity of the testing equipment, therefore, a failure mode for specimen PT was not observed. As a result of comparison with the control specimen, it was determined that post tensioning in the end zone of specimen PT did not adversely affect its shear capacity. Relevant conclusions from the FIB-63 tests are as follows:

- Partial strand debonding was effective in controlling the length and width of the web splitting cracks. Shielding produced a 29% reduction in web crack lengths and a 43% reduction in average web crack widths compared to the control specimen.
- Vertical post tensioning prevented web splitting cracks at the girder end but induced other large web cracks away from the girder end.
- All web cracks within the FIB-63 study were equal to or less than the FDOT requirements for moderate environments, or 0.012 in.
- Increasing vertical end zone reinforcement decreased the length and widths of the web splitting cracks. Specimen LB had 30% more reinforcement and 35% lower average web crack width than specimen CT.
- The measured capacity of all specimens was greater than the ACI 318-14 and AASHTO LRFD calculated nominal shear capacities.

- The increased debonding in specimen SL produced a lower experimental capacity. Bond-shear failure, which was caused by the low number of bonded strands, was the failure mode for specimen SL.

2.5.3. Crispino (2007)

A study by the Virginia Polytechnic Institute and State University and for the Virginia Department of Transportation (VDOT) investigated end zone cracking in Pretensioned Bulb-Tee bridge girders in 2007. The study included the investigation of end zone cracking in current VDOT girders, the examination of a new strut-and-tie model-based design, and the fabrication of a PCBT-63 girder to verify the effectiveness of the model-based design.

Through the investigation of a variety of recently cast VDOT PCBT girders at a Virginia precast plant, the research team was able to notice trends in the end zone cracking of the girders. The girders ranged in depth from 37 in. to 93 in. Horizontal cracks in the girder ends typically developed at the bottom flange-web interface and extended up to 25 percent of the girder height. Examples of the investigated girders can be seen in Figure 2-11. Diagonal cracks typically developed inches from the beam end and extended up to 75 percent of the girder height. Cracking occurred most frequently in deeper beams while smaller beams usually performed better when designed to AASHTO LRFD standards. Girders with more reinforcement in the end zone usually contained less cracking, however, diagonal cracking in some of these girders was still observed.

Figure 2-11 Examples of end zone cracking in PCBT-77 girders (Crispino, 2007)

The research team used the strut-and-tie modeling approach to simulate the end zones of 134 different beams with normal-weight concrete and 137 different beams with light-weight concrete. The models included a variety of girders with a wide range of variables; most notably, depth, strand pattern, and strand diameter.

The study showed a positive linear relationship between the splitting force and the prestressing force for all cases except for the cases wherein the bottom flange contains a large amount of strands. For these cases, the relationship is positively linear until approximately 80 percent of the prestressing force is reached, after which a slight decrease in the splitting force ensues until the final prestressing force is reached. Furthermore, the authors reported a 19 percent increase in splitting force for girders with 0.6 in. strands, compared to girders with 0.5 in. strands. Observations from the field study in the first portion of this research further supported these results. A comparison between girders with similar jacking force but differing strand diameters can be seen in Figure 2-12. T1 and T2 represent the resulting splitting tensile forces from the application

of the prestressing (P_{jack}) forces in the strut-and-tie models. As a result of these models, the authors concluded that a strand diameter of 0.6 in. is more susceptible to end zone cracking. There are currently no AASHTO provisions for strand diameter and eccentricity of the prestress force on the cross section.

Number of strands	P_{jack} (k)	Eccentricity at *h* from beam end (in)	T1 (k)	T2 (k)
48 ½ in. strands	1,491	22.8	95.1	68.0
34 0.6 in. strands	1,498	25.3	113	81.0

Figure 2-12 Tensile force in girders with variable strand diameter (Crispino, 2007)

The splitting resistance required in the *h*/4 region of a PCBT-61 girder varied from 3 to 5 percent of the prestressing force, while the splitting resistance required in PCBT-85 sample girders varied from 4.75 percent to 5.5 percent of the prestressing force. The splitting resistance required in the *h*/4 region of a PCBT-93 girder was calculated to be approximately 7.8 percent of the prestressing force.

The research team used the strut-and-tie model to create design aids for VDOT girders based on cross-sectional size. The design aids were used to convert the results from the strut-and-tie models into area of reinforcement needed. The design model was then compared to other recommendations from Marshall & Mattock (1962), Tuan (2004), and Castrodale & White (2002). These comparisons can be seen in Figure 2-13.

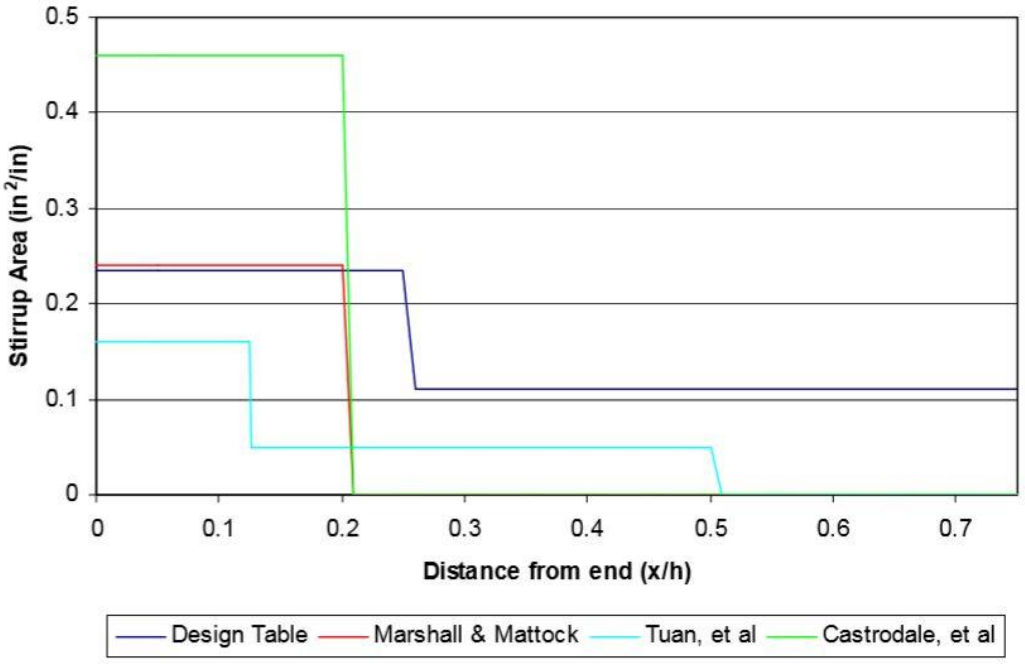

Figure 2-13 Design method comparison, PCBT-77, NWC, 34-0.6 in. strands (Crispino, 2007)

Through the use of the new end zone design model, the research team fabricated an experimental PCBT-53 specimen designed with light-weight concrete. The 53 in. bulb-tee girder was 65 ft long and supported a 7 ft wide, 9 in. deep deck. The vertical reinforcement within one end zone was designed with a stress limit of 12 ksi which corresponded to the research team's early recommendations for controlling crack widths in light-weight concrete girders. The other end of the girder was designed for a working stress limit of 18 ksi in the end zone. The test girder contained 21 -0.5 in. strands, six of which were harped. The release strength of the concrete was mandated to be 5,500 psi. #5 bars were used at the ends of the girders to ensure sufficient spacing and consolidation. Typical AASHTO confinement reinforcement was used in the bottom flange.

After prestress release and crane-lifting of the girder, the end zone containing the 12 ksi stress limit showed very fine cracks in the web (the largest of which was 0.003 in.) and a horizontal crack at the bottom flange-web interface extending about 17 percent of the girder height. At the

end zone containing the 18 ksi stress limit, the acceptable crack criterion were not met. The largest crack width on this end was 0.005 in., which is acceptable based on the authors' early recommendations, however, the crack lengths were not acceptable. A diagonal crack in the top flange extended 70 percent of the girder eight and several smaller cracks extended up to 28 percent of the girder height. These cracks all occurred during the lifting process. The strength of the concrete at prestress release (8,900 psi) was notably higher than the design release strength of 5,500 psi. This suggests more cracking could have occurred, had the strands been released earlier.

The test girder was instrumented with electrical resistance strain gauges to measure the splitting force in the end zones during and after prestress release. In the end zone containing the 12 ksi stress limit, the stress measured in the gauges showed a steady increase. The gauges in the upper portion of the web all measured below 200 microstrains. The gauges in the lower portion of the web were close to the small cracks in the web and reached up to 500 microstrains. After the strains were converted into stresses, they were plotted against their location from the distance from the end of the girder, as can be seen in Figure 2-14. The stresses ranged from 0.68 ksi to 13.8 ksi, with the gauge near the end reaching the highest stress. The stress in the bars decreased as their distance from the girder end increased, much like the trends seen in Tuan (2004).

A greater number of the gauges in the end zone designed for the 18 ksi stress reached higher strains. The strain gauges in the upper portion of the web varied from 0 to 300 microstrain, while the strain gauges in the lower portion of the web varied from 150 to 400 microstrains. The highest strains in the majority of these gauges occurred as the girder was being lifted. The stress distribution over the distance from the girder end was less smooth, for this girder end, however, it did still follow similar trends as the 12 ksi end zone. The maximum

measured stress in the bars was approximately 12 ksi in the end zone designed for an 18 ksi working stress, as shown in Figure 2-15.

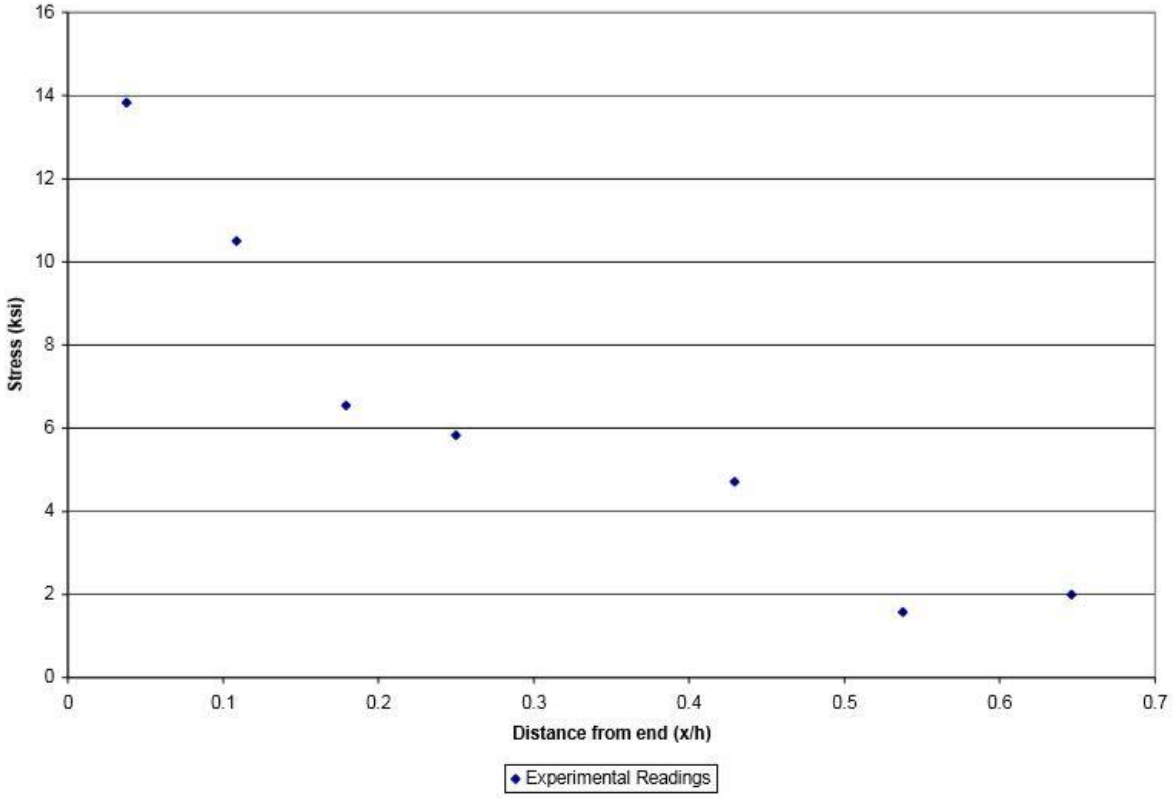

Figure 2-14 Distribution of tensile stress in 12 ksi end zone (Crispino, 2007)

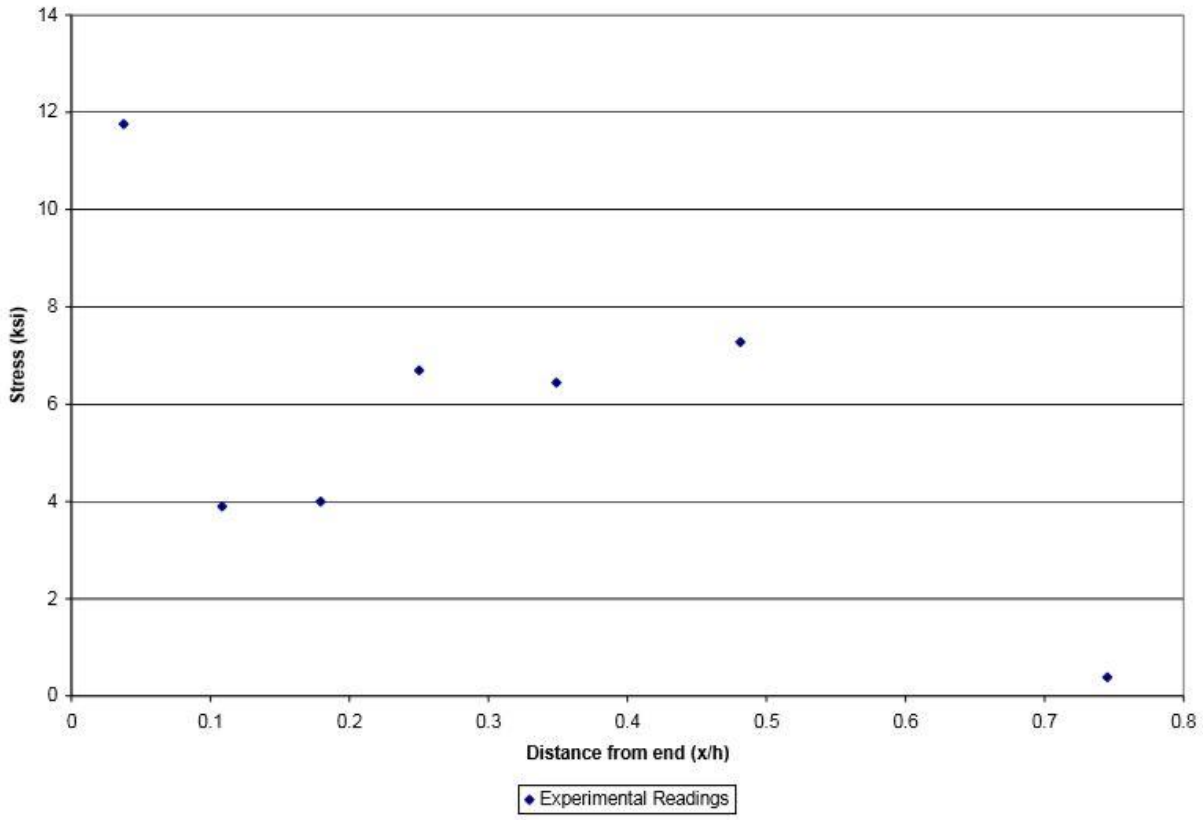

Figure 2-15 Distribution of tensile stress in 18 ksi end zone, (Crispino, 2007)

The girder was shipped to the Virginia Tech Structures Laboratory and a 7 ft wide, 9 in. deep composite deck was added to the top of the girder 77 days after prestress release. The deck was cast and allowed to moist cure for 7 days until the formwork could be removed. After the addition of the deck the girder was again inspected for cracks. The addition of the deck was determined by the authors to have no significant effect on the crack lengths and widths. Relevant conclusions from the author are included in the following:

- For typical PCBT girders below or equal to 61 in. in height, containing 0.5 in. strands, and cast with normal weight concrete, the area of vertical reinforcement in *h*/4 will increase from current practice; however, the slight increase in area will not affect the number of bars used currently.

- For PCBT girders taller than 61 in. in height, containing 0.5 in. strands, and cast with normal weight concrete, the area of vertical reinforcement will increase by one to three stirrups depending on the size selected.
- The number of bars required within the *h*//4 zone for all lightweight PCBT girders, or those containing 0.6 in. strands, should increase. Bundled stirrups to ensure consolidation will be typically needed for these girders.
- For all girders, the area of steel required between *h*/4 and 3*h*/4 is slightly less than the area of reinforcement required within *h*/4. As a general rule, the latter zone should include the same number of stirrups as the former.
- The design aids developed within this study are similar to the standard details used by North Carolina, Florida, and Washington Departments of Transportation.
- An acceptably small amount of cracking occurred within the specimen designed for a working stress of 12 ksi, however, the end zone detail designed for a stress limit of 18 ksi allowed cracks of an unacceptable length.
- A significant tensile force was measured between the *h*/4 and 3*h*/4 region; therefore, this region should still be considered in the end zone reinforcement design.

The author further recommends that more research be conducted on quality control at precast plants to understand the effect of variables that are intrinsic to different precast yards across the country. These variables include casting bed configuration and strand release method. Another recommendation involves administering split cylinder tests before prestress release to validate the concrete's early tensile strength. The author also calls for changes to AASHTO LRFD provisions for end zone reinforcement based on stress limit recommendations based on materials used and

environmental conditions. The final recommendation of the author includes the need for focus on long-term monitoring of girders which have experienced cracks and repairs.

2.5.4. Arab et al. (2014)

Arab et al. (2014) investigated end zone reinforcement modifications for 100 in. deep girders used by the Washington Department of Transportation for the Alaskan Way viaduct in Seattle, Washington. The girder end zone was analyzed using nonlinear finite element analysis and the results were reported and compared against the Gergely-Sozen method (1967), the strut-and-tie method (Castrodale & White, 2002), and the finite element method used by Arab, Badie, and Manzari (2011). A closed-form solution based on shear-friction theory was used to estimate steel tensile stress in the end zone reinforcement at the bottom flange-web interface.

The WF100G girders, which each spanned 205 ft, were pretensioned with eighty 0.6 in diameter strands, 26 of which were harped. The pretensioning force was gradually released through the use of hydraulic movable abutments. The girders were lifted at points 8 ft from the ends during prestress release to remove friction forces between the girder and the casting bed. The typical cross-section details can be seen in Figure 2-16. The longitudinal profile including end zone details is shown in Figure 2-17.

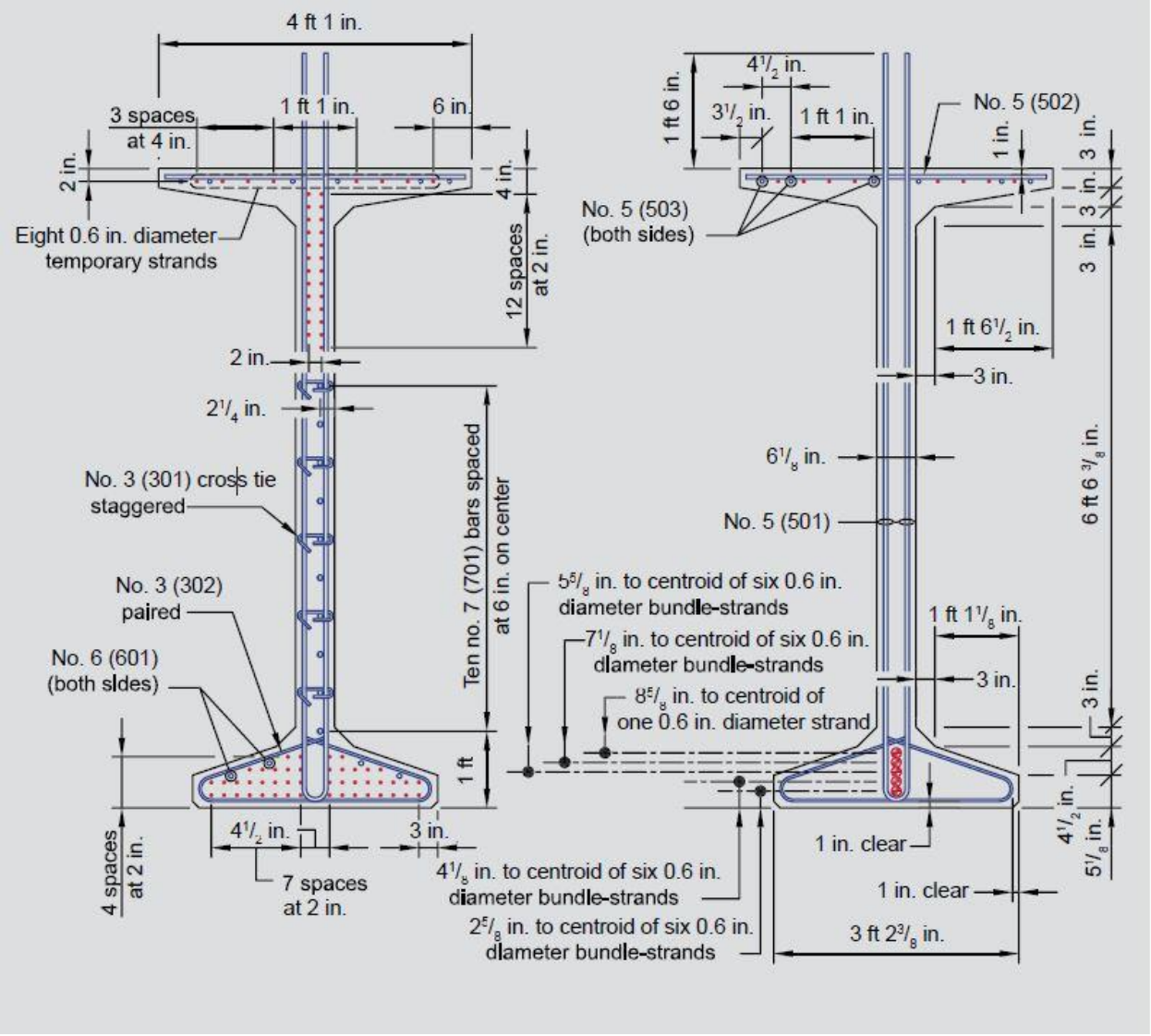

Figure 2-16 Typical cross section details of WF100G (Arab et al., 2014)

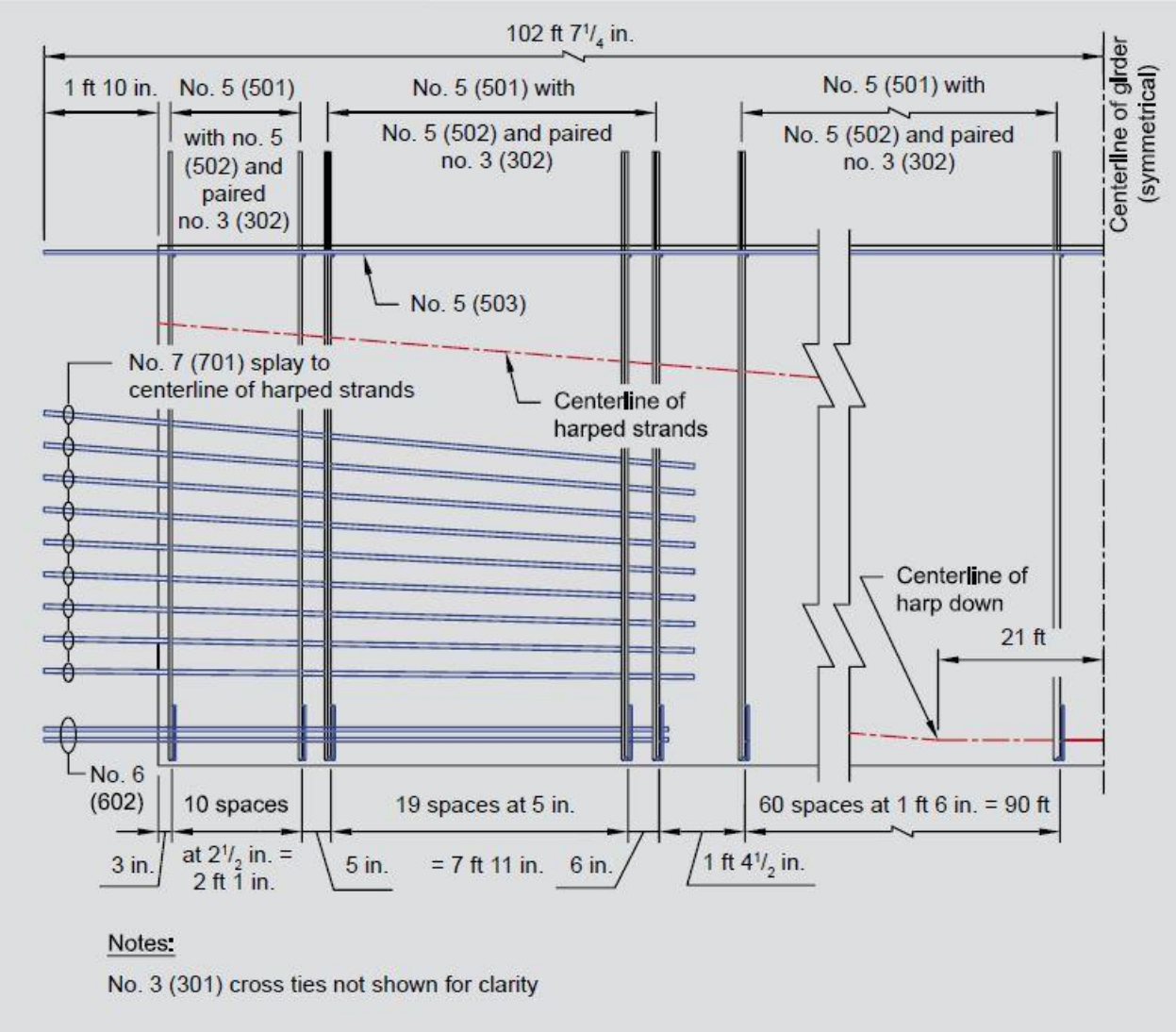

Figure 2-17 Longitudinal profile of WF100G (Arab et al., 2014)

The vertical reinforcement in the ends zones were equipped with electrical resistance strain gauges at three different heights, which were targeted locations at which cracking was most expected. Cracking was most prevalent in three locations: 1) the top one-third of the web, where cracks extended about 36 in. at a 30 degree slope, 2) the bottom one-third of the web, where horizontal cracks extended 20 in., and 3) at the bottom flange-web interface, where cracks extended about 24 in. at a small slope. The crack widths all ranged from 0.006 in. to 0.012 in.

The following observations were made from the strain gauges within the girder:

- The measured strain in the end zone reinforcement was greater than the concrete tensile strain capacity.
- For the multiple strain gauges located 52 in. from the bottom in each girder, the highest measured stress was approximately16.9 ksi.
- The greatest stress recorded in the first row of vertical reinforcement was observed 69.9 in. from the bottom and was about 15.6 ksi.
- The high tensile stresses recorded at the bottom flange-web interface were not predicted by the Gergely-Sozen method.
- The bottom flange-web cracks can be expected with deep girders having thin webs. According to the authors, the large amount strands in the bulky bottom flange create a distinction in behavior between the flange and the thin web. As a result, a clamping force is created by the vertical stirrups in this area, and cracks are therefore created by the large shear stresses at the interface.
- The greatest end zone stress was 85 percent higher than the 20 ksi AASHTO stress limit and occurred about 6 in. away from the girder end, or at 0.06*h*.

Strain gauges were also applied to a prestressing strand in the bottom flange and the strand stress distribution was measured over a 36 in. length from the end of the girder. A parabolic distribution of normalized stress in the strands was observed, as can be seen in Figure 2-18. Current AASHTO LRFD specifications describe a linear transfer length which, according to the authors, may cause designers to significantly underestimate the end zone tensile stresses immediately after prestress transfer. A trend line is presented by the authors which represents the measured stress distribution within the strand. Furthermore, the transfer length of the strand was

measured at approximately 34 in. from the girder end, indicating that the transfer length was smaller than the $60d_b$ length recommended by AASHTO LRFD specifications,

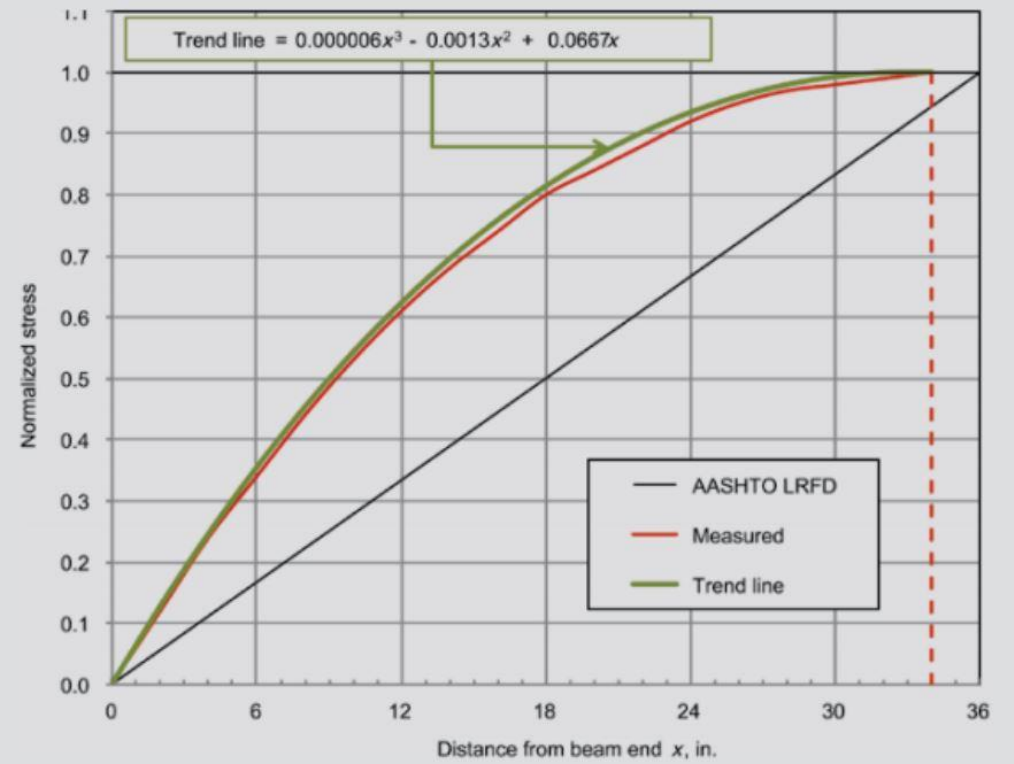

Figure 2-18 Measured strand stress in WF100G girders (Arab et al., 2014)

Two finite element modeling techniques were used to model the behavior of the girders after prestress release: extrusion and embedment. Each method proved to be viable and have advantages over the other. The extrusion method provided more detail at the concrete-strand interface (including slippage, transfer length, and transfer stress distribution) but required much more computational time and power. The embedment method is much less complex, less computationally expensive, and provides acceptable results, however, it treats the concrete-strand interaction as input data, and therefore can only be controlled by adjusting the initial conditions. The embedment technique was used for numerical simulation of the WF100G girders, with the initial condition of the prestressing elements being derived from the measured strain gauge data.

The results of the numerical analysis showed principle tensile stresses much higher than the modulus of rupture within *h*/4, and higher than the modulus of rupture within the *h*/2. The results are shown in Figure 2-19 alongside the actual cracks observed after prestress in a WF100G girder. The authors believe the reinforcement distribution recommended by (Tuan, Yehia, Jongpitaksseel, & Tadros, 2004) most appropriately matches the stress distribution from the finite element analysis. This distribution has 50 percent of the end zone reinforcement contained within *h*/8 of the girder end, and the remaining 50 percent between *h*/8 and *h*/4.

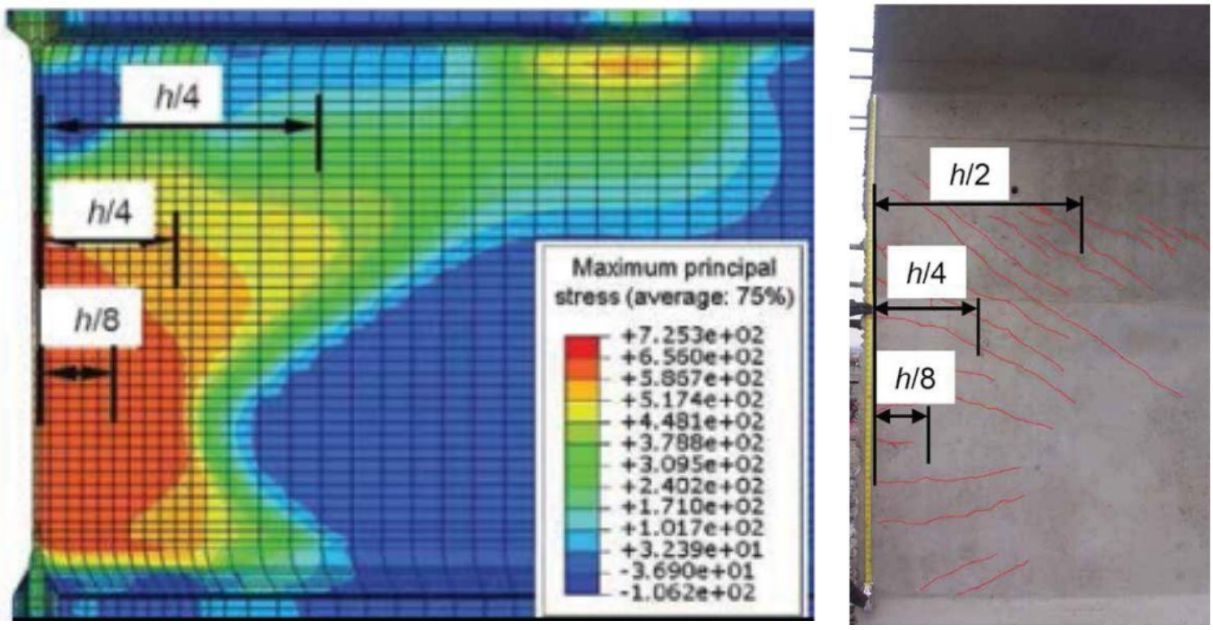

a) Principal stress distribution in numerical model **b) Girder end cracks**

Figure 2-19 Comparison of numerical simulation and cracking behavior (Arab et al., 2014)

The authors also hypothesized that the difference in pretensioning force between the bottom flange and web created shear lag, which resulted in a high concentration of shear stress at the bottom flange-web interface. This shear lag is thought to be partially responsible for the bottom flange-web cracking.

The experiment also measured the lateral stress of the confinement steel within the bottom flange of the girders. The lateral stress was measured at two different heights: 1.5 in. and 12. 625 in. The measured lateral forces were particularly high in the girder ends and at the draping point. The axial tensile stress in the confinement reinforcement was also measured near the member end to determine if the confinement steel in the bottom flange was sufficient for confining the bottom flange. The authors determined that the current minimum required confinement reinforcement in the AASHTO LRFD specifications was sufficient.

The cross ties, which were used in the girder to help with resisting lateral web stresses, were instrumented with strain gauges for the study. The tensile stresses in the no. 3 cross ties were measured between 0.6 ksi and 1.3. As a result it was concluded that these ties had no significant impact on the resistance to lateral stresses.

The following contains relevant conclusions from the study:

- 50 percent of the end zone reinforcement should be distributed within a distance equal to $h/2$ from the girder end, and the remainder should be distributed between $h/8$ and $h/2$.
- In the end zone reinforcement, the tensile stress calculated by the nonlinear finite element solution corresponds to the experimentally measured mean.
- The maximum tensile stress in the end zone reinforcement occurred in the bars near the end of the girder. Similar results were obtained from the strut-and-tie procedure.
- The maximum tensile stresses from the Gergely-Sozen method and shear friction analogy were similar, however, the heights at which these stresses occurred were at 51 in. and 12.625 in., respectively.

- The maximum tensile stress in the end zone reinforcing bar was overestimated by the Gergely-Sozen method, and the vertical location at which it predicted this stress was inaccurate.
- The shear-friction analogy, which was presented in this paper, predicted maximum tensile stress in the end zone reinforcement which was consistent with the experimental results.
- As current AASHTO specifications may not adequately account for the shear lag in the bottom flange-web interface, the closed-form solution proposed in the paper may be an alternative method for estimating tensile stress in the end zone reinforcement.

2.5.5. Oliva & Okumus (2011)

An integrated analytical and experimental study was conducted to further investigate the behavior of end zone cracking in deep prestressed beams used by the Wisconsin Department of Transportation (WisDOT). In particular, the study targeted the Y cracks that occur in the bottom flange of beams because of their high potential to introduce corrosion to prestressing strands. Nonlinear finite element analysis was implemented for the investigation on the effect of different design parameters on end zone cracking, including: increased reinforcement size, cutting sequence, debonding, and lower draping. For the purpose of verification, the results of the analyses were compared to strains measured in two Wisconsin girders during detensioning as well as strains measured by other researchers.

The model girders used in the study were Wisconsin 54W, 72W, and 82W sections. The girders contained 40, 48, and 46 total strands, respectively, with 8 strands draped in each. The girders were picked due to their relatively large amount of prestressing strands. The 54W model

was verified through empirical studies on 54W girders cast at two different prestressing yards in Wisconsin.

The first 54W, a 129 ft long girder manufactured by Spancrete Inc., experienced horizontal and lateral cracking in the web as well as Y cracking at the bottom flange-web interface, as seen in the left side of Figure 2-20. The maximum principal strains from the finite element analysis are shown on the right side. The results in the finite element model are generally compatible with the cracks seen in the 54W. The dark blue areas in the figure correspond with tensile strains near zero, while the red and grey areas represent tension strains of over 2000 με.

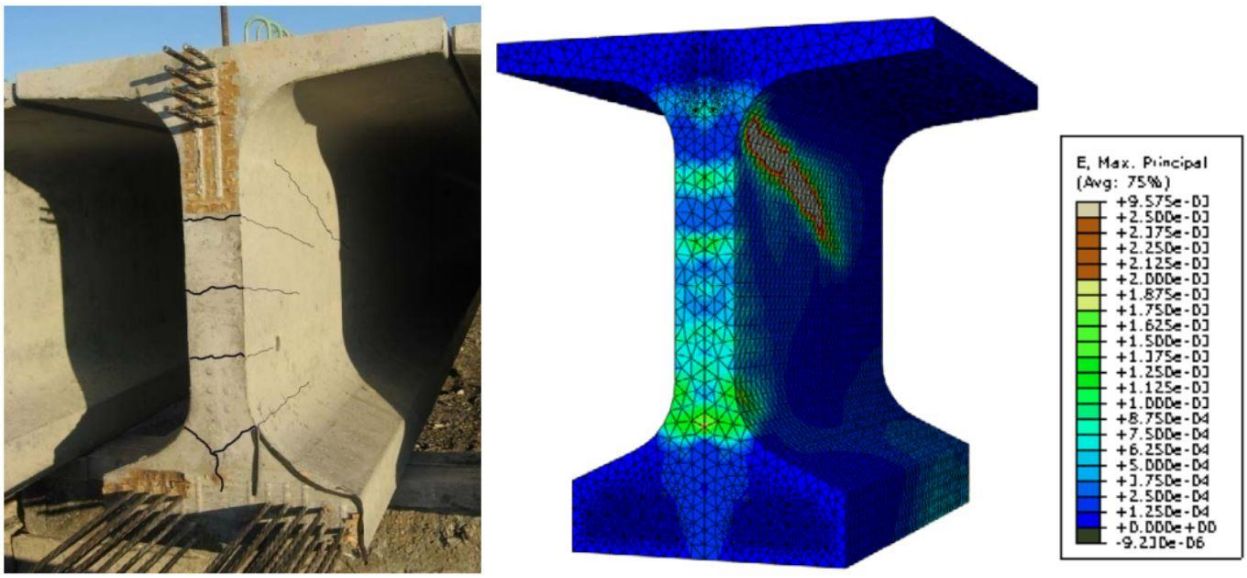

Figure 2-20 Cracks on the first 54W and maximum tensile strains from the FEM (Oliva & Okumus 2011)

A second, 71 ft-2 in., 54W girder, manufactured by County Materials Corporation, was heavily instrumented in the end zone and strain data was measured for the comparison with the finite element model. The steel strain gauges were placed on vertical reinforcement and strands in zones which were predicted by the model to contain the highest principal strains. With the gauges on the strands the authors were able to determine the transfer length and bond stress

distribution between the strands and the concrete. The average of the data produced by the strand strain gauges suggested a transfer length of 44 in., 22% longer than the AASHTO LRFD specification of 36 in. The cracks in the second 54W were also measured against the expected maximum principal strains from the finite element model. This comparison can be seen in Figure 2-21. Again, the results of the finite element model are generally verified by the observed end zone cracking of the girder.

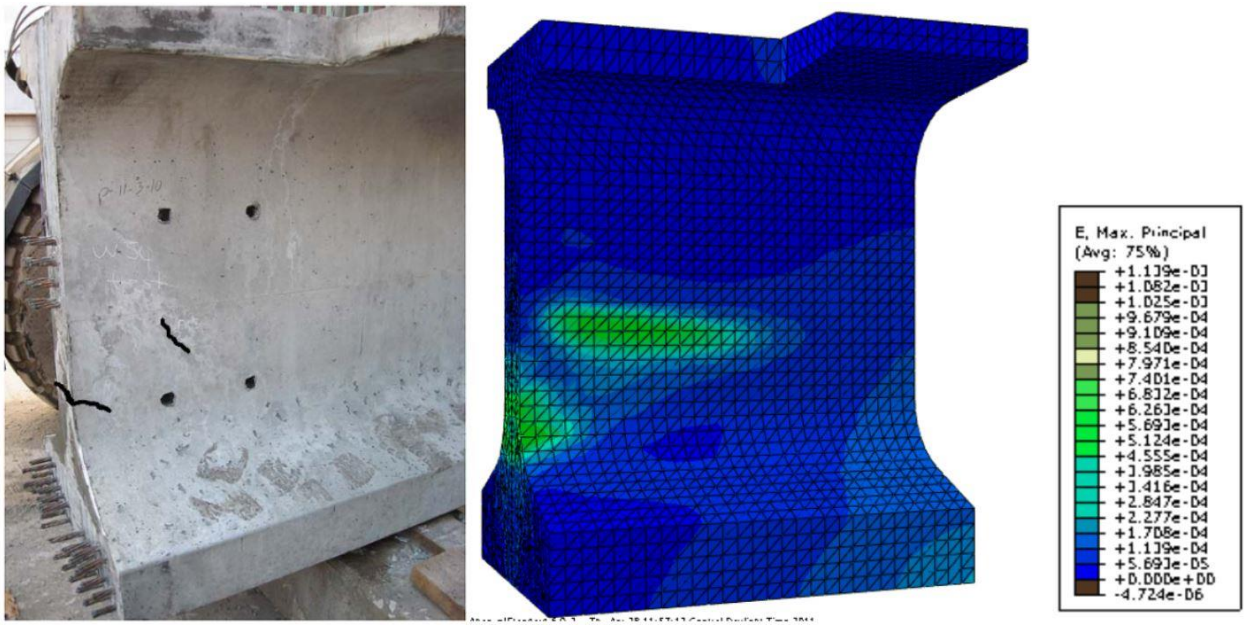

Figure 2-21 Comparison of cracks on the second 54W and maximum tensile strains predicted by the finite element model (Oliva & Okumus 2011)

A third, Tx-70 girder was used to verify the results of the finite element model. The authors verified their model with strain gauge data from the detensioning of a 70 in. deep girder cast for research at the University of Texas, Austin. A comprehensive instrumentation program was used to collect the strains from vertical reinforcement near the girder end. The comparison of the model with the strain gauge data showed very similar trends. One example of this comparison can be seen in Figure 2-22.

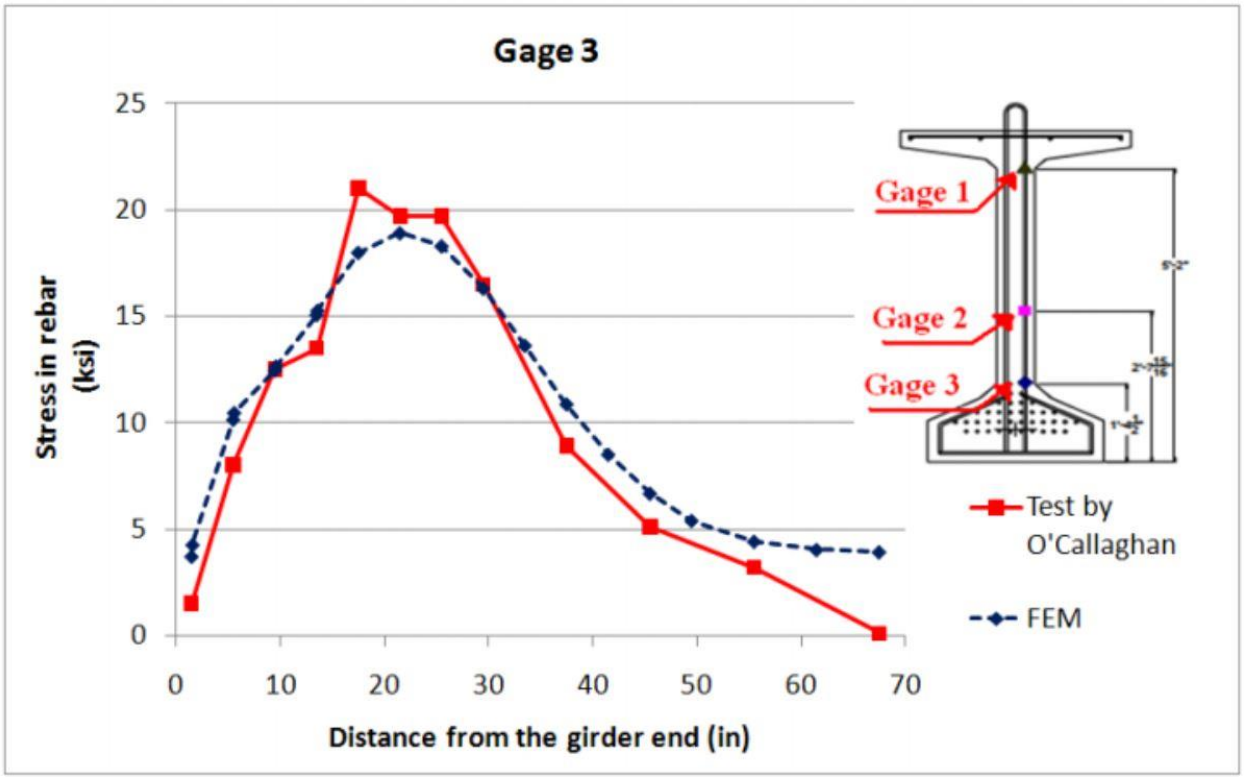

Figure 2-22 Distribution of reinforcement stress in Tx-70 model and strain gauges (Oliva & Okumus 2011)

The predicted maximum tensile strains in the Tx-70 were again matched by the observed cracks in the experimental specimen. As a result, the finite element model was decided to be adequate for further use in the behavioral study of deep girder end zones.

A 54W girder section, much like the Spancrete girder mentioned earlier, was used for the purposes of end zone design calibration. The model also accounted for reinforcing bars using linear elastic truss elements. The tensile stress distribution of the vertical bars within the model reached as high as 14 ksi near the girder end, while the peak stresses in the confinement reinforcement reached as high as 15.5 ksi near the end of the transfer length. The high strains measured in the vertical reinforcement correspond well with the web cracks observed in the Spancrete girder.

The authors implemented several parameters in their model in order to explore the effect of different end zone designs on the strains within the end zone. The investigation of potential solutions included the following parameters: 1) End zone reinforcement pattern, 2) debonding and level of debonding, 3) combination of end zone reinforcement pattern and debonding, 4) strand cutting sequence, 5) lowering, spreading, and removing draped strands, and 6) coping the upper flange. The following sections will discuss the consequence of each end zone modification.

For the investigation of the end zone reinforcement pattern, the authors ran the model with varying reinforcement sizes and spacing. Among the reinforcement designs, the following were included: Five #6 @ 3", five #7 @ 3", five #9 @ 3", five #10 @ 3", five #6 @ 1.785", and two #10 @3" with three #6 @ 3". The modifications in reinforcement design produced a 20-50% reduction of tensile strains level; however, no modification was able to significantly lower the strain level below the expected cracking strain. A comparison between the five #10 @ 3" and two #10 @ 3" with three #6 @ 3" showed very similar strain levels. Through this comparison, the authors determined that two #10 @ 3" with three #6 @ 3" was sufficient for the reduction of strain in the end zone. These findings are similar to the recommendations of (Tuan, Yehia, Jongpitaksseel, & Tadros, 2004). Modifications to other reinforcement (vertical bars beyond $h/2$ and confinement reinforcement) produced no significant reduction in end zone strains.

Debonding and the level of debonding had a significant effect on the reduction of tensile strains in the end zone. The following debonding patterns were implemented in the model: No debonding, 25% debonding, 35% debonding, and 50% debonding. The authors chose to investigate several levels of debonding in which compliance with the AASHTO LRFD specifications was not always adhered. The results of the investigation showed that all levels of debonding reduced the end zone strains. Inclined cracks were eliminated with all debonding

levels. The quantity of web cracks expected generally decreased with the amount of debonded strands at the girder end. Y cracks at the bottom flange-web interface were significantly affected by the distribution of debonded strands in the bottom flange. The most effective distribution contained debonded strands relatively evenly distributed across the entire flange width, as opposed to concentrated in the center of the flange. This distribution of debonded strands was estimated to eliminate Y cracks.

Since changing the reinforcement pattern was successful in reducing horizontal web cracks and the addition of debonding eliminated inclined cracks and Y cracks, the two methods were combined. This combination of design changes resulted in a further reduction of end zone strains. The authors concluded that combining a minimum of 35% debonding with two #10 bars at the girder end reduced the web strains below the cracking limit. For further verification, the authors applied these design modifications to an 82W girder model and similar conclusions were reached.

The effect of strand cutting sequence on cracking was investigated and was determined to have some effect on the crack size and the time at which cracks occur. The authors ran five models with different strand release patterns and determined that releasing the inside strands first produced strains with the smallest magnitude. Thus, they recommended that strand cutting initiate at the interior strands and move outwards if possible.

Three different strand draping design methods were investigated in the finite element model: No draping, lower draping, and fanned draping. The first modification, removing the draped strands, reduced the intensity of the highly concentrated areas of strain near the draped strands, or the area near the inclined cracks. This solution provides great results in the web crack and inclined crack areas, however, it is not practicable since it does not allow the requirement for top fiber tension limits to be met. The lower draping model produced a higher strain concentration near the

location of the strands. This is due to the reduction in area of concrete around the strands in the girder end. Spreading out the draped strands while keeping the same strand centerline at the girder end provided better results for strain reduction in the inclined cracking area when compared to lower draping. Both methods, however, may be purely academic since the lowered strand centerline would produce a lower strand eccentricity which would have to be adjusted by eliminating straight strands and, hence, reducing the capacity of the girder. These modifications were studied for the purposes of investigating the effect of draping patterns on end zone cracking.

The final investigation involved the coping of the girder end. This coping generally occurs on bridges with skew. The effect of coping on the girder end had reportedly no significant impact on the strain in the girder ends. The proposed solutions and their effects on end zone cracks is summarized in Table 2-2.

Table 2-2 Impact of Proposed Solutions on End Zone Cracking (Oliva & Okumus 2011)

SOLUTION		INCLINED CRACKING	WEB CRACKING	Y CRACKS
End Zone Reinforcement	First vertical set from the end	MILD	MODERATE	NONE
	Second vertical set from the end	NONE	NONE	NONE
	Bottom flange stirrups	NONE	NONE	NONE
Debonding		HIGH	MODERATE	HIGH
End Zone Reinforcement & Debonding		HIGH	HIGH	HIGH
Strand Cutting Order		NONE	NONE	MODERATE
Draped Strands	Removed	HIGH	NONE	NONE
	Lowered	NONE	MODERATE	NONE
	Lowered & Spread	HIGH	MODERATE	NONE
Coping the top flange		NONE	NONE	NONE

HIGH = can eliminate cracking
MODERATE = can reduce strains significantly
MILD = can reduce strains
NONE = has negligible impact

2.6. Review of Transfer Length in Pretensioned Concrete Girders

2.6.1. Code Provisions for Transfer Length

2.6.1.1. AASHTO (2015)

Section 5.11.4 of AASHTO's *LRFD Bridge Design Specifications* (2015) explains AASHTO's design requirements for the transfer and development lengths for pretensioned concrete members. To represent the transfer and development lengths, the organization uses Equations (2-3) and (2-4), respectively.

$$l_t = 60 d_b \quad \textbf{(2-3)}$$

$$l_d \geq \kappa (f_{ps} - \frac{2}{3} f_{pe}) d_b \quad \textbf{(2-4)}$$

Where: d_b = diameter of the strand (in.)

f_{ps} = average stress in prestressing steel at the time for which the nominal resistance of the member is required (ksi)

f_{pe} = effective stress in the prestressing steel after losses (ksi)

κ = 1.0 for pretensioned panels, piling, and other pretensioned members with a depth of less than or equal to 24.0 in.

κ = 1.6 for pretensioned members with a depth greater than 24.0 in.

The transfer length is assumed to vary linearly from zero at the point where bonding initiates to f_{pe} at the point where the transfer length ends. According to AASHTO, the development length, l_d, of a pretensioned strand is the length that the strand should be bonded beyond the section required to develop f_{ps}. Section 5.11.4.3 states that for all strands that are debonded where tension exists in the precompressed tensile zone, κ shall be equal to 2.0.

The ACI and AASHTO equations for development length are equivalent expressions for both bonded and debonded pretensioned members. In both cases, the length required for development is governed by diameter size, effective stress, nominal stress, and bonding conditions.

2.6.1.2. ACI 318-14

Section 25.4.8 of the ACI code addresses the development of seven-wire strands in tension. ACI states that the development length can be represented by the following equation:

$$l_d = \left(\frac{f_{se}}{3000}\right) d_b + \left(\frac{f_{ps} - f_{se}}{1000}\right) d_b \quad \textbf{(2-5)}$$

where f_{se} = effective prestress in the prestressing steel (psi)

f_{ps} = stress in the prestressing steel at nominal strength (psi)

d_b = the diameter of the strand (in.)

The first term in the equation represents the transfer length of the strand, or the length required for the prestressing strand to develop the effective prestress, f_{ps}. The second term represents the additional length required for the stress of the prestressing strand to develop. According to section 25.4.8.1 (b), for strands that are debonded and designed for tension in the precompressed tension zone, the calculated development length, l_d, should be doubled.

2.7. Previous Research Associated with Transfer Length

Many studies have been conducted over the years to enhance our understanding of transfer and development length in prestressed members. The following section provides a summary of the equations developed in these studies and brief descriptions of the investigations.

2.7.1. Hanson and Kaar (1959)

The current ACI predictive equations for the transfer and development length of prestressed members were developed based on research conducted by Hanson and Kaar (1959). These transfer and development length equations are shown in Equation (2-6) and Equation (2-7), respectively.

$$l_t = \left(\frac{f_{se}}{3}\right) d_b \quad \textbf{(2-6)}$$

$$l_d = \left(\frac{f_{se}}{3}\right) d_b + \left(f_{ps} - f_{se}\right) d_b \quad \textbf{(2-7)}$$

where f_{se} = effective stress in prestressing strand, ksi

f_{ps} = stress in prestressing strand at nominal strength, ksi

d_b = nominal strand diameter, in.

The study investigated four main variables: strand diameter, concrete compressive strength, percentage of reinforcement steel used in a section, and the surface condition of the strand Overall, forty-seven beams were studied, prestressed with ¼, 3/8, and ½ in. diameter, stress-relieved, 250 ksi strands. The first phase investigated eighteen beams with varying strand diameters and embedment lengths of the strands. The second phase examined nine beams with concrete compressive strengths that varied between approximately 3700 psi, 5400 psi, and 7200 psi. The third phase investigated the effect of the percentage of reinforcement by comparing beams with two, four, and six strands. The final phase investigated the effect of strand surface condition by casting two groups of four beams: one group with smooth, clean strands, the other group with rusted, weathered strands. The ACI equations were derived by Alan H. Mattock and first used in 1963 by ACI. (Riding et al., 2015)

2.7.2. Martin and Scott (1976)

In 1976 Martin and Scott reexamined the ACI transfer and development length equations after studying the bond failure of a pretensioned member. The study took into consideration the release method of the prestressing strands. As Hanson and Kaar's study only included strands released slowly rather than the commonly used method of flame-cutting or saw-cutting. The study also took into consideration strands with the ultimate strength of 270 ksi, rather than the less common 250 ksi used by Hanson and Kaar. As a result of this research Martin and Scott proposed a much more conservative equation for transfer length than that found in the ACI building code. The expression recommended a transfer length equal to eighty times the diameter of the strand, as shown in Equation (2-8).

$$l_t = 80 d_b \tag{2-8}$$

This expression produces a much higher estimation of the transfer length than the recommendations of Hanson and Kaar, which can be equated to 50 times the diameter of the strand. (Riding et al. 2015).

2.7.3. Shahawy & Issa (1992)

The investigation of experimental findings from three research projects funded by the Florida Department of Transportation (FDOT) led Shahawy (Shahawy & Issa, 1992) to develop his own transfer length equation. Shahawy proposed a transfer length expression which replaced the term for effective prestress, f_{se}, with a term for initial stress before prestress losses, f_{si}. The expression can be seen in (2-9).

$$l_t = \frac{1}{3} f_{si} d_b \tag{2-9}$$

2.7.4. Russell and Burns (1993)

A study published in 1993 by Russell and Burns involved extensive testing on rectangular beams, AASHTO-type beams, and Texas Type-C girders at the University of Texas at Austin. The tests included a total of 65 prestressed girders with both 0.5 in. and 0.6 in. diameter strands. (Russell & Burns, 1993). The study investigated the effect of strand diameter, strand spacing, debonding, size of cross-section, and confinement reinforcement on beam transfer lengths. The research team found the transfer lengths by using the 95% Average Maximum Strain (AMS) method. The team also found that strand bond failure only occurs when cracks propagate into the transfer zone of the prestressing strands. After review of the FHWA's five-year ban on the use of 0.6 in. strands, Russell and Burns concluded that the restrictions should be reconsidered. As a result of the study Russell and Burns recommended transfer lengths to be expressed by Equation (2-10).

$$l_t = \frac{1}{2} f_{se} d_b \qquad \textbf{(2-10)}$$

Consequentially, the recommended equations by Russell and Burns were reviewed by Dale Buckner on behalf of the FHWA. Buckner determined that the existing ACI expression for transfer length was non-conservative due to the use of 250 ksi of Hanson and Kaar's study (Buckner, 1995). The increasing use of low relaxation strands adds an additional 20 percent to the expected transfer length predicted by the ACI expression. He determined that Equation (2-9), proposed by Shawawy et al., (1992) provided a more accurate transfer length (Riding et al., 2015).

Buckner also found that the ACI expressions for development length were non-conservative and presented the Equation (2-11 for development length. Buckner specified that both recommendations should be multiplied by a factor of 1.3 for draped or straight strands which end

in the upper 1/3 of the depth of the member and have at least one ft of concrete cast underneath them. Following Buckner's review, the FHWA repealed the ban on 0.6 in. diameter strands for use in pretensioned members.

$$l_d = \frac{1}{3} f_{si} d_b + \lambda (f_{su} - f_{se}) d_b \quad \textbf{(2-11)}$$

2.7.5. Ramirez and Russell (2008)

In 2008, a report by Ramirez and Russell was published for the National Cooperative Highway Research Program (NCHRP). The intent of the study was to incorporate a factor for concrete compressive strength into the transfer and development length expressions. The authors used both 0.5 in. and 0.6 in. diameter strands and concrete release strengths which varied from 4 ksi to 10 ksi. As a result of the study, it was determined that concrete release strength and transfer length have an inverse relationship. Furthermore, the study suggested that the development length is also reduced with an increase in concrete release strength. Equation (2-12 and Equation (2-13 are proposed as a result of this study (Riding et al., 2015).

$$l_t = \frac{120 d_b}{\sqrt{f'_{ci}}} \geq 40 d_b \quad \textbf{(2-12)}$$

$$l_d = \left(\frac{120}{\sqrt{f'_{ci}}} + \frac{225}{\sqrt{f'_c}} \right) d_b \geq 100 d_b \quad \textbf{(2-13)}$$

2.8. Previous Research Related to this Study

2.8.1. Dunham (2011)

A research study was conducted at Auburn University to investigate the transfer length in bulb-tee girders constructed with self-consolidating concrete (SCC). The transfer length of twelve bulb-tee girders, cast for use in an ALDOT bridge project, were studied as a part of the program.

Six bulb-tee girders with a height of 54 in. (BT-54) and six bulb-tee girders with a height of 72 in. (BT-72) were cast using either SCC or conventionally vibrated concrete (CVC). The transfer lengths of the girders were measured immediately after prestress release, as well as at 7, 14, and 28 days after release. The transfer length results were compared against each other, as well as against the transfer length equations given in previous literature.

All twelve specimens used in the experiment were plant-cast at Hanson Pipe & Prestress in Pelham, Alabama. The BT-54 girders had a span of 97 ft 10 in. with a skewed end of 15 degrees. A total of forty ½ in. diameter strands were used in the BT-54 girders, with eight being draped. The BT-72 girders spanned 134 ft 2 in. with an identical skew of 15 degrees. Ten additional ½ in. diameter strands were used in the BT-72 girders, creating a total of fifty strands, of which eighteen were draped. Furthermore, to satisfy allowable stress limits, a total of four and six strands were debonded for 10 ft in the ends of the BT-54 and BT-78 girders, respectively.

The transfer length of each girder was measured at both ends and the transfer length of the debonded strands within ten of the twelve girders was measured. This resulted in the capturing of thirty-four transfer zones: 24 at the girder ends, and 10 at the location of debonding. The transfer lengths were measured using demountable, mechanical (DEMEC) target screws which were cast in the side of the bottom flange of the girders. The cast-in-place mounting system allowed for the DEMEC target screws to be easily and quickly installed in the girder after fabrication. Metal strips were used to mount the threaded inserts which would eventually hold the target screws in place. The mounting system was held in place by tying the threaded rods to the strands contained in the bulb. After the concrete was cured thirty-four target screws were ultimately screwed into the threaded inserts and a distance of approximately 5 ft could be measured. The cast-in-place

DEMEC mounting system is shown in Figure 2-23. The installation of the DEMEC target screws after the removal of the metal strip can be seen in Figure 2-24.

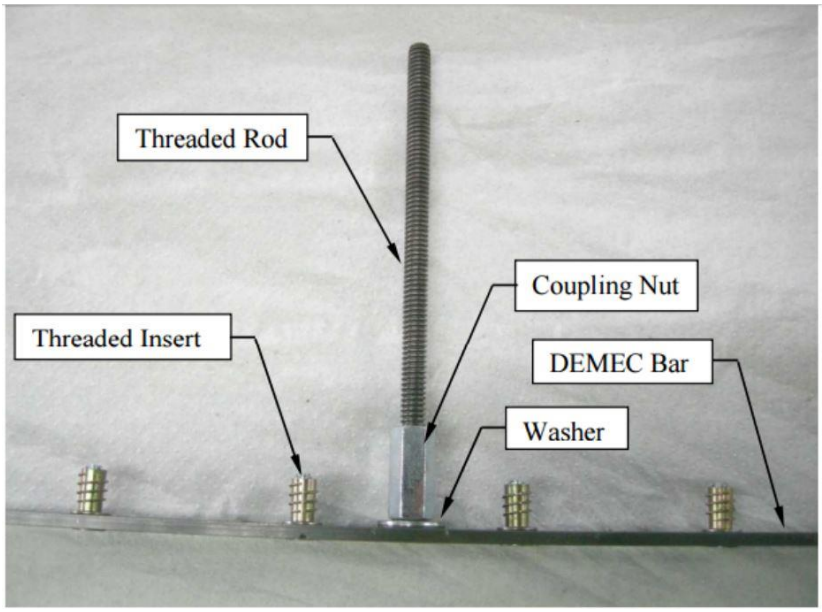

Figure 2-23 Cast-in-place DEMEC mounting system (Dunham, 2011)

Figure 2-24 Installation of the DEMEC target screws (Dunham, 2011)

The transfer lengths were measured immediately after prestress release, and at 7 days, 14 days, and 28 days after prestress release. The transfer lengths were acquired through the use of an analog DEMEC strain gauge and the DEMEC target screws. The distance between each DEMEC

target screw was measured before prestress release, and the subsequent measurements were compared to the initial values to represent a change in distance between the points over time. The change in distance value between each point was converted into a change in strain. These values were then averaged with the values from the surrounding target screws to produce a smoother trend line. To eliminate the effect of the skew at the girder ends, the transfer length on both faces of the girder were measured and averaged together. Finally, the transfer lengths were reported by plotting the measured change in strain vs. the distance from the girder end of the central point between the target screws. The transfer lengths were determined by calculating the distance between the girder edge and the point along the girder length at which 95% of the average maximum strain (AMS) was measured. An example strain profile with the transfer lengths marked can be seen in Figure 2-25.

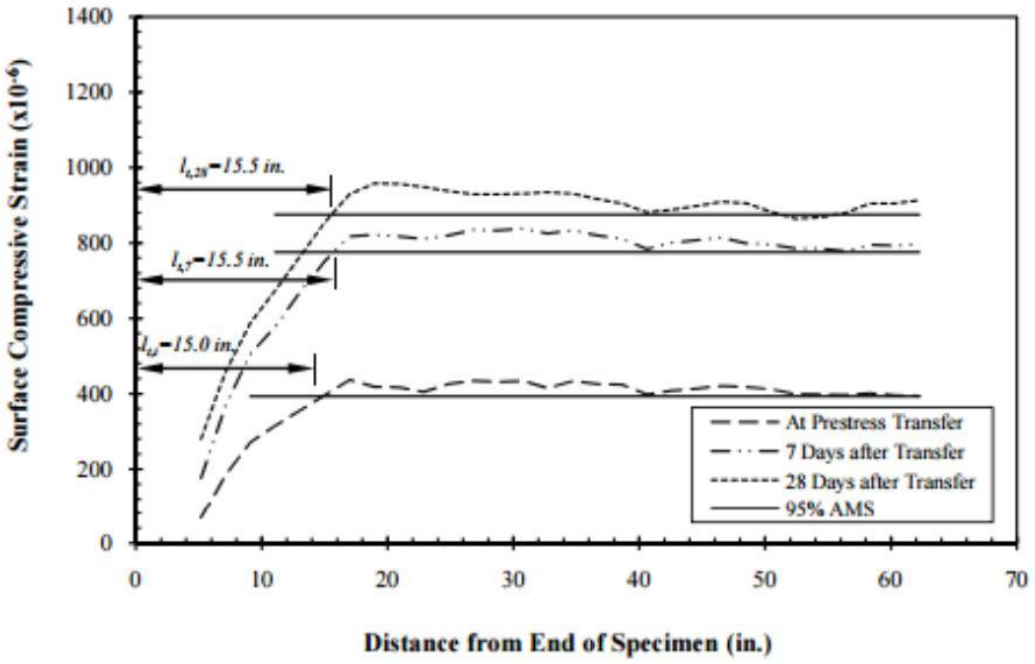

Figure 2-25 Determination of transfer length and 95%AMS (Dunham, 2011)

The transfer lengths were found and compared for several variables including: Concrete mixture, strand diameter, end of girder from which concrete was first poured, strand debonding, mark end vs. opposite end, and time since prestress release. The transfer lengths measured from the fully bonded strands at end A (mark end) and end B (non-marked end) are shown in Table 2-3.

Table 2-3 Summary of Transfer Length Results for Fully Bonded Strands (Dunham, 2011)

						End A			End B		
Concrete	Depth (in.)	Girder ID	f'_{ci} (psi)	f_{pj} (ksi)	f_{pt} (ksi)	Initial (in.)	7-Day (in.)	28-Day (in.)	Initial (in.)	7-Day (in.)	28-Day (in.)
SCC	54	2S	9010	202.5	190	15.0	15.5	15.5	15.5	17.5	17.0
		4S	8680	202.5	190	20.0	19.0	20.5	14.0	15.0	15.5
		7S	8760	202.5	190	14.0	16.0	16.5	9.5	10.5	10.0
	72	2S	8220	202.4	188	16.0	17.5	17.5	14.5	19.0	17.0
		4S	7860	202.4	188	9.5	12.0	13.5	18.0	19.0	20.0
		7S	8120	202.4	188	9.0	9.5	9.0	20.0	19.5	18.5
CVC	54	8C	7940	202.5	190	9.0	12.0	11.5	15.0	19.0	17.0
		11C	7860	202.5	190	10.0	10.5	12.0	12.5	13.5	14.5
		13C	8790	202.5	190	9.0	12.0	11.0	12.0	14.5	14.0
	72	8C	8290	202.4	190	11.0	13.0	15.0	11.0	13.5	15.0
		11C	8320	202.4	190	10.5	13.0	14.0	9.0	11.5	11.5
		13C	8770	202.4	190	7.5	9.0	10.0	12.5	16.0	16.0

As a result of the transfer length test program, the following relevant conclusions were reported:

- Transfer lengths grow in length for weeks after prestress release. A significant amount of this growth occurs between prestress release and seven-days after prestress release.
- Since transfer lengths grow up to 18 percent over the course of 28 days, initial transfer length measurements cannot solely determine long-term transfer lengths.
- Transfer lengths in CVC grows more over time than in SCC.
- Transfer lengths of partially debonded strands grow less over time than those of fully bonded strands.

- Although strands with partial debonding have shorter transfer lengths than those of fully bonded strands, there is no reason to adjust the code provisions for these partially debonded strands since they are not subject to cracking.
- SCC girders produced transfer lengths 20 percent and 18 larger than CVC girders for fully bonded and debonded strands, respectively.
- No apparent correlation was found to describe how much longer transfer lengths are in SCC than in CVC. Though larger cross sections seemed to produce longer transfer length differences between SCC and CVC.
- No significant difference was found in transfer lengths between girders with different strand diameter.
- The additional transfer length associated with SCC in the study was not enough to produce non-conservative transfer lengths when compared to code predictions.
- Both ACI and AASHTO recommended equations were conservative but inaccurate for high-strength concrete. Previous research was reported to show that these codes produce non-conservative values for transfer length in lower-strength concretes.

Chapter 3 Design and Finite Element Modeling of the BT-78

3.1. Introduction

The purpose of this study was to develop an optimal design for a 78 in. bulb-tee girder with a span of 180 ft and a minimal potential for end zone cracking. As a result of goal it was necessary to use higher-order analysis tools to understand the effect of various factors on end zone cracking as well as to determine possible solutions. After an in-depth literature review on current analysis methods for girder end zones, the research team decided upon the use of non-linear finite element modeling for the girder analyses and design optimizations. The objectives for the preliminary design and analysis phases of this study are as follows:

- Design and analyze a prestressed girder which spans 180 ft and conforms to current AASHTO specifications.
- Develop a non-linear finite element model (FEM) to explore the end zone behavior.
- Understand the effect of various factors on end zone cracking and propose optimized test specimens.
- Analyze and verify the design of test specimen spanning 54 ft.
- Identify optimal positions for the placement of strain gauges in test specimens using FEM.
- Analyze and correlate field data to verify the validity of FEM.
- Perform a parametric analysis to understand the effects of various modeling assumptions on the FEM.

3.2. Preliminary Design of the BT-78

The design for the new girder section was chosen for its structural efficiency and relative ease of construction. The formwork for the BT-78 was easily produced by using modified BT-74 formwork which was readily available at the precast yard from past ALDOT projects. The section was designed with 66 strands, 22 of which were draped. 4 strands in the top flange were tensioned to 8 kips of force. These strands are not included in the total force reported in Table 3-2. Using a bearing-to bearing span of 178.25 ft, the BT-78 girder was designed for a bridge with the parameters shown in Table 3-1. The section properties of the girder are shown in Table 3-2. Cross section details can be found in Chapter 4.

A moment curvature analysis was performed for the full-span BT-78 section at 1 ft intervals along the length of the girder. The maximum service level demand is 10,646 kip-ft, or roughly 90 percent of the 11,694 kip-ft available cracking moment capacity. The maximum factored load demand is 14,673 kip-ft, or about 65 percent of the 22,442 kip-ft available nominal moment capacity. The calculated shear demand is 398 kips while the assumed total nominal shear capacity is 1022 kips. The shear and moment demand vs. capacity graphs are shown in Figure 3-1 BT-78 moment demand vs. capacity and Figure 3-2. The top and bottom stresses can be seen in Figure 3-3. The girder was designed for zero tensile stresses in the top fibers at release.

The preliminary design of the BT-78 was used as the control specimen throughout the project and will be referred to as the "standard design" in later chapters. This design serves as a starting point for all other end zone modifications proposed in this study. Further specifications of the BT-78 can be found in Chapter 4.

Table 3-1 Bridge Design Parameters

Overall width (ft)	30.42
Curb-to-curb width (ft)	28
Number of lanes	2
Lane width (ft)	12
Effective deck thickness (in.)	7
Bridge cross section moment of inertia (in^4)	6,974,849
Bridge Design Loading	HL-93
Girder Spacing (ft)	6

Table 3-2 BT-78 Section Properties

Area of section	$\mathbf{A_c}$	=	1,049	in^2
Center of gravity in x-direction	$\mathbf{CG_X}$	=	13.5	in
Center of gravity in y-direction	$\mathbf{CG_Y}$	=	41.2	in
Moment of inertia about CG_X	$\mathbf{I_c}$	=	67,829	in^4
Height of section	**D**	=	78	in
Section modulus at top fiber	$\mathbf{S^t}$	=	23,555	in^3
Section modulus at bottom fiber	$\mathbf{S_b}$	=	21,086	in^3
Radius of gyration of the section	$\mathbf{r^2}$	=	827.29	in^2
Design 28-day strength	$\mathbf{f_c'}$	=	10,000	psi
Compressive strength at release	$\mathbf{f_{ci}'}$	=	8,500	psi
Number of prestressing strands		=	66	
Area of prestressing strands	$\mathbf{A_p}$	=	14.32	in^2
Total force in strands	$\mathbf{P_i}$	=	2,932,172	lbs
Young's modulus of strands	$\mathbf{E_{ps}}$	=	28,500,000	psi
Ultimate strength of strands	$\mathbf{f_s'}$	=	270,000	psi
Yield strength of strands	$\mathbf{f_{py}}$	=	243,000	psi
Weight of concrete	**W**	=	150	lb/ft^3
$E = w^{1.5}33\sqrt{f_{ci}'}$	$\mathbf{E_{ci}}$	=	89,337	psi

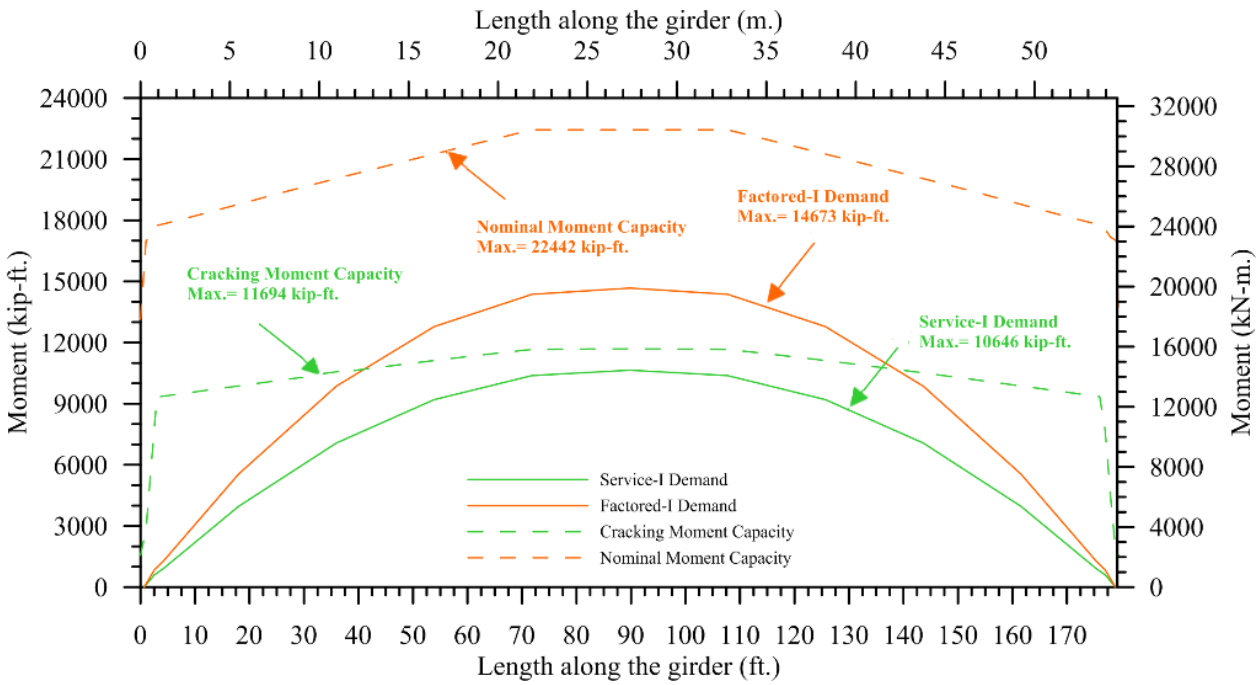

Figure 3-1 BT-78 moment demand vs. capacity

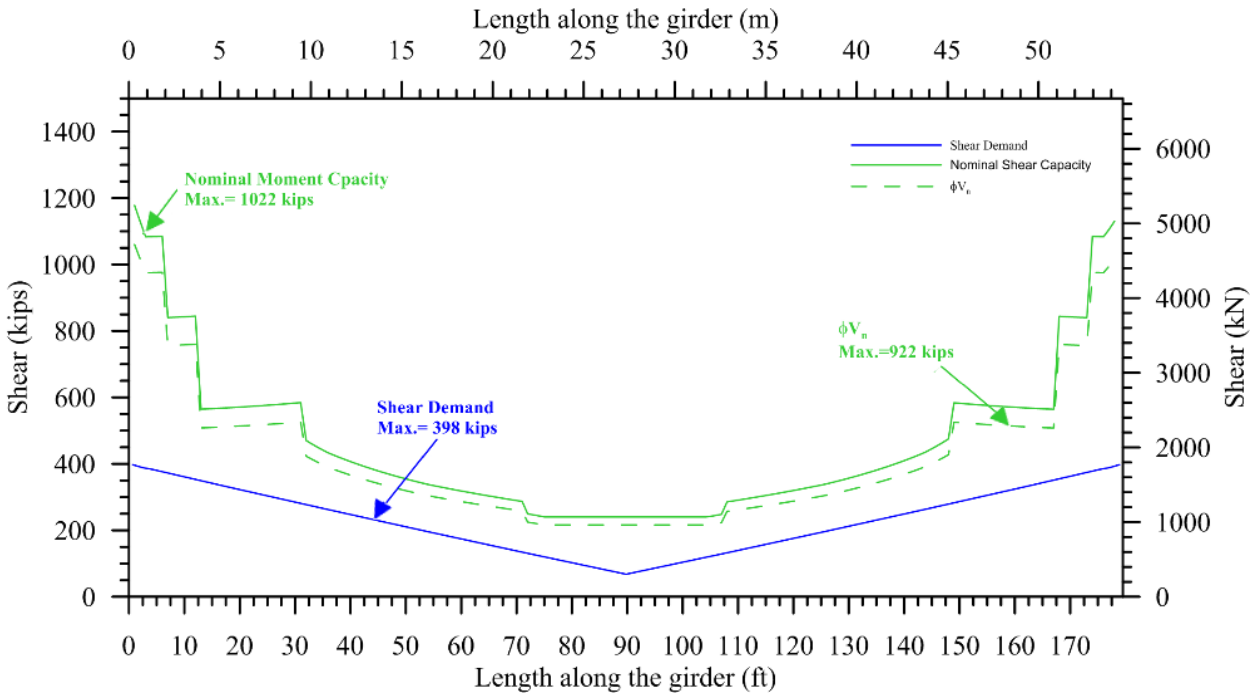

Figure 3-2 BT-78 shear demand vs. capactiy

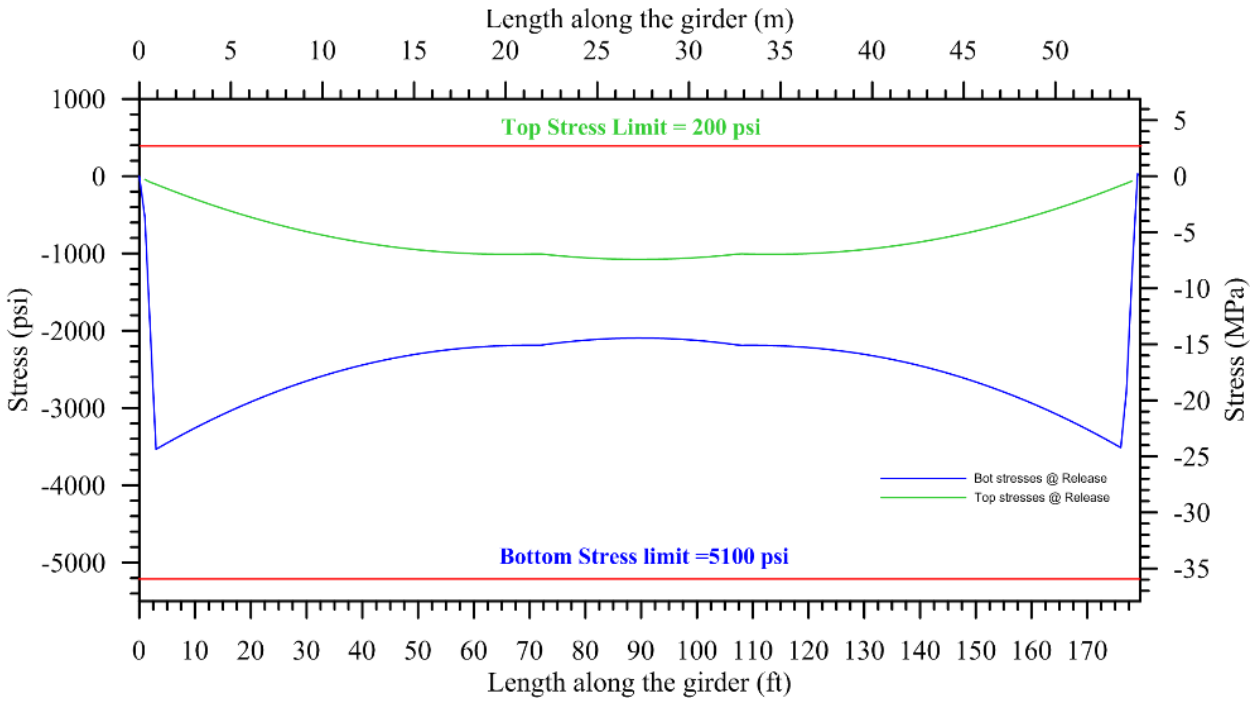

Figure 3-3 BT-78 top and bottom stresses

3.3. Finite Element Model Properties

Finite element analysis software called Abaqus (version 6.12) was used in this study. Abaqus was developed by Dassault Systems for the simulation of a wide variety of material models under various physical conditions (Dassault Systèmes Simulia Corporation, 2012). The software's capabilities include material non-linearity, simultaneous loading conditions, and various boundary conditions. For the purpose of modeling end zone cracking in prestressed concrete girders, the ability to model elements with material non-linearity, such as concrete, is a necessity. Furthermore, the simultaneous loading of prestressing strands and girder self-weight during prestress transfer demonstrate the need for a model capable of simulating multiple loading conditions

The FEM is able to approximate physical reality of prestressed girder end zones only when realistic constraints are applied and considerations are taken to include the non-linear behavior of models. The post-cracking behavior of concrete induces a redistribution of stresses from the concrete to the reinforcement elements and results in a loss of stiffness in the concrete. These factors were taken into consideration in this study particularly through the use of a material model packaged within the Abaqus software referred to as the concrete damaged plasticity model. This model is intended for general purpose modeling of concrete and can account for non-linear behavior in both the tension and the compression of concrete. It also provides a sufficiently high degree of accuracy and the ability to visualize maximum principle strain vectors across node points within the model. To some degree, this model is also able to account for effects related to the steel-concrete interface such as dowel action and bond slip. Consequentially, the damaged plasticity model was used for the FEM in this study.

The material model used in this study adopted concrete with compressive elastic behavior corresponding to the values provided in ACI 318-14. For the concrete inelastic region the model determines behavior through a plasticity model defined by the input parameters of yield criterion, the hardening/softening rule, and the flow rule. Concrete tensile behavior corresponds to the ACI 318-14 tensile stress limits of concrete. The reinforcing bars were modeled as a linear elastic material with an elastic modulus of 29,000 ksi and a Poisson's ratio of 0.3. The use of non-linear material properties for reinforcing bars would have resulted in a decreased computational efficiency without much gain in accuracy. The effect of the prestressing strands was applied as surface traction along the transfer length, or $60d_b$, as recommended by AASHTO (2015).

By definition, the behavior of large objects are simulated in FEM software through the modeling of a combination of miniscule elements. These elements can vary in size and shape, and

some enable greater computational cost efficiency than others. For the purpose of modeling the concrete, solid (continuum) elements were used in this study. Two examples of these elements are provided in Figure 3-4. The tetrahedral element has advantages in modeling irregular geometric patterns, such as draped strands. The hexahedral element provides more volume at a low computational cost.

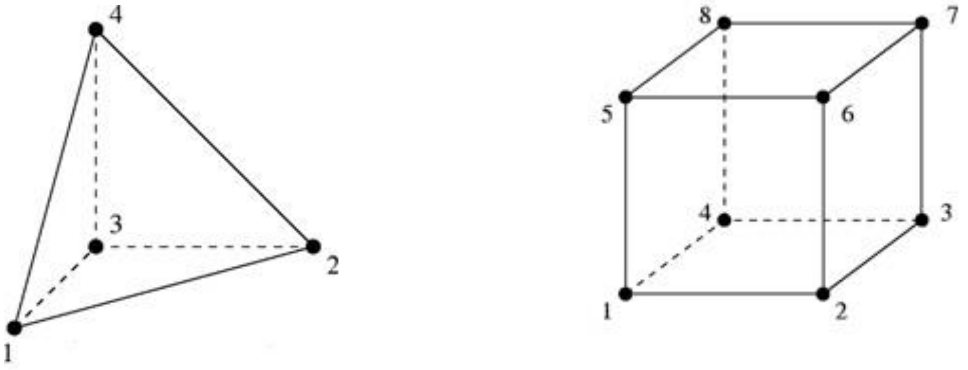

a) Tetrahedral element used in the end zone region **b) Hexahedral element used outside of the end-zonoe region**

Figure 3-4 Abaqus solid elements used in FEM

The steel reinforcement was modeled using truss elements. It was believed by the research team that beam elements would have negatively impacted the computational efficiency without significantly enhancing the accuracy of the model.

3.3.1. Analysis Model for a Typical Prestressed Girder

Within the context of this study, the modeling of prestressed girders was enhanced through the use of symmetry and mesh zones. The symmetry of the BT-78 allowed for the model to be divided in half at both the span centerline and the cross sectional centerline. This allowed the model to be one-fourth of the full beam size. Secondly, mesh zones enabled the girders to be modeled with greater accuracy in areas of interest while other areas were modeled with less accuracy to reduce computational cost. The end zone of the girder was modeled with a very fine

mesh which produces a very accurate model. This zone extended a length equal to 60 times the diameter of the strand. An adjacent area, named "End Zone 2" in Figure 3-5, was modeled with a slightly coarser mesh, and extends the length of two time the grider height for the purpose of observing propagated cracks. The final zone, "Zone 3", was modeled with a coarser mesh with material properties limited to the elastic range since cracks were not expected in this zone.

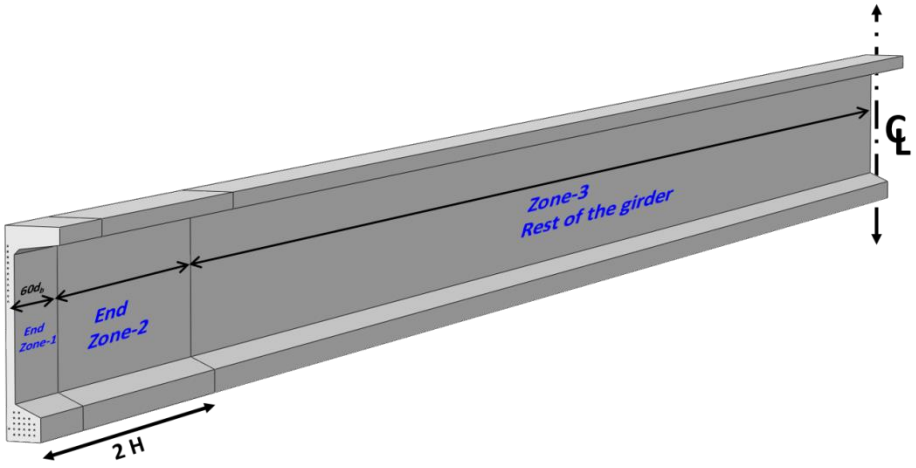

Figure 3-5 Abaqus model with mesh zones marked

A typical girder model in the FEM contains two layers: a strain contour and principle strain vectors. The strain contours, shown on the model in Figure 3-6, represent strain intervals on the girder surface. Although the cracking within these contours is impossible to locate, the contours serve as a general area in which strains in the concrete are more likely to produce cracks. The principle strain vectors show the magnitude and direction in which the cracking is likely to occur. A series of parallel vectors represents the potential location and orientation of cracks. Cracks are predicted to form in a perpendicular orientation to the maximum principal strain vectors.

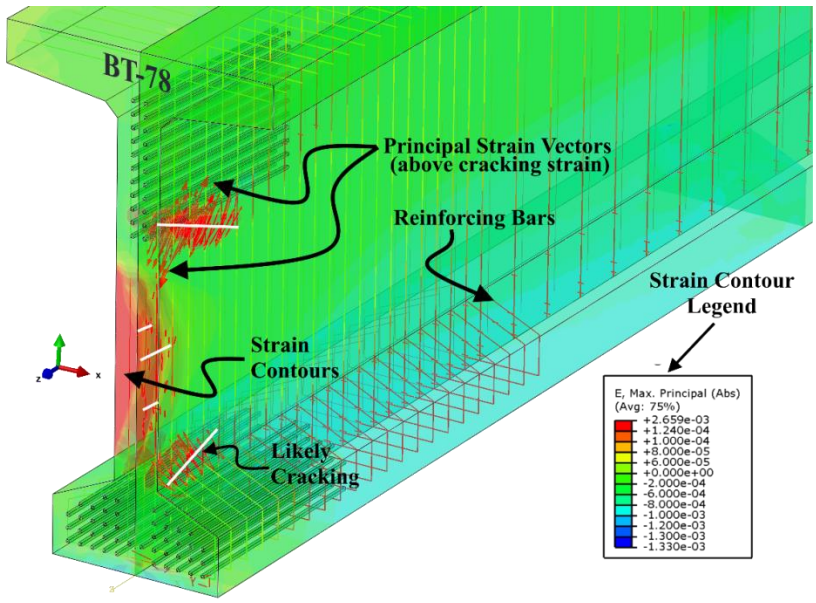

Figure 3-6 Typical girder model in the FEM

3.3.2. Calibration of the FEM

The Abaqus model was verified through the creation of models for several similar girder for which both the design specifications and the end zone crack locations after prestress were known. The Washington WF100G girder (Arab A. , et al., 2014) and the Virginia PCEF 95.5 girder were used for calibration. The results of the WF100G model and a photograph of the corresponding end zone cracks can be seen in Figure 3-7.

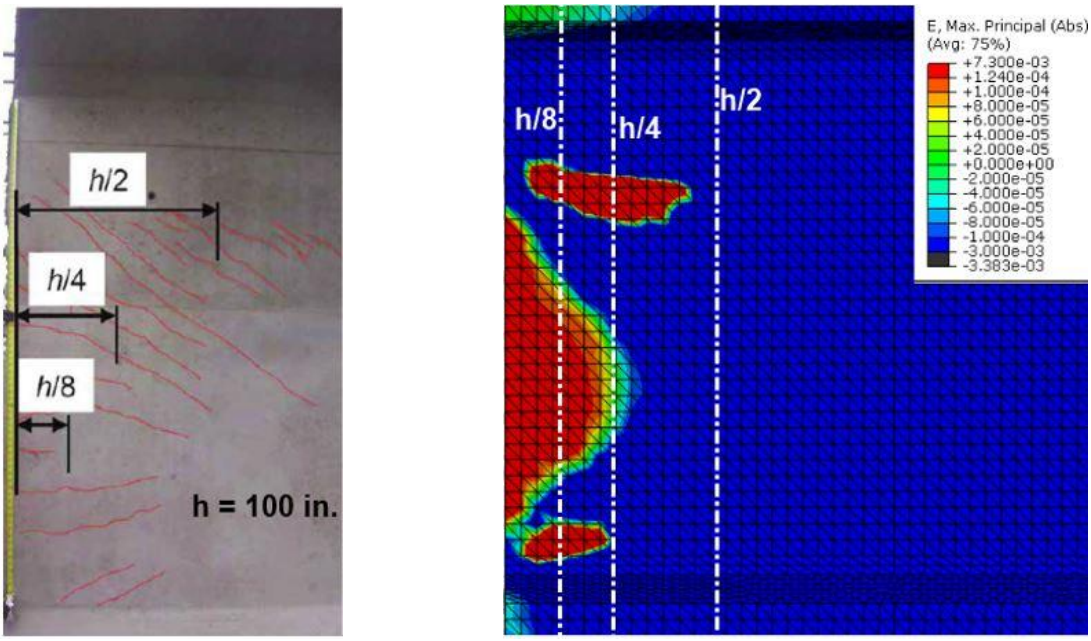

a) WF100G cracks **b) WF100G modeled in Abaqus**

Figure 3-7 Comparison of WF100G end zone cracks with Abaqus model

3.3.3. Modeling the BT-72

The addition of horizontal reinforcement to the end zone is a prescribed method used by ALDOT to control the cracks in the end zones of BT-72 girders. The horizontal reinforcement in the BT-72 girders includes four pairs of #5 bars spaced at 4 in. vertically in the lower section of the web beginning one ft above the bottom of the girder. These reinforcement bars extend 5 ft from the girder end. The effect of these bars on controlling end zone cracking was investigated. The results of this investigation are presented in Figure 3-8. The resulting strain contours of the BT-72 show no clear reduction of principle strains in the model containing the horizontal reinforcement. As a result of this investigation, horizontal bars were not used to control cracking in any of the BT-78 models.

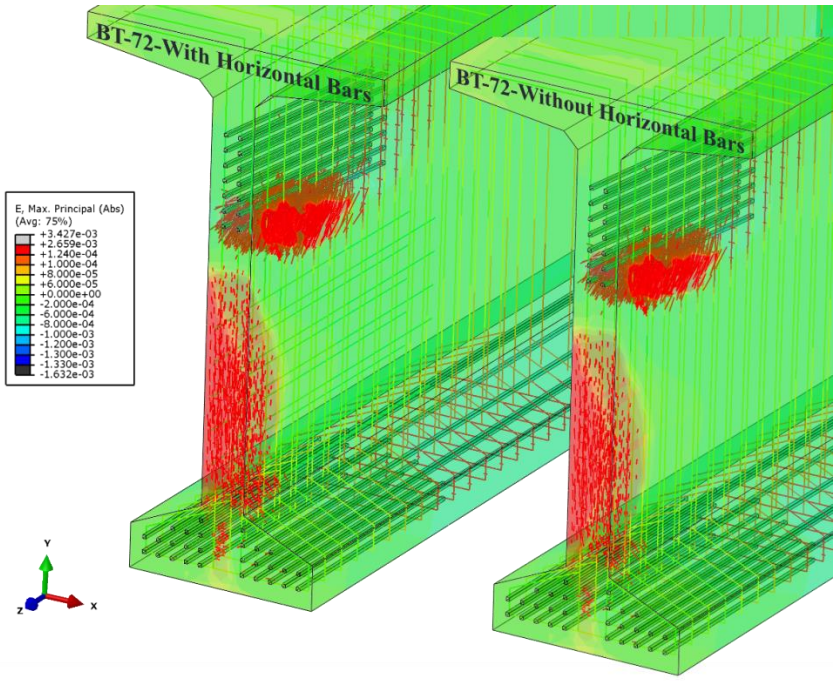

Figure 3-8 FEM comparison of BT-72 with and without horizontal reinforcement

3.4. Modeling the BT-78

The full-span BT-78 was modeled using the FEM. The standard design resulted in a large strain contour around the web and underneath the draped strands. The results of the standard design can be seen in Figure 3-9a. Several end zone modifications were investigated using the Abaqus model: Strand draping, debonding, a combination of draping and debonding, and increased vertical reinforcement. The modifications are discussed in the following sections.

3.4.1. Additional Vertical Reinforcement

The increased vertical reinforcement end zone modification consisted of larger reinforcement at smaller spacing. Instead of using five #7 bars at 4 in. spacing, the modifications included five #8 bars at 3.25 in. spacing. This increased the amount of steel within the *h*/4 region from 6 in^2 to 7.9 in^2. The results of the FEM with modified vertical reinforcement

produced the results shown in Figure 3-9b. As can be seen in the figure, the addition of #8 bars to the end zone produced similar results to the standard design. Since the results suggest only a minimal reduction in principal strains in the end zone, the vertical reinforcement modification was abandoned and other alternatives were explored.

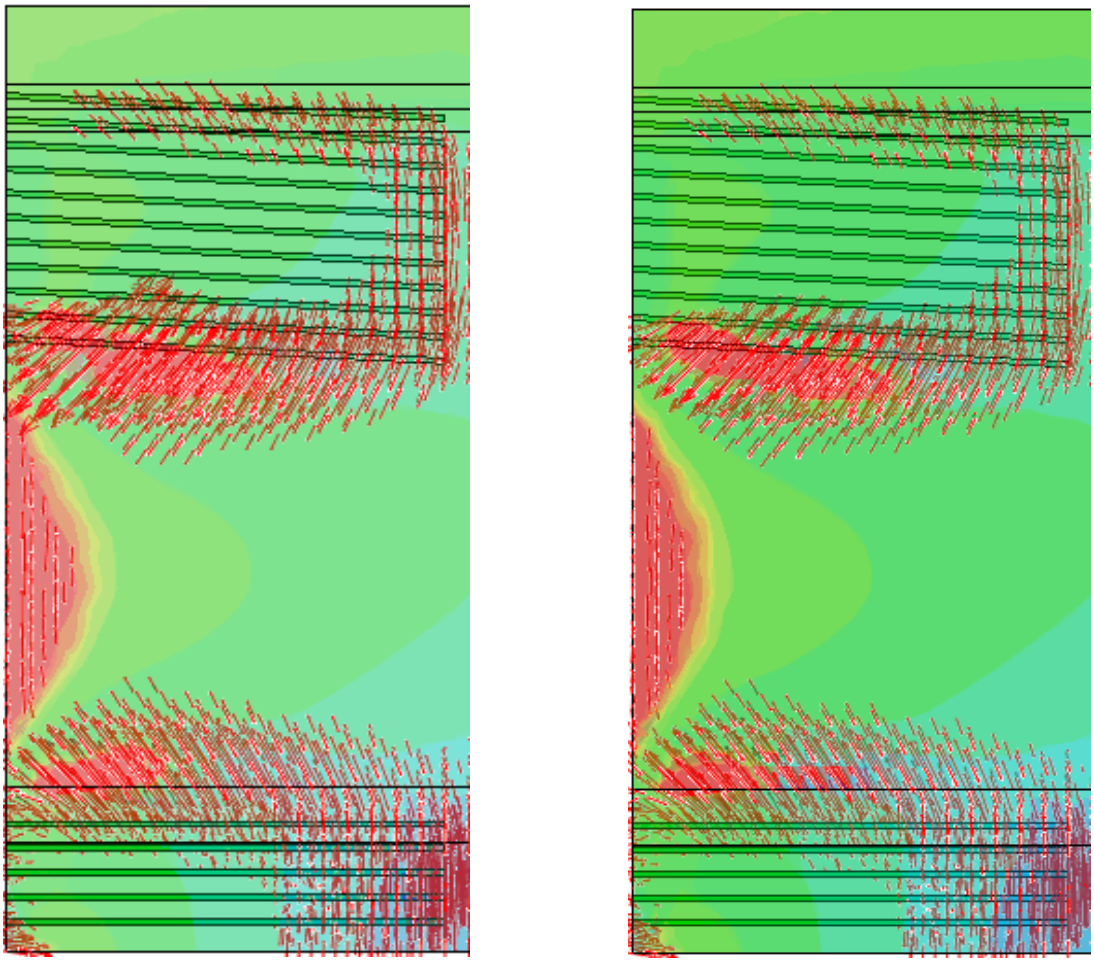

a) Standard design **b) Modified vertical reinforcement**

Figure 3-9 FEM comparison of standard design and modified vertical reinforcement

3.4.2. Partial Debonding

The next end zone modification investigated included partial debonding of strands. Twelve of the strands in the bottom flange of the BT-78 were debonded at varying lengths of 5, 10, and 15

ft. The specifications of this design can be seen in Chapter 4. The results of the BT-78 FEM with partial debonding produced a reduced area of strain around the web. The area under the draped strands contained a lower amount of principle strain vectors than the standard design. The BT-78 with standard draping and partial debonding can be seen in Figure 3-10.

3.4.3. Lower Draping

The effect of a lower draping angle on the BT-78 was studied. The draping was lowered 14 in. at the girder end for a total decrease in the draping angle from 2.9 degrees to 1.7 degrees. The results of the FEM with the lower draping angle produced a concentration of principle stresses at a lower elevation below the draped strands. The BT-78 FEM with lower draping can be seen in Figure 3-10.

3.4.4. Lower Draping and Partial Debonding

An FEM was created for an end zone modification which included the combination of a lower draping angle and partial debonding. The combination of the two modifications produced the lowest concentration of principle stresses of the four designs. The resulting model showed a reduction in strains in the web and below the draped strands. The BT-78 model with lower draping and partial debonding can be seen in Figure 3-10.

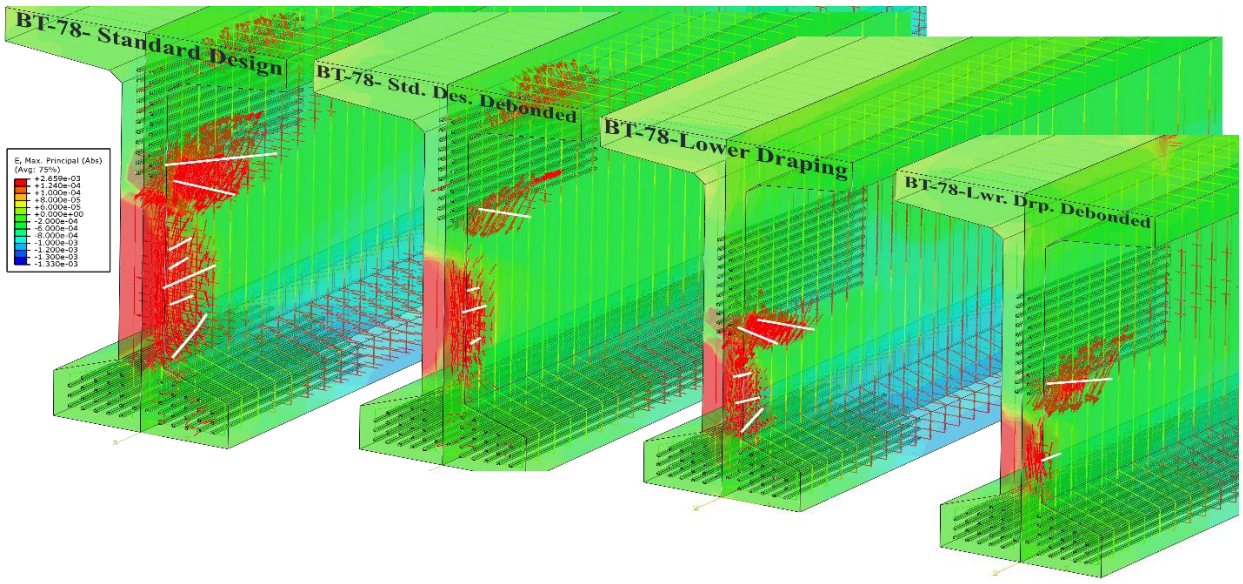

Figure 3-10 FEM comparison of BT-78 girders with end zone modifications

3.5. End Zone Strain Gauge Placement

The models were also useful in determining locations for placement of the internal steel and concrete strain gauges. The research team used the strain contours to determine areas of likely cracking in both the steel and the concrete. Figure 3-11a shows the steel strain gauge placement on top of the local stress contours from the FEM in the end zone reinforcement of Specimen 1 at prestress release. The dark red color on the bars represents the highest levels of stress. Figure 3-11b shows the concrete gauge placement with the principle strain vectors from the FEM of Specimen 1 at prestress release. These locations were similar to locations chosen by Tuan et al (2004), Oliva and Okumus (2011) and Arab et al (2014). The final position of the strain gauges can be viewed in Chapter 4.

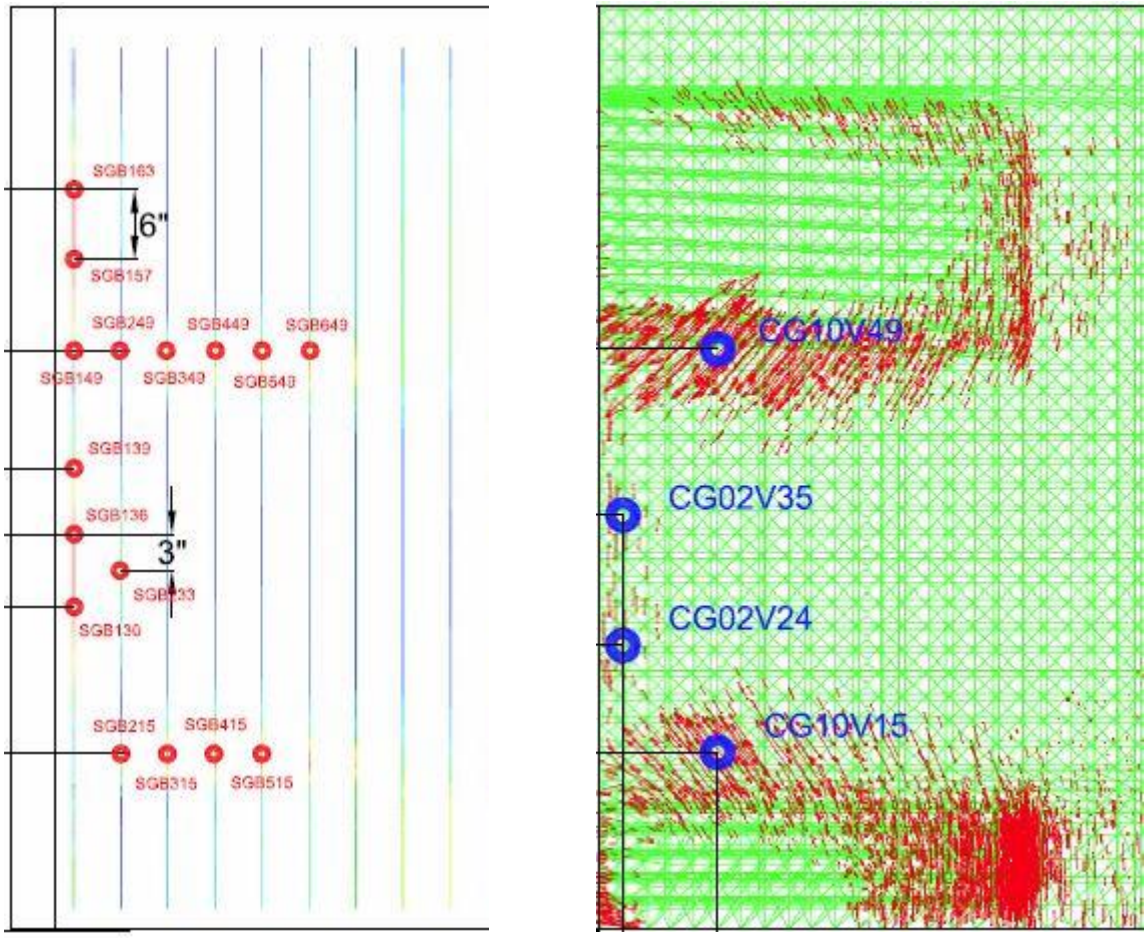

a) Steel strain gauge placement with bar stress contours

a) Concrete strain gauge placement with principle strain vectors

Figure 3-11 Gauge placement based on FEM

3.6. Summary of the Finite Element Analysis Program

The analysis used in this study was for the purpose of predicting likely areas of cracking for potential end zone modifications in the BT-78 girder. The results of this analysis provided the research team with four conclusive BT-78 end zone designs which could ultimately reduce the amount of cracking within the girder ends. The models were also useful in the placement of steel and concrete girders within the end zone. The FEM was a crucial tool in determining the final design of the four specimens to be fabricated.

Chapter 4 Design and Fabrication of Experimental Specimens

4.1. Introduction

The experimental specimens for this study were designed in collaboration with the University of Alabama, Hanson Pipe & Precast, and Alabama Department of Transportation (ALDOT). For the experimental program, a total of four, 78 in. deep, bulb-tee (BT-78) girders were designed with varying configurations of the prestressing strands with the intent of investigating the effect of these modifications on end zone cracking. The four experimental specimens were each 54 foot long and contained a total of 66 – 0.6 in. diameter strands with the following internal strand configurations: (1) 44 straight strands and 22- draped strands with standard draping angle in line with current ALDOT practice (Specimen 1); (2) 44 straight strands with ten strands partially debonded and 22- draped strands with standard draping angle (Specimen 2); (3) 44 straight strands and 22- draped strands with lower draping angle (Specimen 3); and (4) 44 straight strands with ten strands partially debonded and 22- draped strands with lower draping angle (Specimen 4). All specimens were fabricated at Hanson Pipe & Precast in Pelham, Alabama. Specimens 1 and 2 were fabricated during the week of July 27-31, 2015 and Specimens 3 and 4 were fabricated during the week of August 3-7, 2015. A detailed discussion regarding the design, fabrication, and in-field data acquisition of the specimens will be presented in this chapter.

4.2. Specimen Design

A major motivation of the project was to develop a girder detail that can surpass the current span length capabilities of standard ALDOT BT girders. In the past, ALDOT girders have not

typically been produced with spans in excess of 165 ft. The designs for the four specimens were decided upon through the consideration of both the experience of the designers, as well as the results from the detailed 3D finite element model in ABAQUS, as described in Chapter 3. A 78 in. deep, bulb-tee shape was chosen for several reasons. The estimated maximum span length that can be achieved of a BT-78 girder meeting the AASHTO requirements, and with 6 ft center-to-center girder spacing is approximately 180 feet. Furthermore, developing new deep beams is expensive, due to the cost of new formwork for production, the research team chose the deepest beam that a local Alabama fabricator (Hanson Pipe & Precast) could produce with minimal modifications to their existing formwork. The precast fabricator was able to economically modify their existing BT-74 formwork by welding 3-inch tubes to the top and adding 1 inch of depth to the bottom of the side forms. For these reasons, the use of the BT-78 was agreed upon and the designs of the individual specimens were then planned.

Although the production span length for the BT-78 girder can reach up to 180 ft, the girder test specimens were limited to a span of 54 ft each, due to restrictions on the weight and length capacities for transportation and testing of the girder in the laboratory. Since the draped portion of the full-length girder was 72 ft-3 in. long, the hold down points were embedded within a central waste block that was cast between the two specimens on the same bed. The profile for the full 180 ft BT-78 girder can be seen in Figure 4-1.

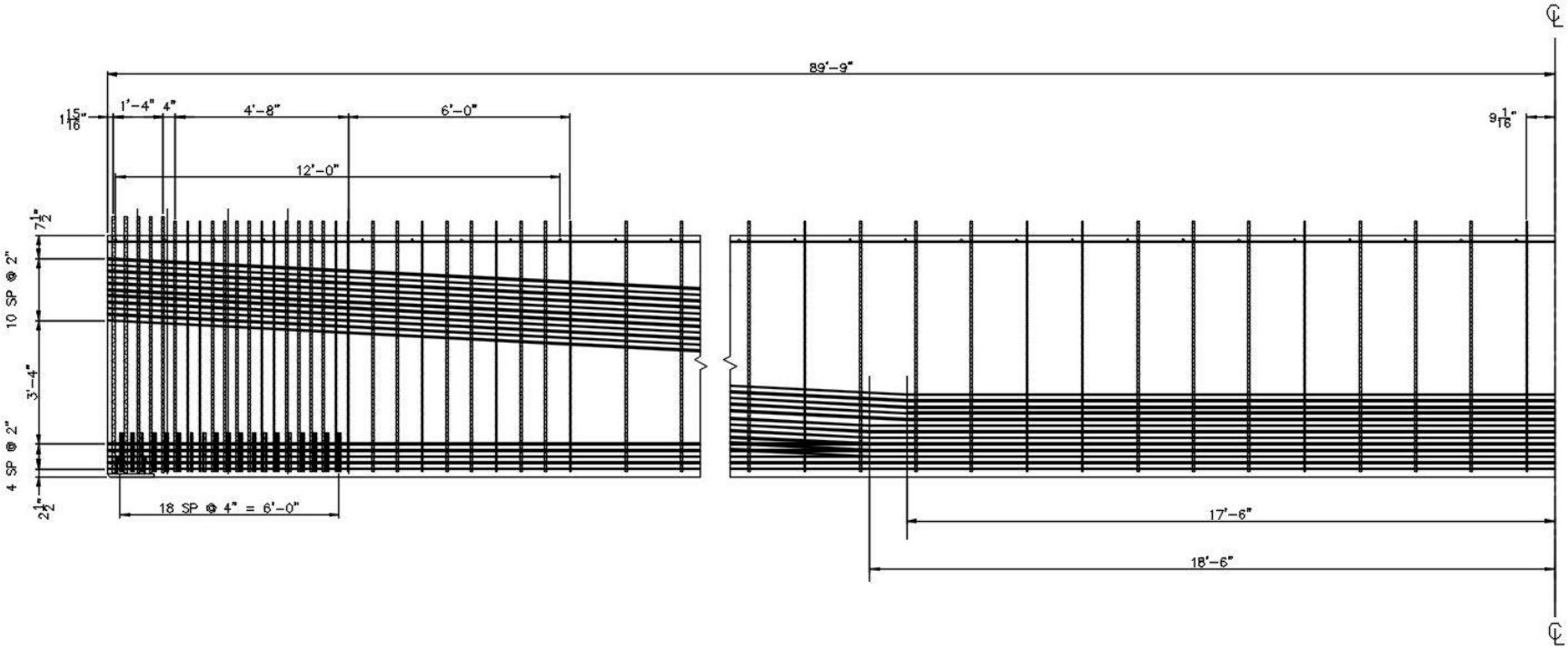

Figure 4-1 Standard design for full-scale BT-78 girder

Specimen 1 and Specimen 2 contained a standard draping angle of 2.9 degrees and were cast together on the same bed. Specimen 3 and 4 contained a lowered draping angle of 1.67 degrees and were cast together on the same bed. Sheathing was added to lower flange strands in Specimens 2 and 4 according to the debonding requirements given in section 5.11.4.3 of AASHTO LRFD Specifications. A summary of different design parameters altered among the four test specimens is shown Table 4-1. The elevation views for the test specimens are shown in Figure 4-2 and Figure 4-3 . The typical cross section dimensions of the BT-78 are shown in Figure 4-4. For simplification purposes, the end of the specimen in which the draping strands area at higher elevation will be referred as the mark end, and the end in which the draping strands are close to the bottom will be referred as the opposite end as shown in Figure 4-1 and Table 4-2.

Table 4-1 Strand Design Comparison

	Specimen 1	Specimen 2	Specimen 3	Specimen 4
Draping Angle	Standard (2.9°)	Standard (2.9°)	Lower (1.67°)	Lower 1.67°)
Debonding	No	Yes (18%)	No	Yes (18%)

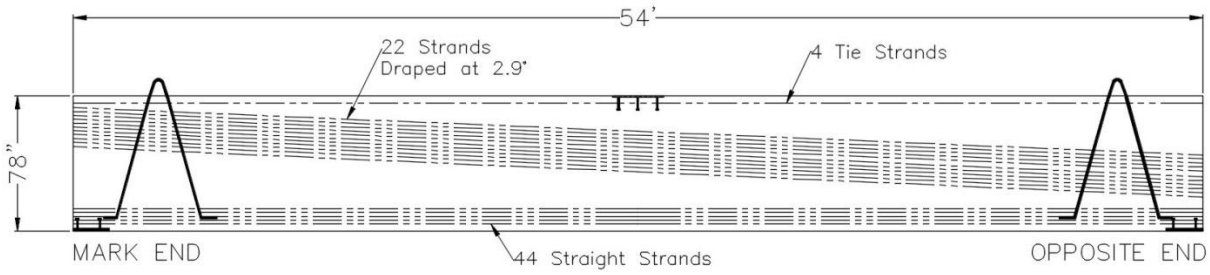

Figure 4-2 Specimen 1 and 2 elevation

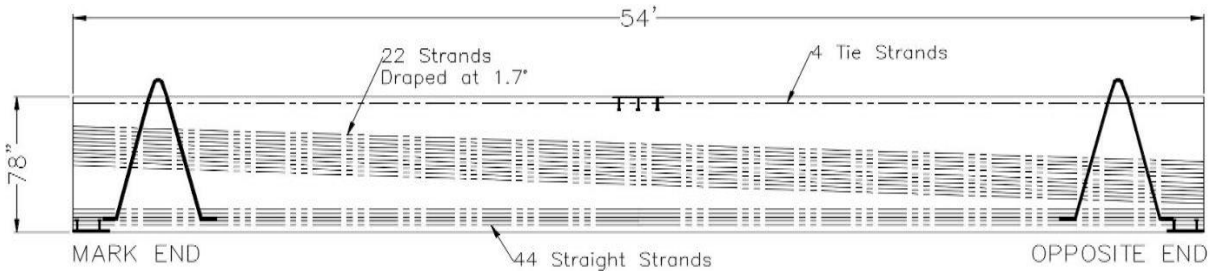

Figure 4-3 Specimen 3 and 4 elevation

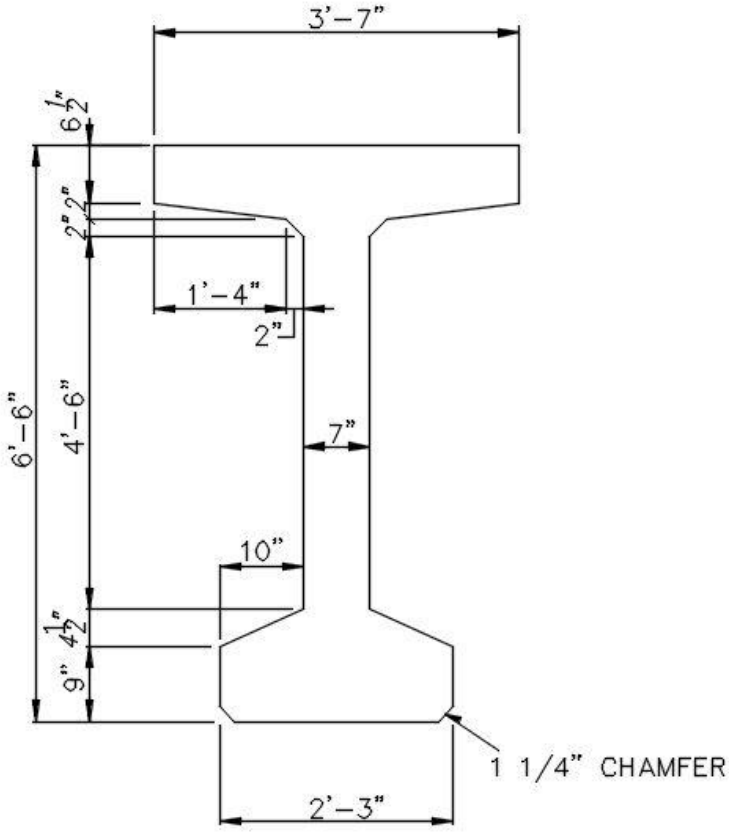

Figure 4-4 Typical BT-78 cross section

4.3. Prestressing Strands

Each girder contained a total of sixty-six 0.6-in. diameter strands, each pre-tensioned to a force varying between 44,500 and 44,900 lbs. Four tie strands, each pre-tensioned to 8,000 lbs, were included in the top flange of the specimens. The prestressing strands were uncoated, low-relaxation, seven-wire steel strands, with a grade of 270 ksi steel. All of the strands for the

specimens were supplied by Sumiden Wire Products Corporation of Dickson, Tennessee. The strands were stored outside and the recommended ALDOT weathering practices for strands used within prestressed concrete girders were followed.

Each girder contained 22 draped strands and 44 straight strands. The draping angle for Specimens 1 and 2 was 2.9 degrees while the draping angle for Specimens 3 and 4 was lowered to 1.67 degrees. For Specimens 2 and 4, 12 of the 66 strands, or 18%, were debonded in a typical "checkerboard" pattern with no more than 40% of the strands in any row being debonded. Furthermore, the debonding was discontinued at 5, 10, or 15 ft, depending on the row in which the debonding was contained. The design of the partial debonding satisfies the conditions presented in AASHTO LRFD Section 5.11.4.3. The total design prestressing force of the 66 strands was 2,977.8 kips. The strand pattern at the girder ends for all the test specimens are shown in Figure 4-5 through Figure 4-8.

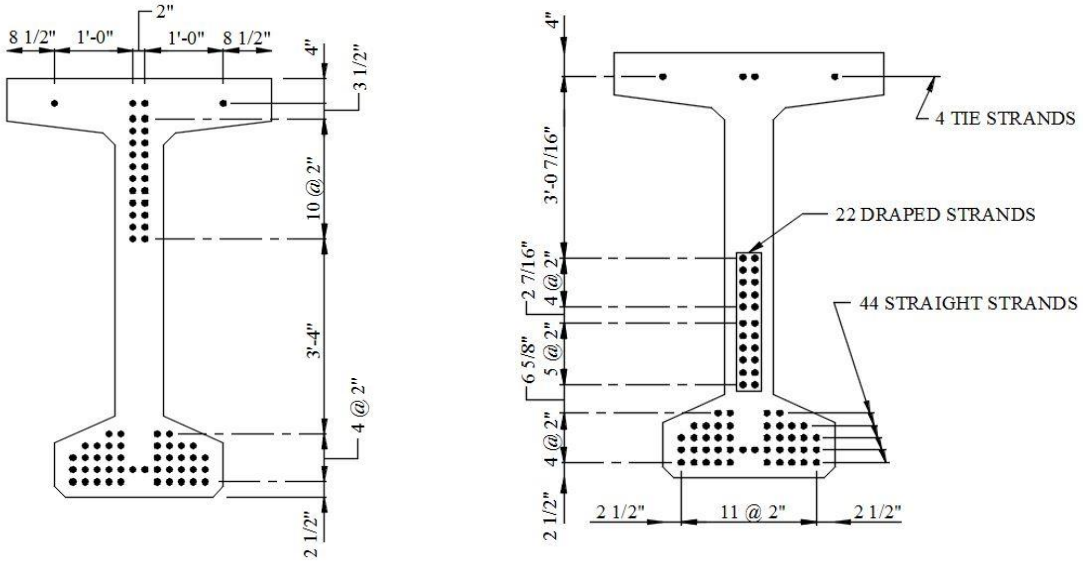

Mark End **Opposite End**

Figure 4-5 Specimen 1 Strand Pattern

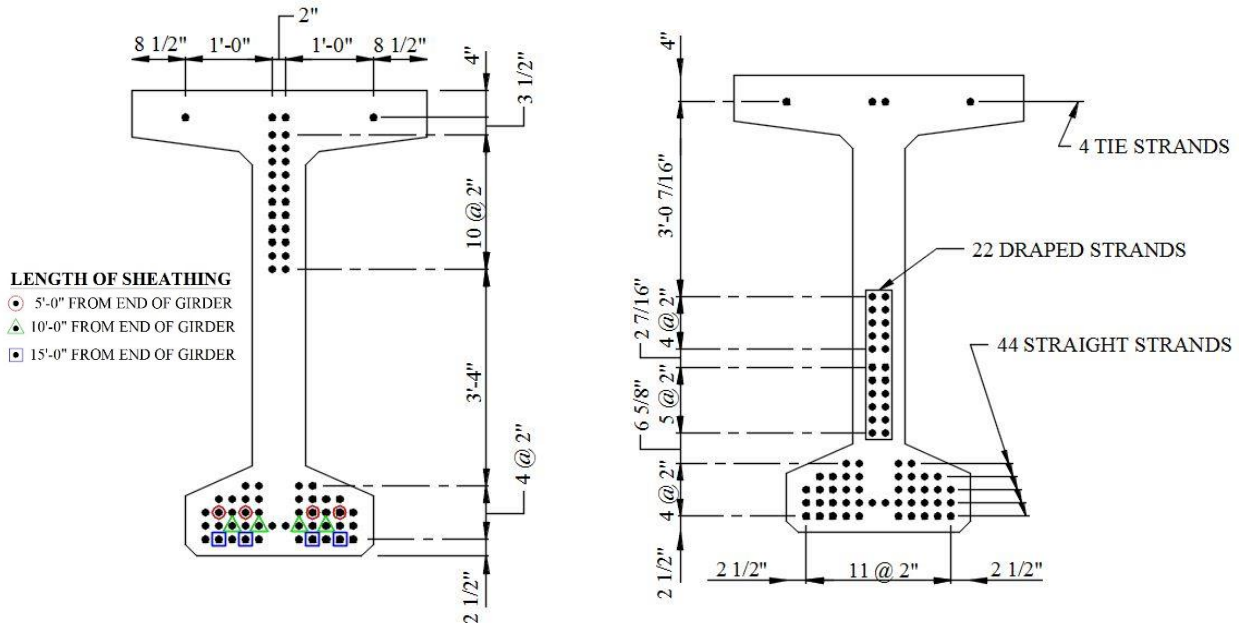

a) Mark End **b) Opposite End**

Figure 4-6 Specimen 2 Strand Pattern

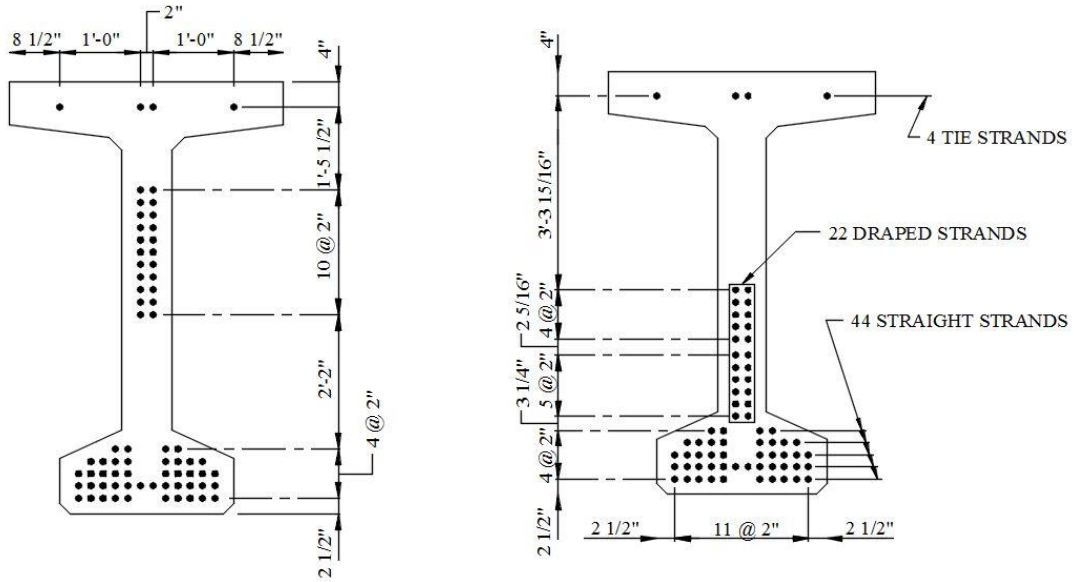

a) Mark End **b) Opposite End**

Figure 4-7 Specimen 3 Strand Pattern

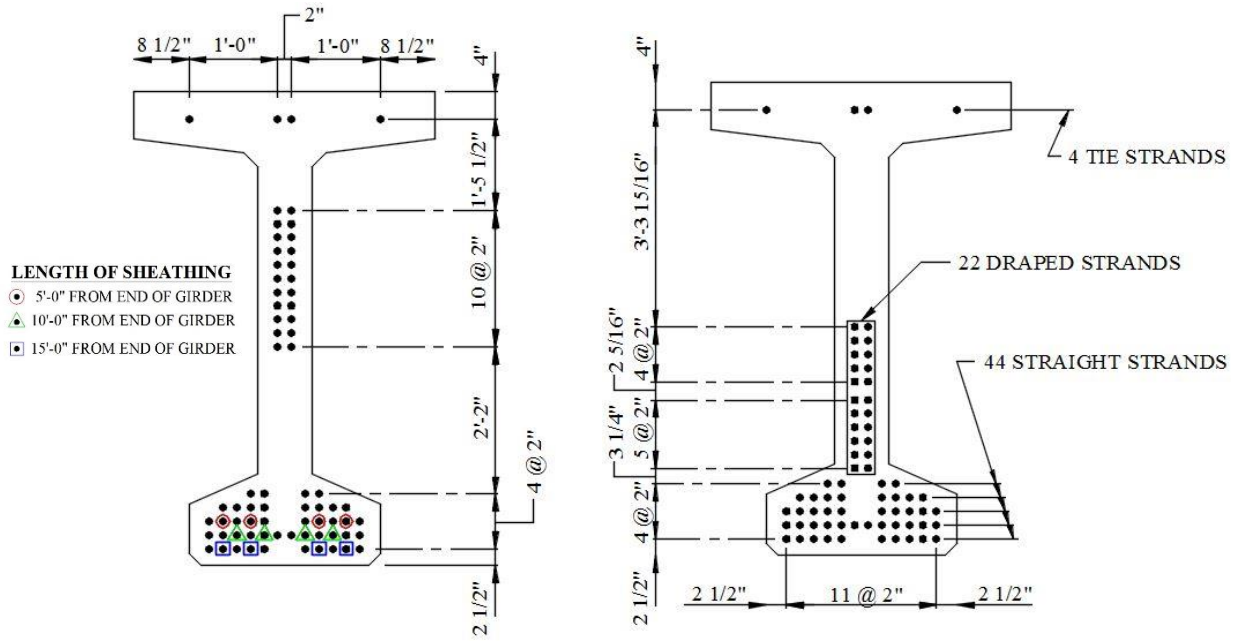

a) Mark End **b) Opposite End**

Figure 4-8 Specimen 4 Strand Pattern

4.3.1. Steel Reinforcement

The steel reinforcement used was consistent for all four test specimens. There were five different types of steel reinforcement used in the specimens including: V#7, V#5, S#8, S#4, and B#3. All reinforcement used was uncoated, grade 60, mild steel. The size of the reinforcement bar is indicated within the label by the numeral following the "#" symbol. For example, V#7 represents a V-bar made from #7 rebar (diameter = 7/8 in.). The pattern of all bars, except the S#8 bars, was symmetric on either side of the mid-span. Each V bar and B bar was tied to a counterpart which faced the opposite direction. The bar shape specifications are shown in Figure 4-9. A 3D model of the prestressing strands and mild reinforcement is shown in Figure 4-10.

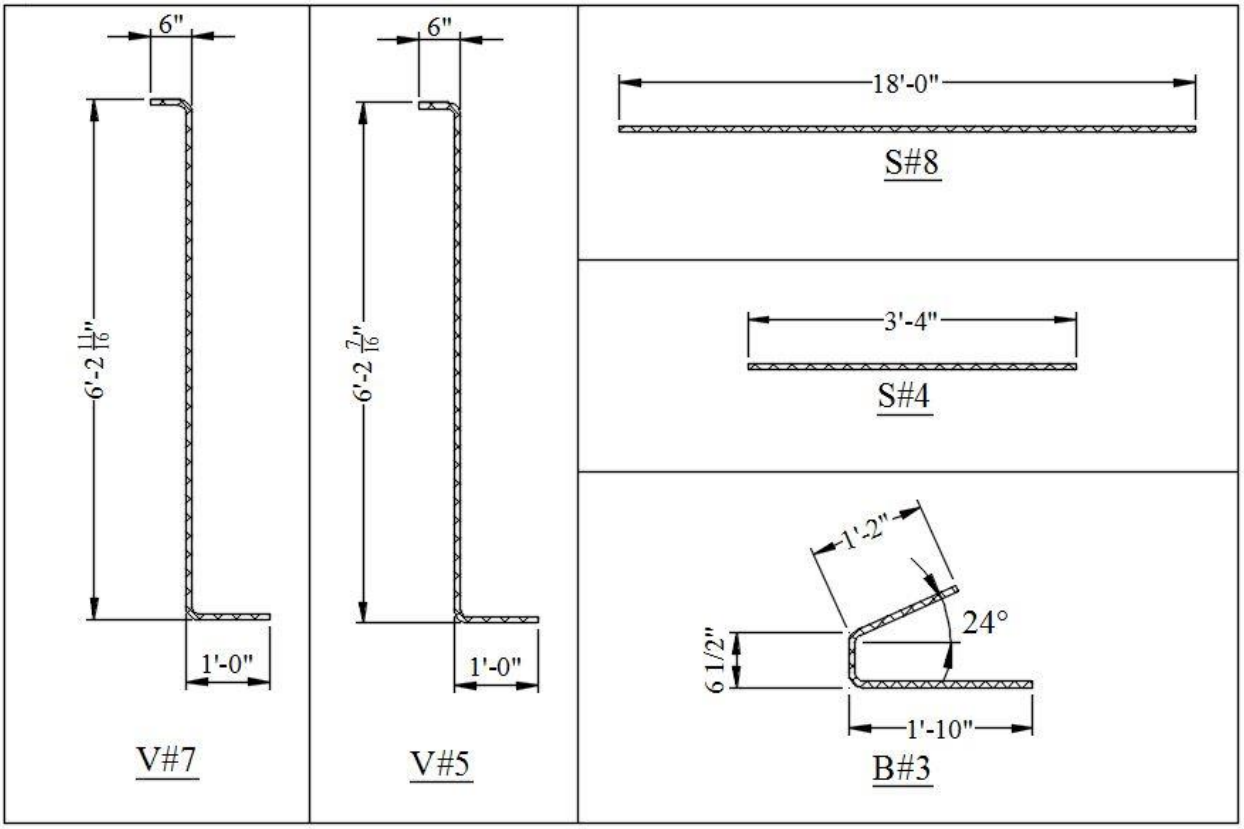

Figure 4-9 Typical reinforcement specifications

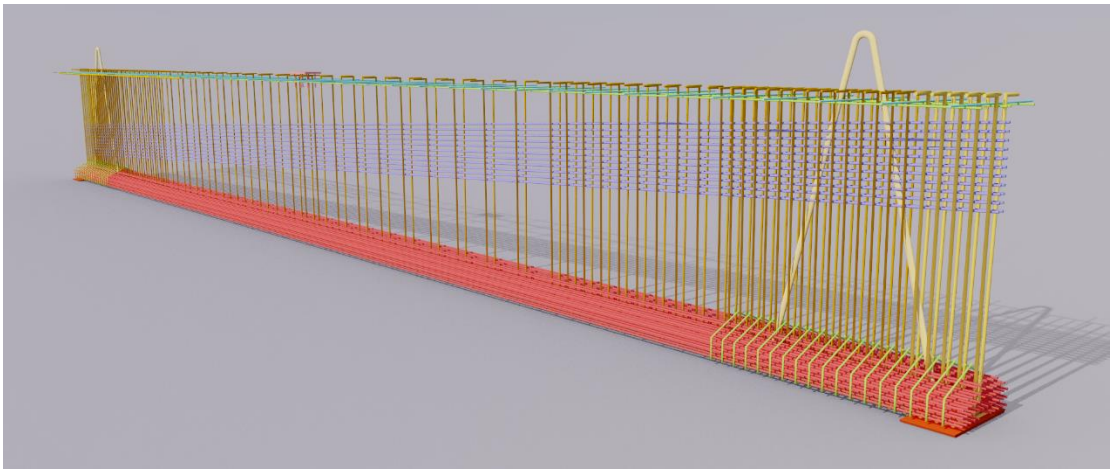

Figure 4-10 Three dimensional model of prestressing and reinforcement

4.3.1.1. Splitting Reinforcement

The V bars were vertically oriented z-shaped bars whose main purpose were resisting splitting but also helped in providing resistance to shear cracking. In accordance with current AASHTO LRFD specifications, five V#7 bars were placed at a spacing of 4 in. on center through the *h*/4 region of the end zone (where *h* is the height of the girder), or the first 19.5 inches. The V#5 bars, were continued at a 4 inch spacing through the rest of the end zone region, or 78 inches from the girder end. The V#5 bars were also used as shear reinforcement at higher spacing throughout the remainder of the girder (from the end zone region to mid-span). For all specimens, the end zone splitting reinforcement was symmetric about the mid-span centerline.

The splitting reinforcement in the end zone adheres to the distribution first recommended by Tuan et al (Tuan 2004). As shown in Table 4-2, 3.6 in^2 of vertical reinforcement, or 60 percent of the AASHTO requirement for *h*/4, is contained within the *h*/8 region.

4.3.1.2. Confinement Reinforcement

As required by current AASHTO guidelines, the strands within the bulb were surrounded with B#3 bars, serving as confining reinforcement through the girder end zone. Two B#3 bars were tied together as a bundle and each bundle was spaced at 4 in. on center through a distance, h, from the girder end. The total area of splitting and confinement reinforcement along the end zone divisions can be seen in Table 4-2.

4.3.1.3. Reinforcement in the Top Flange

The S#4 bars were used in the top flange at a 12 in. spacing for the first 84 in. and at less frequent spacing for the rest of the girder until mid-span. The S#8 bars were used as additional longitudinal reinforcement in the top flange at the opposite end of the test girders. This additional reinforcement was needed to meet the AASHTO tensile stress limit requirements of 200 psi at

prestress release. This condition was a result of the nonconventional configuration of the strands within the test specimens due to the shortened length of the specimen. The lower elevation of the strands at the opposite end created a lower strand eccentricity, which, in result, required more steel in the top flange to resist tensile strains. The calculated tensile stress at the opposite end of the test girder was approximately 380 psi. Four longitudinal bars were placed in the top flange to control cracking in the area around the high tensile zone. This reinforcement was used only to control the tensile stress at the opposite end of the girder and had no effect on the end zone behavior of the mark end. The end zone reinforcement design can be seen in Figure 4-11.

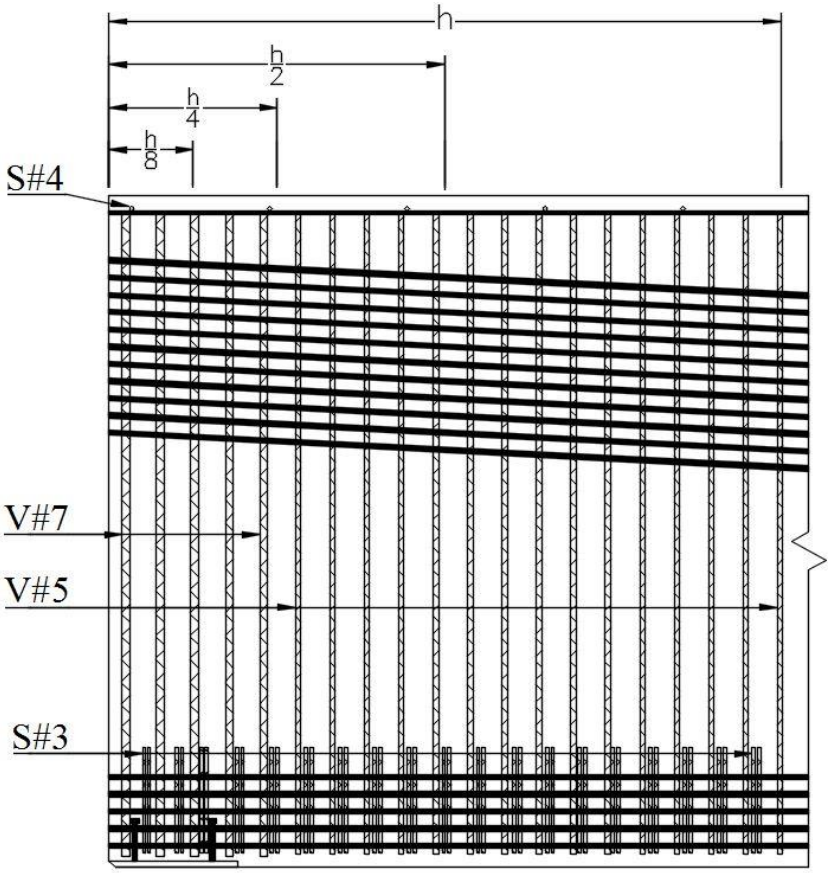

Figure 4-11 End zone reinforcement design

Table 4-2 Area of Steel Reinforcement within End-zone Divisions

	h/8	h/4	h/2	h
Area of Vertical Steel	3.6 in^2	6.0 in^2	9.1 in^2	15.3 in^2
Area of Confinement Steel	0.22 in^2	0.55 in^2	0.99 in^2	1.9 in^2

4.3.2. Concrete Mix

The prototype full-length BT-78 girder was designed with a 10,000 psi SCC mix with a one-day release strength of 8500 psi. The SCC mix design included Type III portland cement, #100 sand from Red Bluff Sand & Gravel in Prattville, Alabama for the fine aggregate and #67 limestone sand from Vulcan Materials Company in Helena, Alabama for the course aggregate. The admixtures included an air entraining admixture (MasterAir AE 90), a Type D hydration controlling admixture (MasterSet DELVO), a Type F high-range water reducing admixture (MasterGlenium 7700), and a Type S viscosity modifying admixture (MasterMatrix VMA), all of which were produced by BASF Admixtures in Cleveland, Ohio. The mineral admixture used was a grade 100 GranCem ground granulated blast-furnace slag admixture produced by Holcim, Inc. in Birmingham, Alabama. The concrete mix design proportions are shown in Table 4-3.

The concrete for all four specimens were mixed in two separate pours. The concrete was mixed at the mixing facility on site at Hanson Pipe & Precast in Pelham, Alabama. The mix design for all four specimens was the same, however weather conditions were different for the two pours.

The weather for the first pour was sunny and the temperature at the time of batching was 96 degrees Fahrenheit. For the second pour, the weather was overcast and the temperature at the time of batching was 86 degrees Fahrenheit. The differences in temperature did not affect any fresh concrete properties. The measured concrete properties are presented in Table 4-4.

Table 4-3 Concrete Mixture Proportions

	Proportions (per cubic yard)
Type III Cement (lb)	782
GGBF Slag (lb)	138
Water (gal)	34.8
Fine Aggregate #100 (lb)	1420
Coarse Aggregate #67 (lb)	1440
Air Entraining Admixture (oz)	1.04
Hydration Controlling Admixture (oz)	18.40
High-range Water-reducing Admixture (oz)	101.2
Viscosity Modifying Admixture (oz)	36.8

Table 4-4 Measured SCC Properties for the Test Specimens

		Specimens 1 and 2	Specimens 3 and 4
Fresh Properties	Spread (in.)	27	27.5
	Visual Stability Index (VSI)	0.5	0.5
	Air (%)	2.9	2.5
	Unit Weight (lbs/ft^3)	148.6	--
Hardened Properties	Release Age (hrs)	17	16
	f'_{ci} (psi)	9,205	8958
	f'_c (psi)	11,639	11,850

4.4. Specimen Fabrication

4.4.1. Casting Configuration of Specimens

The test girders were cast, two at a time, on the same casting bed at the precast plant. Since the test specimens were only segmented versions of the full-length specimens, two test girder specimens were cast at once on a single bed. This casting technique minimized the wastage of prestressing strands and optimized the labor cost for fabrication. Specimens 1 and 2 were cast together during the first week of the pouring since they both contained the standard draping angle. The mark end of Specimen 1 was in the eastern-most position, and the mark end of Specimen 2 was in the western-most position. The following week, Specimens 3 and 4 were cast together on the same bed since they both contained the lower draping angle. The mark end of Specimen 3 was in the eastern-most position, and the mark end of specimen 4 was in the western-most position. The configuration of the girders in the casting bed can be seen in Figure 4-12 and Figure 4-13.

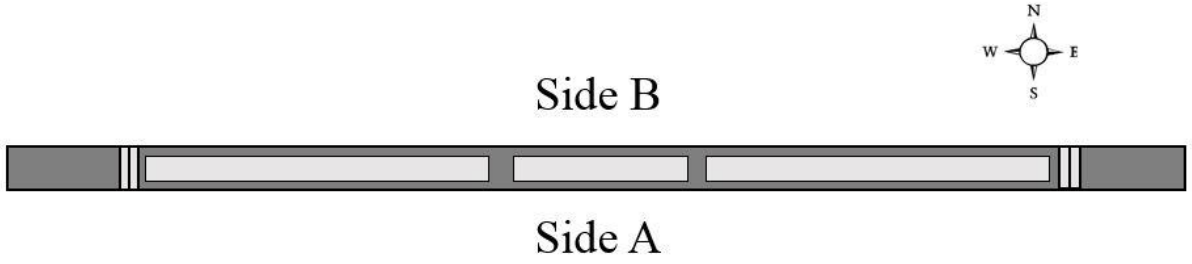

Figure 4-12 Casting bed top view

Figure 4-13 Casting bed elevation view

4.4.2. Fabrication of Specimens

The specimens were fabricated using standard plant casting procedures. The casting bed was first cleaned off and necessary materials for the two specimens being casted were laid out beside the bed. The 66 prestressing strands were then pulled through the headers and the hold-down points in the correct configuration. These strands were then partially stressed to 5,000 lbs, so that the material could be checked for any defects. The hold-up points were then placed and the strands were tensioned using a hydraulic jacking device. The strand properties were checked against the design according to standard ALDOT procedures. The measured elongation for strands in both specimens were between the values of 24.375-26 in. Plastic sheathing with an open slit was placed around certain strands for debonding. The strands were debonded at three different lengths, 5 ft, 10 ft and 15 ft. This practice is typical of ALDOT debonding procedures. The debonded strands can be seen in Figure 4-6 and Figure 4-8.

The pre-bent mild steel reinforcement bars were then tied to the fully-prestressed strands. Because the reinforcement bars in the end zones contained sensitive strain gauges, they were carefully put in the correct place and the lead wires were draped off to the sides. The placement of the reinforcement bars can be seen in Figure 4-14. More details about the steel strain gauges are discussed in section 4.6.1. After the steel reinforcement cage was placed, the research team placed the DEMEC mounting system and the concrete gauges as discussed in sections 4.5.3 and 4.6, respectively. Reinforcement was also placed within the waste block during this time.

Figure 4-14 Placement of reinforcement bars

The forms were then lubricated with form oil that helped to prevent the concrete from sticking to the forms. The casting bed and the DEMEC strips were also sprayed with form oil before the concrete was poured. The side forms were set in segments using a moveable crane. Each segment of the side forms was guided into position and then latched from the top with steel latches at approximately every 4 feet. The bottom of the forms was clamped together using post-tensioned threaded rods at roughly the same spacing as the latches.

As mentioned previously, the forms used for the BT-78 specimens were a modified version of existing BT-74 formwork. The extra height was achieved by building a steel platform for the base of the side forms which raised the entire cross section by 1 inch. A wooden chamfer form was also built into the sides of the casting bed. Furthermore, 3 in. by 3 in. hollow steel tubing was

welded on to the inside face of the forms to add an extra three inches of height to the girder. As a result, it was necessary to modify the existing top latches. These latches, which were normally bolted in place to the sides, had to be raised to clear the top of the 3-inch tubing on the modified side forms. To achieve this, small lengths of 3 in. by 3 in. steel tubing were cut and welded to the top of the latch connection points. The latches were then bolted into this tubing. The modification of the formwork was performed prior to placement of the formwork.

Figure 4-15 Placement of side forms

The concrete was batched in a facility on site. Before the concrete from each mix was approved to be poured, a small batch was taken aside and its properties were tested. Sample cylinders were also poured for later use. The concrete was transported and poured using a rotation of several Tuckerbilt transporters which each had a capacity of 6 cubic yards. In both cases the

concrete was poured starting from the mark end of the western-most specimen and finishing with the mark end of the eastern-most specimen. The transporter used an auger-driven chute to move the fresh concrete from the hopper to the girder. In order to preserve the steel and concrete strain gauges, the concrete was never poured directly over the end zones of the girder. The SCC required no vibration and easily flowed through the strands and reinforcement, however, to speed up the process, the concrete was still poured by moving the transporter from end to end. Trowels were used to level and smooth off the top of the girders after all of the concrete had been poured. Since the girders were solely for research purposes, it was not necessary to perform the typical top surface roughening.

Figure 4-16 Pouring of concrete for Specimen 3

During the second week of fabrication, the formwork burst while pouring Specimen 4. The failure first occurred at a weld on the pinned end of a latch on Side B of Specimen 4. The failure occurred after the level of the concrete had reached the bottom of the top flange on the mark end, or the side from which the concrete was being poured. The level of the concrete during failure was approximately 15 inched above the top draped strand along the whole girder. Immediately after the first failure, several or all of the other top latches failed in succession due to the higher stresses caused by the first failure. The forms were held in place by the bottom clamps along the whole length of the girder. Because of the low viscosity of SCC, concrete from within the formwork immediately started leaking out of the mark end of the specimen. Since pouring on Specimen 3 had not yet begun, the fabricators decided that the best course of action was to take the forms off, remove all of the concrete, and restart pouring again the following day.

The forms were held in place by a crane while the bottom clamps were loosened. As soon as the bottom clamps were free, the forms were removed one by one using the crane. With the use of two fire hoses, concrete retardants, shovels, vibrators, and eventually a jack-hammer, the casting bed was cleaned and ready to be prepared for pouring the following day. During the process of cleaning the bars, the DEMEC mounting systems were removed, however it was necessary to keep the concrete and steel strain gauges in place. Inevitably, there may have been some damage to the strain gauges due to the high pressure caused by the fire hoses. The following day the same procedures as before were followed during preparation for pouring. As an extra precaution, the form top latches were re-welded with longer welds. The DEMEC mounting systems and the sides were then replaced and both Specimen 3 and Specimen 4 were poured.

Figure 4-17 Specimen 4 side form failure

Some inconsistencies in the cross-sectional shape of Specimen 3 and Specimen 4 were noticed prior to the detensioning process. First, a void in the concrete was noticed around the lifting loop of the mark end of Specimen 3. Moreover, an inch thick layer of concrete had seemingly leaked through the mark end heading of Specimen 3 and had hardened on the casting bed around the bottom strands. The concrete was broken up with a jack hammer before the strands were detensioned. Secondly, the thickness along the webs of Specimen 3 and Specimen 4 varied by ½ inch. These inconsistencies could be explained by the use of modified side forms and probably had little to no effect on the outcome of the experiments.

After the specimens were poured, a weatherproof tarp was draped across the entire casting bed to prevent any rain from affecting the girders and to aid in curing. The following morning the

forms were removed using the cranes in the reverse order of which they were added. Tests were run on the cylinder samples and the average compressive strengths of two cylinders were recorded. When the average compressive strength of the two cylinder samples was higher than 8500 psi, the detensioning process could begin. For Specimen 1 and Specimen 2 it took approximately seventeen hours to reach an average compressive strength of 9205 psi, while for Specimen 3 and Specimen 4 it took approximately sixteen hours to reach 8958 psi.

After the forms were removed the research team began the process of connecting the strain gauge lead wires to the data acquisition system. The lead wires were connected to a system of cables and boxes that led to the data acquisition system. Each girder had its own data acquisition computer which was housed inside of a vehicle parked next to the girder end zone. As the cables were being connected, another member of the research team prepared the DEMEC system for use. The first DEMEC reading was taken before the detensioning process began. More details about the DEMEC data collection process can be found in Section 4.6. After the first DEMEC readings were completed and the data acquisition systems had been checked, both data acquisition systems began collecting data.

The prestressed strands were detensioned in three phases. Four workers were required for the detensioning process: The strands were cut using a propane-fueled flame torch and the cuts were made simultaneously a few inches outside of each of the four headers. The workers followed a predetermined cutting sequence which can be seen in Figure 4-18. In the first phase, the workers cut the bottom corner strands, the top (tie) strands, and all the draped strands. The second DEMEC readings were taken after the first cutting phase. The next phase included cutting all the strands in the top two rows of the bulb. The third DEMEC readings were taken after the second cutting phase. Finally the remaining three rows on the bottom of the bulb were cut. The fourth DEMEC

readings were then taken and the data acquisition systems were simultaneously turned off. Within each row, the strands were cut beginning with the outside strands and ending with the inside strands, alternating sides between every cut.

The following business day the girders were picked up with cranes and moved into the storage yard. The sides of each girder was then white washed, except for the area around the end zones which was susceptible to end zone cracking. In the storage yard, each end of the girder rested on two adjacent 4 in. x 4 in. wooden members. The 7-Day DEMEC readings for Specimens 1 and 2 were taken with these support conditions.

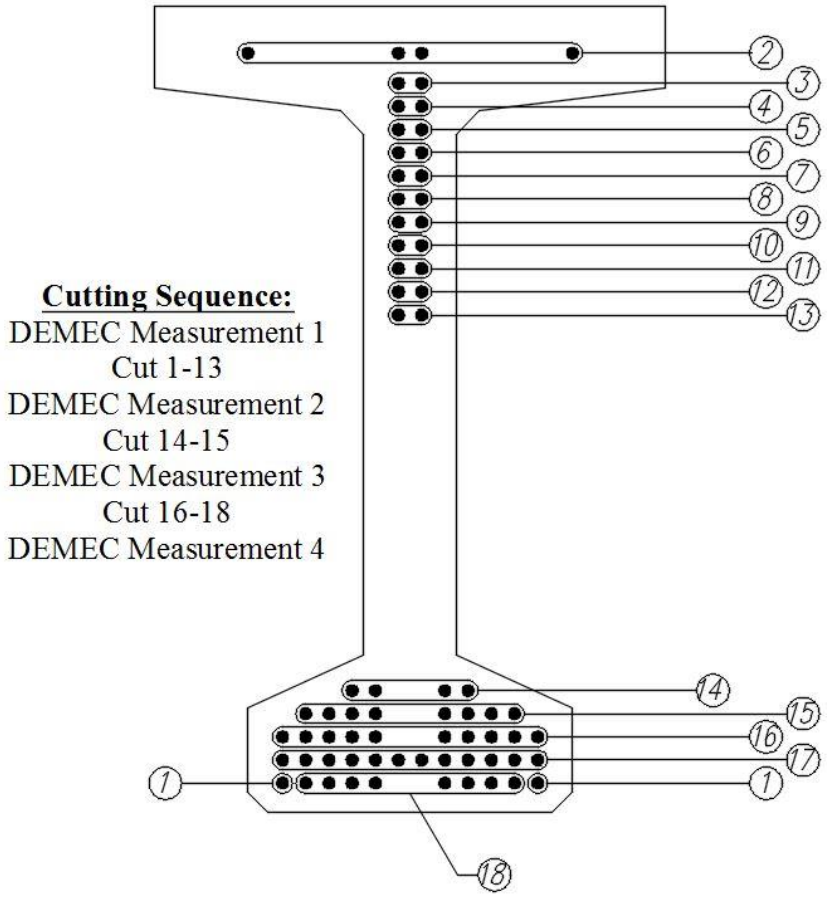

Figure 4-18 Strand cutting sequence

4.5. Transfer Length Acquisition

The transfer length acquisition methodology used in this study is a modified version of the methodology used in previous ALDOT research projects (Dunham, 2011). The determination of the transfer length was decided through the analysis of concrete surface strains using demountable-mechanical (DEMEC) gauges. The following section describes the process used to obtain the transfer length data.

In order to capture the transfer lengths of the four girders with minimum disruption to workflow of the fabricators, steel strips were prefabricated to embed the DEMEC hardware within the girder. Steel strips were used on both faces of the mark end of each girder so that results could be compared for higher accuracy. Since the opposite ends of the girders (the ends with lower strand elevation) did not contain strains which were representative of an actual girder end, they were of little interest to the experiment and their transfer lengths were not recorded. There were a total of eight strips used to embed the DEMEC hardware into the four specimens. The following describes the procedure for the prefabrication and application of the strips.

First, eight strips of steel were cut and a computerized numerical control machine was used to drill 34 holes at 50 mm intervals starting from the end of each strip. These holes were beveled at 82 degrees to allow for a flat surface after machine screws were inserted into the holes. Once the machine screws were inserted into the holes, threaded inserts were fastened around the machine screws on the backside of the steel strips. These threaded inserts were to eventually serve as housing for the DEMEC screws. Another five holes, beveled at 82 degrees, were drilled into the steel strip to accommodate the threaded rods which were used to tie the strips in place to the straight strands before casting. Smaller machine screws were then inserted into the five holes on the front side. On the backside of the strips couplings and threaded rods were attached to the five machine

screws. Finally, each component was hand tightened and two layers of masking tape were placed on the face of the strips to protect the machine screw heads from any contact with the concrete. The final setup of the DEMEC mounting system without the threaded rods is shown in Figure 4-19.

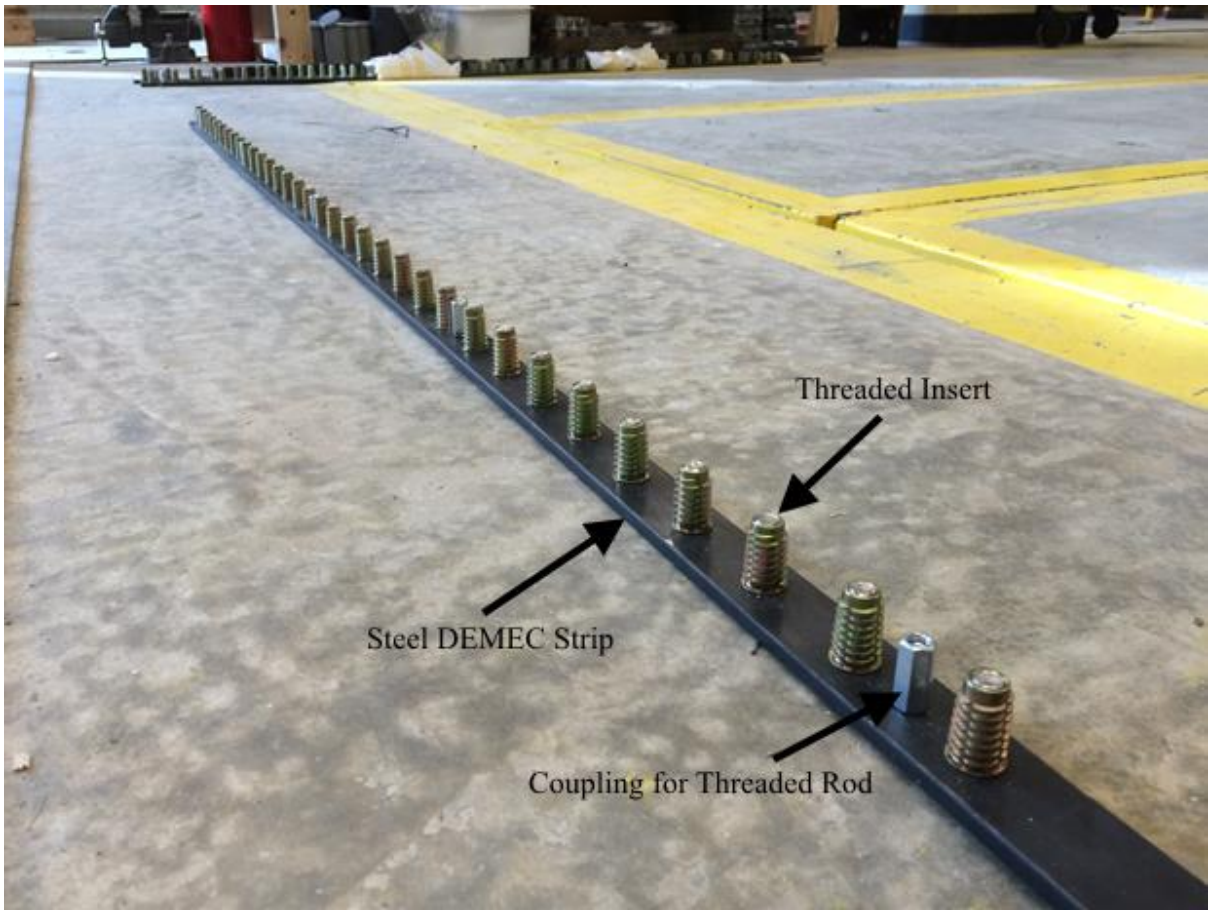

Figure 4-19 Initial setup of the DEMEC mounting system

Additionally, DEMEC screws had to be fabricated from standard DEMEC discs and hex head screws. The disks contained small pinpoint hole that was manufactured for use with DEMEC strain gauges. Small holes for the discs were drilled into the head of the hex head screws using a human operated drill press and the discs were glued into the holes using an epoxy for metals. An

assembled DEMEC screw is shown in Figure 4-20. This method of attaching DEMEC targets to the screws was successful for the majority of the screws, however, a few of the DEMEC discs became loose during the time between the installation of the discs and the reading of the concrete surface strains. The loose DEMEC discs could have been a product of either using an insufficient amount of epoxy or drilling too large of a hole in the screw head. The problem was realized during the reading of the concrete surface strains when the measured value was dramatically shifting as a result of small amounts of lateral pressure on the DEMEC strain gauge. The few data points which were affected by the loose DEMEC screws were not considered in the reported results and had little effect on the accuracy of the transfer length determination program.

Figure 4-20 Assembled DEMEC Screw

During the fabrication of each girder, the DEMEC mounting system was installed after the prestressed strands were stressed to the designed value and the conventional steel reinforcement

was tied in. The five threaded rods on the DEMEC mounting system were attached to the top of the second row of strands using zip-ties. For all specimens, the final location of the DEMEC mounting system was approximately 5 in. above the bottom surface. The DEMEC strip was intentionally placed slightly outside of the girder so that it would be pushed in when the side formwork was placed and there would be a low chance for concrete to enter the area between the side formwork and the DEMEC strip. Immediately before the sides were set, the outside faces of the DEMEC strips were sprayed with form oil to resist bonding with the concrete. The final configuration of the DEMEC mounting system before the placement of the formwork can be seen in Figure 4-21.

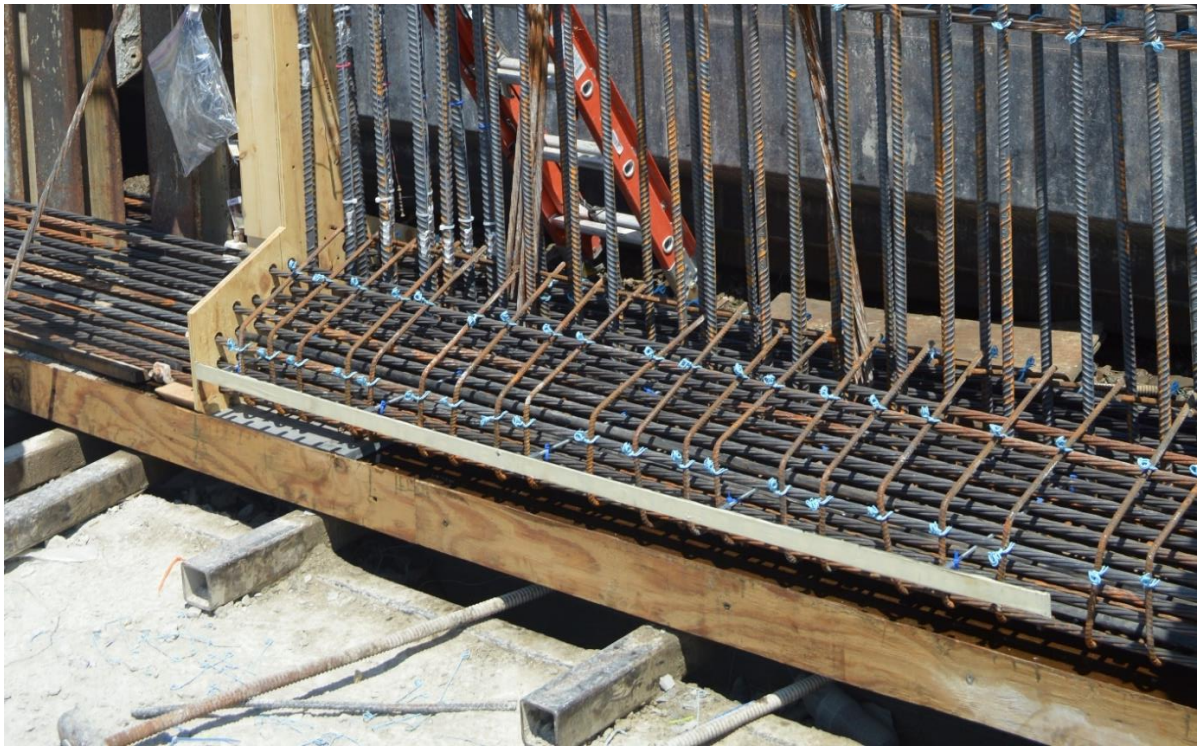

Figure 4-21 Installation of the DEMEC mounting system

The concrete was placed and allowed to harden overnight. The following day, the formwork was removed and the DEMEC mounting system was disassembled. The first step in

disassembling the mounting system was removing the masking tape from the face of the steel strip. Although precautions were taken to keep the concrete from bonding to the DEMEC mounting system, a thin layer of concrete still bonded with the face of the DEMEC strip. The concrete was eventually chipped away with a hammer. The masking tape was then removed and the machine screws were removed with a drill. The steel bar was then free to be removed from the concrete. A hammer and pry bar were used to pry the steel strip from the surface of the concrete. The removal of the DEMEC mounting system is shown in Figure 4-22.

Figure 4-22 Disassembly of the steel DEMEC strip

After the steel strip was removed, the openings of the 34 threaded inserts were visible on the surface of the concrete. The DEMEC screws were then inserted into the threaded inserts and snugly fastened with a socket wrench so that they would be stationary during the detensioning process. The concrete above each screw was then numbered with a permanent marker to avoid

confusion during the data collection process. The application of the DEMEC screws is shown in Figure 4-23.

Figure 4-23 Application of DEMEC screws

4.5.3. Concrete Surface Strain Measurement

Great efforts were taken throughout the process to ensure that the measuring of the concrete surface strain was consistent for the four girders. Because several readings were to be taken during the detensioning process, two 150 mm Mayes Instruments digital DEMEC strain gauges were needed to speed up the process. The strain gauges had different calibration coefficients, so readings from both strain gauges were taken and compared to ensure consistency between the two. The gauges were deemed to be consistent acceptable for use in the field for testing. In the field, the strain gauges and their users were kept consistent for each specimen so that no differences in

strain gauge factor or in user operation were introduced in different readings of the same specimen. One of the DEMEC strain gauges can be seen in Figure 4-24 and Figure 4-25aa.

Figure 4-24 DEMEC strain gauge with gauge factor

For measuring the distance between two DEMEC screws, the first step was calibration using a Mayes Instruments reference bar with a low variance in thermal expansion. This allowed for more accurate readings in environments with varying temperatures. When using the DEMEC strain gauge, it was necessary to hold the gauge in a position completely perpendicular to the plane of the surface being measured. This ensured that the conical points of the gauge were fully inside the target holes on the DEMEC screws.

Figure 4-25 DEMEC strain gauge

The distance between the DEMEC screw targets was measured by first inserting the moveable conical point on the right-hand side of the strain gauge in Figure 4-25 into the target on the right side of the 150 mm span being measured. Next, the stationary conical point on the left-hand side of the strain gauge was inserted into the target on the left hand side of the 150 mm span. The strain gauge was then rotated into the horizontal position and held stationary until the digital meter settled upon a value. This value was then recorded and the strain gauge was completely removed from the target holes. In most cases, three readings were taken at each 150 mm span to ensure the precision of the readings. Due to the time consuming nature of reading the surface strains, only two readings were gathered in some cases.

This process of reading surface strains was implemented in the field beginning with the target hole on the mark end of the specimen and ending with the target hole furthest away from the mark end of the specimen. Once all 31 spans were read at least two times, the DEMEC targets

on the opposing face of the specimen was read. Since transfer release of both specimens was simultaneous, the surface strains of both specimens were read simultaneously, starting with face A and then moving to face B. The process of reading the surface strain is shown in Figure 4-26.

Figure 4-26 Concrete surface strain reading

Surface strain readings were taken at four different times for specimen 1 and specimen 2: before prestress release, after release of strands on rows 1-13, after release of strands on rows 14-15, and after release of all strands. Specimen 3 and specimen 4 had two additional readings: one reading seven days after prestress release, and the other during the week of lab testing. The first surface strain reading for all girders was taken to serve as a benchmark reading to which all other readings would be compared.

4.6. Strain Gauges

Another form of instrumentation used to collect strain data during the detensioning of the girders was strain gauges. Both concrete and steel strain gauges were used in all four girders.

Within the end zone on the mark end of each girder there were 40 strain gauges—31 steel gauges attached to the non-prestressed reinforcement, and 9 concrete gauges suspended in the concrete using wire. The planned position of the gauges were decided upon using the results of the finite element model presented in Chapter 3. These gauges were useful in arriving at a strain contour in the end zone of the girder and estimate critical stress value in end zone reinforcement. During the data collection procedure, it was observed that some of the gauges were potentially damaged during the placement of the bars and pouring of the concrete. The following section describes the configuration and implementation of the strain gauges used in the field evaluation phase of the project.

4.6.1. Steel Gauges

The use of steel strain gauges on the non-prestressed reinforcement within the girder end zone was for measuring the critical stresses in the V bars. The planned locations of the 31 steel strain gauges are shown in Figure 4-29. Each bar location in the figure represents two bars facing opposite directions. For all of the #7 bar locations, both bars were instrumented with a strain gauge. For the first #5 bar location, only one bar was instrumented with a strain gauge. The steel gauges were placed on the bars using the following process.

1) The end zone reinforcement, which would contain strain gauges for all four test specimens, were brought to the University of Alabama campus and the location of the strain gauges were marked.
2) The surfaces of the reinforcement bars were smoothed out with a grinder so that the strain gauges could be applied to a flat surface in an orientation parallel with the length of the rebar. The surface was grinded as flat as possible with careful considerations not to compromise the strength of the bar by grinding off too much of the cross section.

3) Two different grits of sandpaper were then used to physically clear any grease, rust, or other oxides from the surface to which the strain gauge was to be bonded.
4) A neutralizer was applied to the area using a single stroke of a gauze sponge. The surface was then dried with several single strokes from clean gauze sponges with careful considerations not to redeposit any of the removed contaminants back to the area of interest.
5) A conditioner was then applied to the area using the same application and drying precautions that were used with the neutralizer.
6) 6 mm TML strain gauges were removed from the plastic encasement and held in one hand. The other hand was used to place a drop of epoxy on the backside of the strain gauge. The strain gauge was then immediately placed in its position on the prepared area of the bar and held in place for several minutes with a firm press of the thumb. The gauge was positioned so that the lead wires would run vertically up the bar and exit the girder from the top. After several minutes, thumb pressure was released and the bond between the strain gauge and the bar was checked by gently pulling on the lead wire to check for movement. If the bond was incomplete, the strain gauge was then pulled completely off the bar at a low angle and checked for any visible damages. For any incompletely bonded gauges, the process was started over from step 3).
7) For well-bonded gauges, the process continued by taking a roll of tack and covering the top of the gauge with a protective flat layer. The edges of this layer were then pressed firmly around the outsides of the gauges to prevent any moisture from making contact with the gauge. Precautions were also taken to keep the exposed portion of the lead wires separated from each other since this could cause issues when reading the

gauges. Finally a thin strip of aluminum tape was placed on top of the tack and wire so that only the aluminum tape and insulated wire were exposed.

This process was used for the application of the steel gauges to the reinforcement bars for all four specimens. For all girders the strain gauges were oriented so that the side of the bar with the strain gauge would be facing the center of the girder. The wires leaving the strain gauges were gently secured to the bars using zip-ties at roughly 18 in. intervals to avoid any chance of the wire getting caught on something and pulling out the strain gauge.

A system for labeling the steel strain gauges was created to avoid confusion during both the placing of the bars and the wiring of the gauge wires to the data acquisition system. This system can be seen in Figure 4-27. The wires for each strain gauge were carefully labeled with the correct bar identification number near the end of the wire. These labels were then covered with clear packaging tape to prevent damage that could occur during the pouring process. The labeling system proved to be useful for attaching the wires to the data acquisition system.

During the fabrication of the specimens the bars containing the strain gauges were carefully placed and tied into position so that the strain gauge wires were not being pinched, pulled, or twisted. The wires were then draped over a bar that was connected to the lifting loop and stacked near the outside of the end formwork.

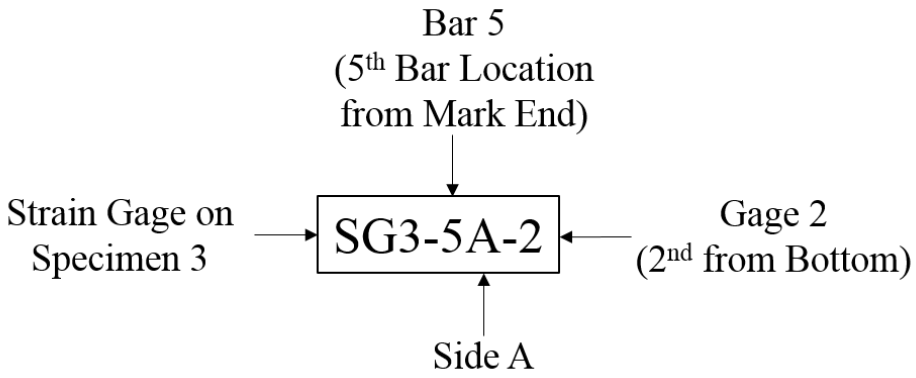

Figure 4-27 Identification system for the steel strain gauges

Figure 4-28 Configuration of steel strain gauges during fabrication

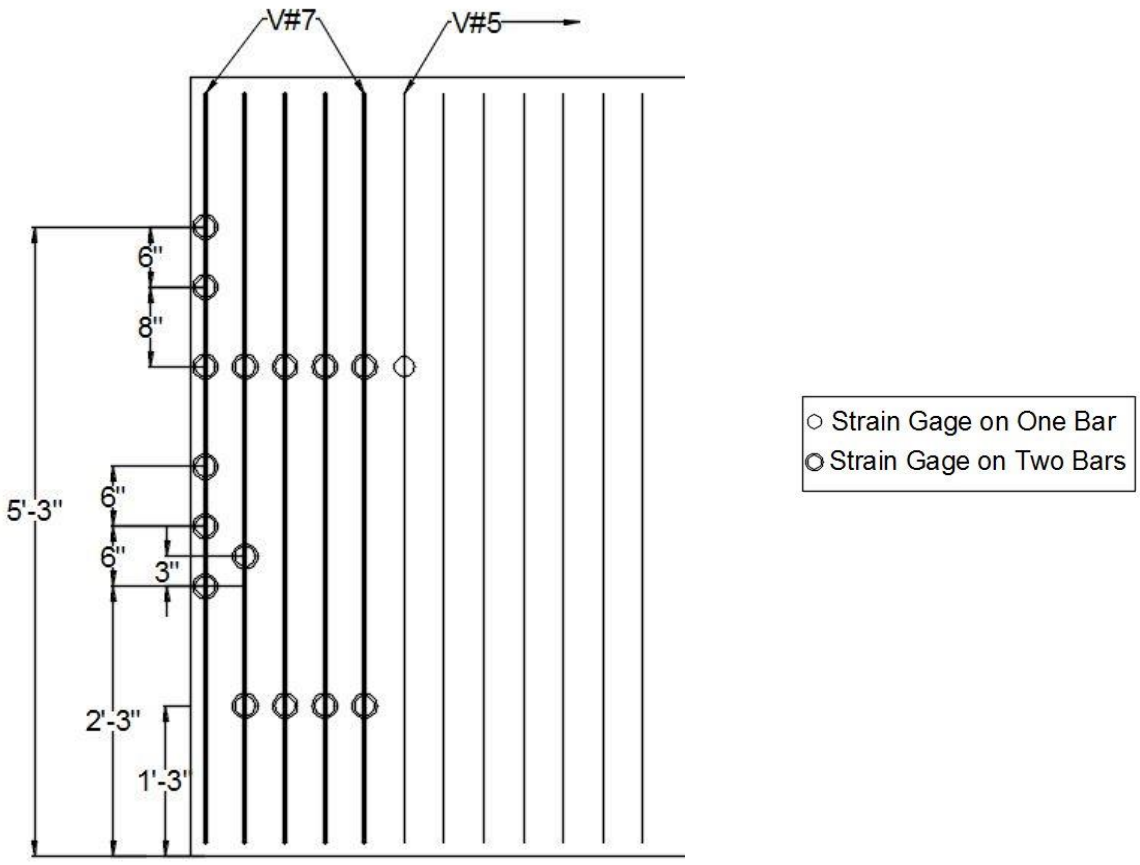

Figure 4-29 Location of the steel strain gauges

4.6.2. Concrete Gauges

A total of nine concrete gauges were used in the end zone of each specimen. The concrete gauges were strategically placed to capture the strain in the concrete within the end zone, as well as around the h/4, h/2, and h locations (19.5 in., 39 in., and 78 in., respectively). The planned concrete gauge locations can be seen in Figure 4-30.

During fabrication, the gauges were hung by twisting a wire in few small helical loops around the body of the concrete gauge. The ends of the wire were then tied to adjacent reinforcement bars in a secure fashion. The concrete gauges was then checked to make sure it was

positioned in its proper orientation and that it could move freely in the direction in which it was oriented. An example of the concrete gauge configuration within the girder can be seen in Figure 4-31. A concrete identification system, similar to the steel gauge identification system, was devised to eliminate confusion of wires during fabrication. This system can be seen in Figure 4-32.

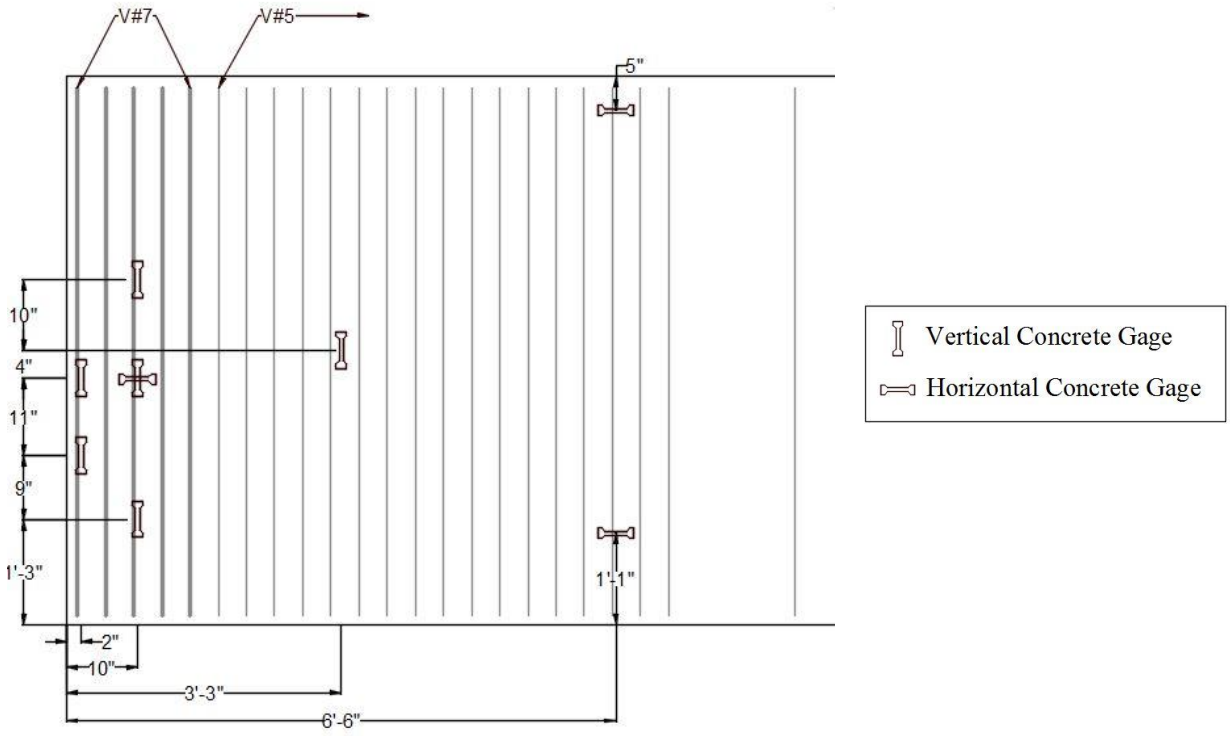

Figure 4-30 Location of the concrete strain gauges

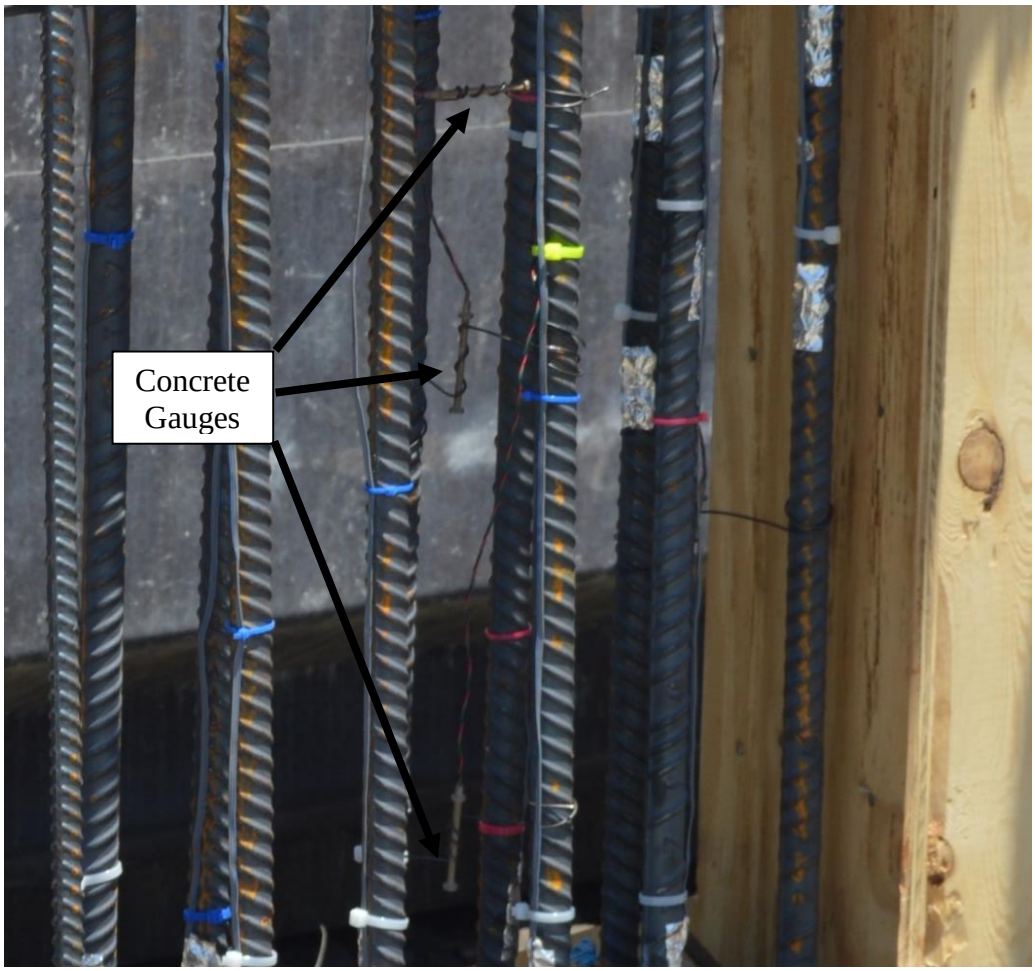

Figure 4-31 Configuration of concrete gauges during fabrication

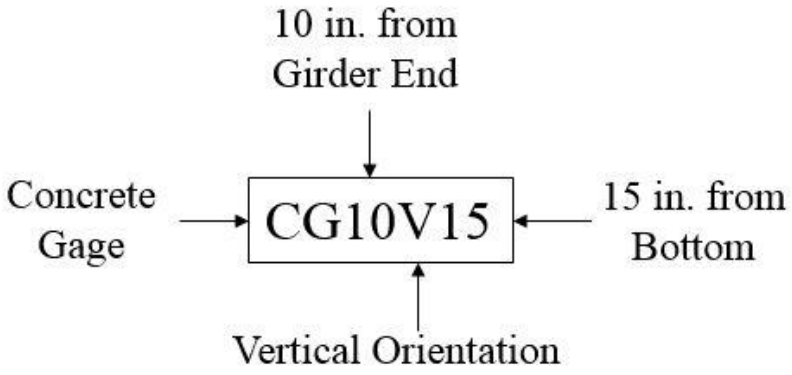

Figure 4-32 Identification system for the concrete strain gauges

Chapter 5 Experimental Testing

5.1. Introduction

After the fabrication of the specimens, the girders were brought to the Large-Scale Structures Laboratory (LSSL) on the University of Alabama campus for load testing. The girders were equipped with multiple forms of instrumentation and tested until the cracking load was reached. This chapter will outline the details regarding the test setup, instrumentation used, loading procedure.

5.2. Test Configuration

Each girder was individually transported to the testing site, tested, and removed before the transportation of the following girder. The following process was used in the testing of all four test specimens. The girder was transported to and from the testing site on an adjustable flatbed utility trailer and picked up by two cranes upon arrival and before departure. A photo of a test specimen being delivered to the LSSL can be seen in Figure 5-1.

5.2.1. Girder Supports

The sole plate on each of the girder ends was then lowered directly on top of the foundation block bearing plate. The girder was supported by a roller connection at one end and a pinned connection at the other end. The roller connection consisted of a 2-inch diameter steel rod centered between two 1-inch thick steel plates. To ensure the system was level and full bearing was achieved, the bottom steel plate was leveled on the top surface of the concrete foundation block with a thick layer of 10,000 psi strength USG Hydro-Stone® gypsum cement. The pinned

connection consisted of the same components as the roller connection, however, on the pinned connection the rod was welded to the center of the top steel plate. The girder supports can be seen in Figure 5-2 and Figure 5-3. The bearing-to-bearing length of the test specimens were 52 ft-9 in.

Figure 5-1 Transportation of Specimen 3 in the LSSL

Figure 5-2 Roller end support

Figure 5-3 Pinned end support

5.2.2. Load Point

The loading point of the load jack was placed at mid-span for the fully bonded specimens (Specimens 1 and 3) as seen in Figure 5-4, however, it was necessary to adjust the loading point for the debonded specimens (Specimens 2 and 4) to account for the transfer and development length of the debonded strands. AASHTO (2015) and ACI 318-14 transfer and development length equations were used to determine the adjusted loading point for Specimen 2 and Specimen 4. The adjusted loading point was 34.5 ft from the debonded end of the girder. The adjusted loading point can be seen in Figure 5-5. The load was applied through a hydraulic Power Team hydraulic ram with a maximum capacity of 1,400 kips.

The load was distributed through a 1-inch thick steel plate which rested on top of an 8-inch x 6-in. x 14-in. ultra-high performance concrete spreader beam. Two spreader beams were cast, and after testing 2-inch x 2-inch cube samples from the same pour, the average compressive strength of the two spreader beams was approximately 24,000 psi. The first spreader beam was used for the Specimen 1 and Specimen 3 tests, however, due to vertical cracks that formed in the spreader beam after the second test, the second spreader beam was used for the Specimen 2 and Specimen 4 tests. In order to ensure the spreader beam was level and in full bearing with the girder, USG Hydro-Strone® gypsum cement was poured underneath the spreader beam for each test. Careful measurements were taken to perfectly center the jack and spreader beam above the center of the web to avoid a punching failure in the top flange. During fabrication of the girder, the load plate was not perfectly placed before embedment in the top of the girder, therefore, in some cases the position of the spreader beam was up to 3 inches off-center with the load plate. A typical configuration of the load point spreader beam can be seen in Figure 5-6.

The load jack was held in place by a steel reaction frame which was tied to the strong floor using six high-strength 2-inch dia. all thread post-tensioning bars. The reaction frame was moved with a crane for positioning above the loading plate.

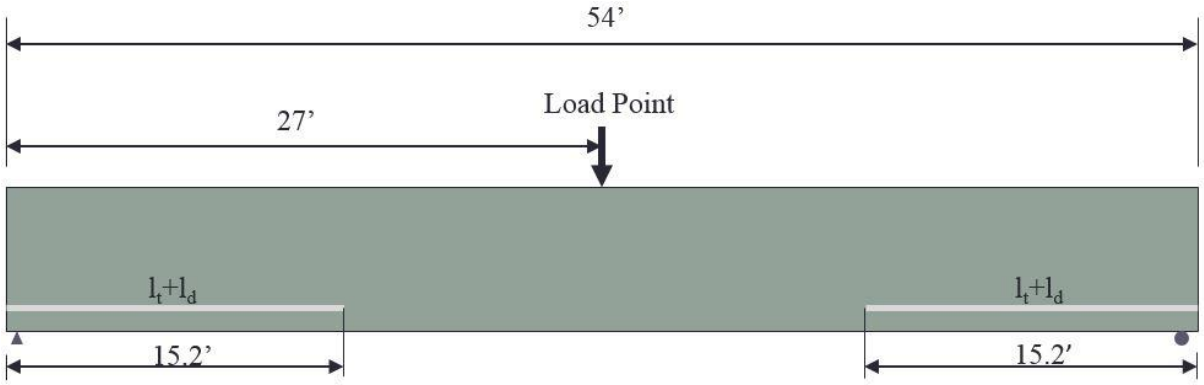

Figure 5-4 Load point for Specimen 1 and Specimen 3

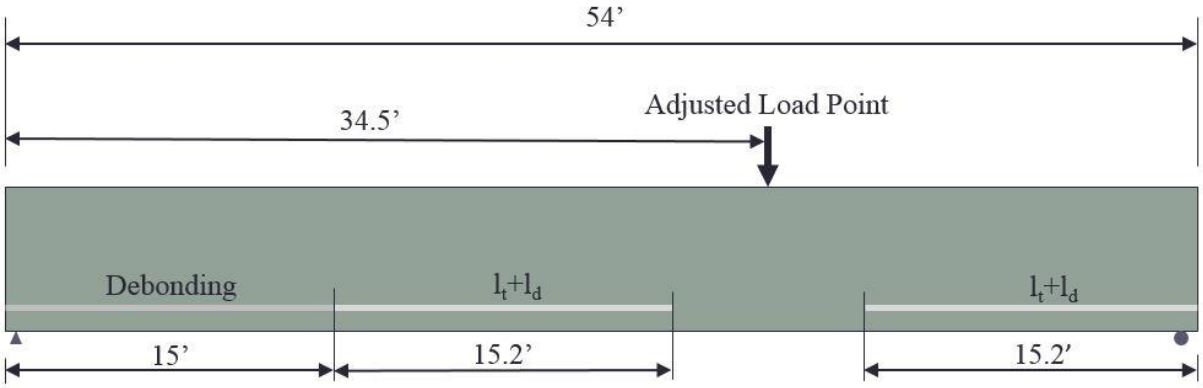

Figure 5-5 Adjusted load point for Specimen 2 and Specimen 4

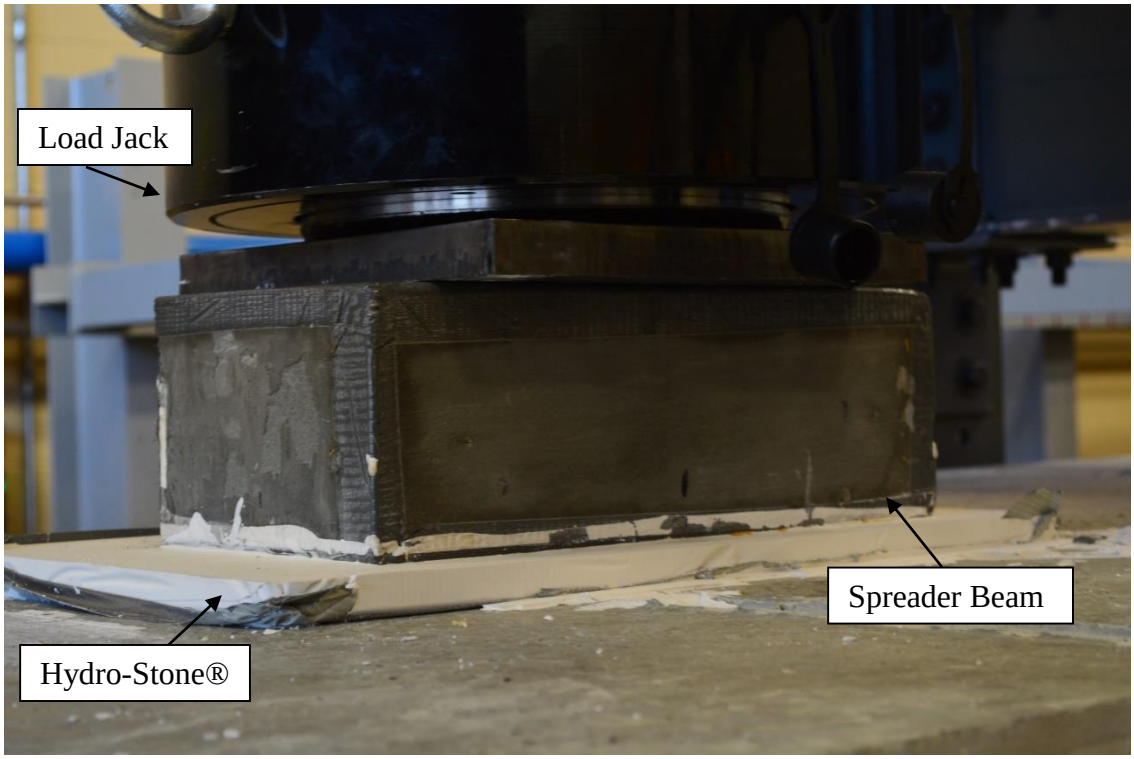

Figure 5-6 Load point spreader beam

5.3. Instrumentation

Instrumentation used in the laboratory tests included direct current displacement transducers (DCDT), string potentiometers, demountable mechanical gauge targets (DEMEC), internal steel strain gauges, internal concrete strain gauges, a non-contact, 3D optical tracker with 40 sensors, a photogrammetry camera, and a 3D LiDAR scanner. The results of the data collection will be presented in Chapter 6.

5.3.1. DCDTs

The DCDTs were used in three separate areas: at the load point, in the end zone, and at the girder end. The specifications and positions of the DCDTs are shown in Appendix A.

There were eight DCDTs used at the load point to capture the average strain distribution along the height of the girder. The load point DCDTs were held by aluminum angles which were fixed to thin wooden blocks. A typical load point DCDT can be seen in Figure 5-7. Several epoxies and glues were tested for attaching the blocks to the girder face, but ultimately the research team decided that hot glue created the best bond strength between the wood and the concrete face. Two DCDTs were placed on the upper flange, four were placed along the web, one was placed on the bottom bulb, and one was placed on the bottom face of the girder. The entire load point DCDT configuration can be seen in Figure 5-8.

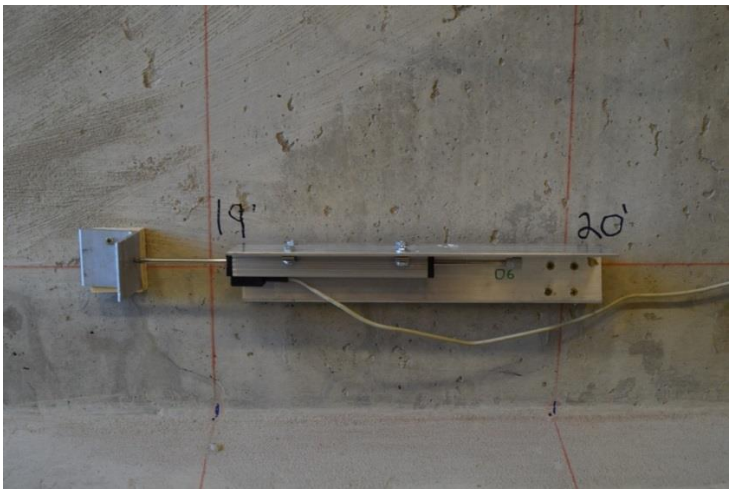

Figure 5-7 Typical load point DCDT configuration

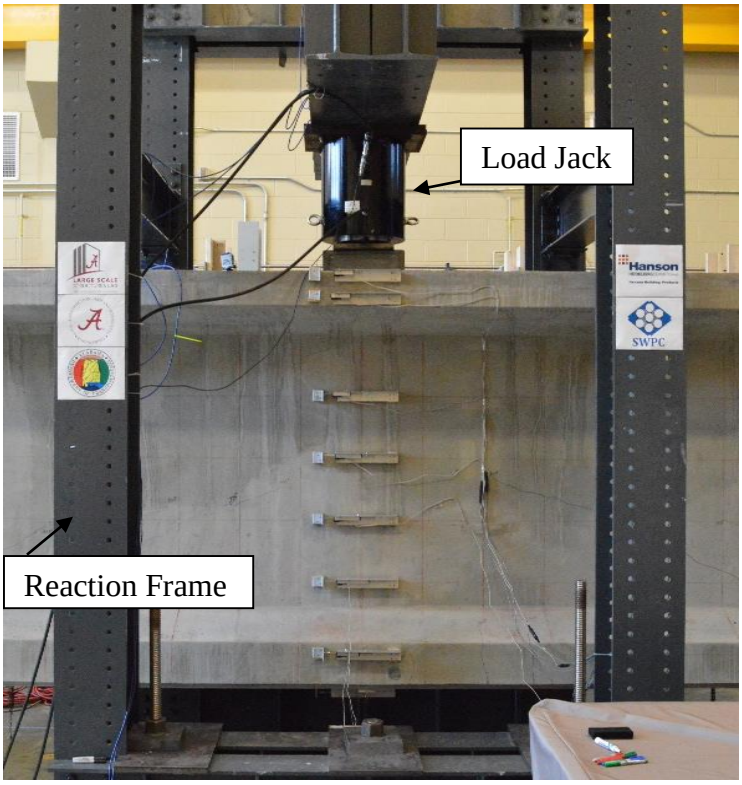

Figure 5-8 Load point DCDT positions

Five DCDTs were used to capture the shear deformation in the end zone region near the mark end of the girder. The points used in the DCDT shear deformation study were located on the web in a 3 ft x 3 ft square starting 3 feet from the mark end of the girder. A DCDT was also placed diagonally across the 3 ft x 3 ft square to help determine the shear deformation behavior of the end zone. The shear deformation DCDT configuration is shown in Figure 5-9. Finally a DCDT was placed on the face of the bulb for the purpose of measuring any shifts on the roller end of the girder. The rod of the DCDT was attached to an aluminum angle that was fixed to the stationary foundation block. The configuration of the roller end DCDT can be seen in Figure 5-10.

Figure 5-9 Shear deformation DCDT configuration

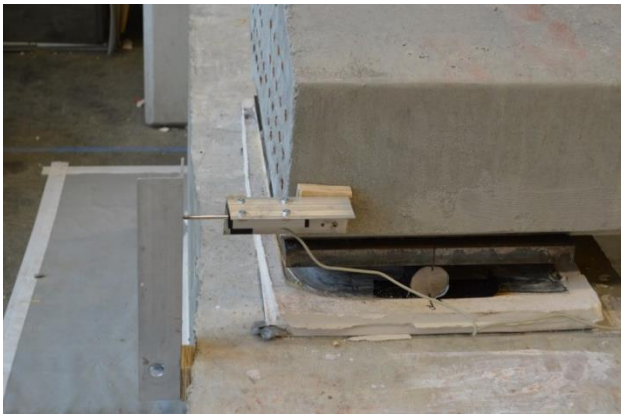

Figure 5-10 Roller end DCDT configuration

5.3.2. String Potentiometers

Eight string potentiometers were used to measure the change in deflection during loading along the length of the girder. Each potentiometer was screwed to a wooden plank which was held down by a lead block to ensure fixity to the floor. A wooden block was then centered directly above the potentiometer and fastened to the girder with hot glue. A hook and chain hung from the block and were connected to the moveable end of the string potentiometer. The specifications and positions of the string potentiometers are shown in Appendix A. The configuration of the string potentiometers can be seen in Figure 5-11.

Figure 5-11 String potentiometers

5.3.3. Strain Gauges

The internal steel and concrete strain gauges which were installed in the end zones of the girder during fabrication were re-attached to the data acquisition system before the laboratory tests. Many of the gauges were compromised during installation or pouring of the concrete, however, the rest were used to read strains in the girder during the load tests.

5.3.4. NDI System

The shear deformation of the girders was also measured with the use of the NDI system on the opposite end. Forty NDI sensors were attached in a 1 ft x 1 ft grid pattern along the outside

face of the web. Readings from an NDI Optotrak Certus HD tracker were recorded during the girder load tests and used to develop a shear deformation gradient along the recorded area.

Figure 5-12 NDI tracker

Figure 5-13 NDI sensor configuration

5.3.5. Photogrammetry

The photogrammetry camera was used in various areas throughout the girder tests. On Specimen 1, the photogrammetry camera was used in the web of the end zone to record the shear deformation much like the DCDTs and NDI sensors were used. For the other three specimens, the camera was used in the web of the loaded area. The photogrammetry camera took incremental pictures of an area on the girder marked with small dots. Before the dots were applied, the area was painted with a thin solution of white latex paint and water to create higher contrast between the dots and the background without inhibiting surface cracks with the paint. The variance of the dots in the pictures were then used to obtain a strain gradient for the recorded area. A typical photogrammetry pattern and the photogrammetry camera can be seen in Figure 5-14.

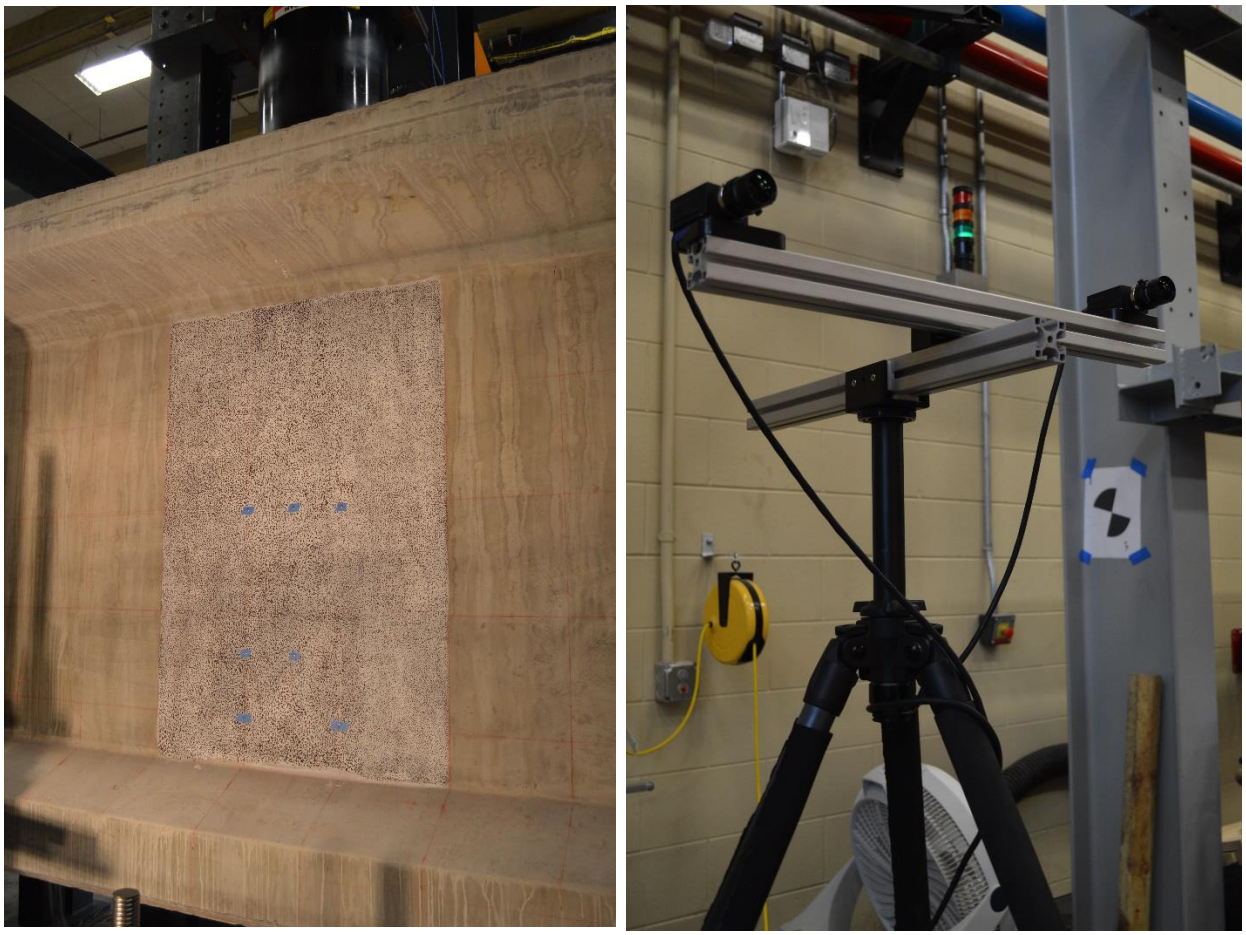

a) Photogrammetry pattern **b) Photogrammetry camera**

Figure 5-14 Elements of the photogrammetry system

5.3.6. LiDAR Scanner

For Specimen 3 a Light Detection and Ranging (LiDAR) scanner was used to scan a 1-foot x 1-foot area of the girder both before and during the application of the load. A "highest resolution" scan was used for both scans. Five targets were positioned in stationary locations around the testing area for later use in establishing a global coordinate system. The Leica Scan Station C10 scanner can be seen in Figure 5-15.

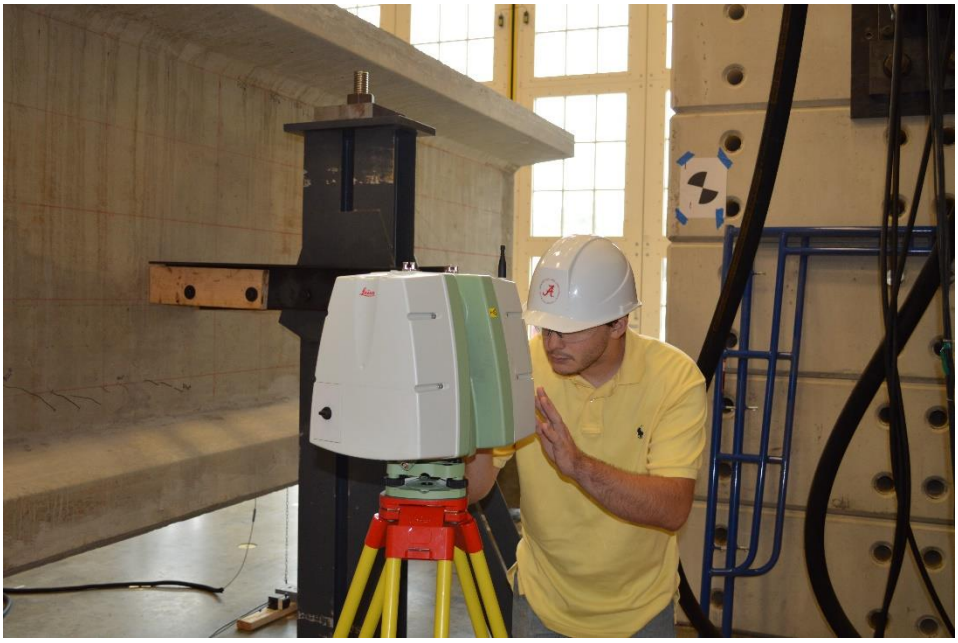

Figure 5-15 Shear Deformation Readings Using the Leica Scan Station C10

5.4. Test Procedure

The girders were tested in a different order from which they were cast due to the changed loading point of Specimens 2 and 4. The testing schedule is shown in Table 5-1.

Table 5-1 Testing Schedule

	Pour Date	Test Date	Age at Testing
Specimen 1	July 29, 2015	September 18, 2015	51 days
Specimen 2	July 29, 2015	November 2, 2015	96 days
Specimen 3	August 6, 2015	October 9, 2015	64 days
Specimen 4	August 6, 2015	November 20, 2015	106 days

The day prior to the full load test, the girder was loaded to 200 kips for the purpose of checking the equipment and instrumentation. Once all equipment and instrumentation was checked, the load was released from the girder.

On the day of testing the instrumentation was powered on and each of the data acquisition systems were manually triggered at the same time. The hydraulic pump was then manually pumped until the load of 200 kips. The research team decided that manually pumping the jack, rather than using an electronically controlled pump, would allow for more control over the loading process. After the initial load, the research team loaded the girder by 25-50 kip increments and then paused to check for cracks and take pictures. The load was then incrementally increased until the initial cracks were formed. The team then carefully traced the cracks with permanent markers and measured the crack widths. After all the cracks had been traced and labeled with a cracking load, the loading continued with 25 kip increments. When more cracks formed, the loading paused and the new cracks were mapped. With process was repeated until it was determined that the safe loading limit had been reached. Girders were not loaded to ultimate failure. After the final load was applied for Specimen 3, a LiDAR scan of the same girder area was taken. The load was then slowly removed from the girder and the data acquisition equipment was manually stopped. The tests each generally lasted roughly two hours from the first load to the removal of the load.

The day of each test, three cylinders were broken for use in determining the concrete compressive strength. The results of the tests can be seen in Table 5-2.

Table 5-2 Test Day Cylinder Results

	Test Day Compression Strength (psi)			
Specimen	Test 1	Test 2	Test 3	**Average**
Specimen 1	11,470	12,340	11,738	**11,849**
Specimen 2	12,672	12,972	13,062	**12,902**
Specimen 3	11,854	12,233	12,158	**12,078**
Specimen 4	12,130	12,950	12,802	**12,627**

Chapter 6 Results and Discussion

6.1. Introduction

The end zone regions of four BT-78 specimens with varying end zone details were studied with the intent of analyzing and comparing the internal and surface strain states of the girders and determining a practical girder design that best minimizes end zone cracking. The following chapter presents the results of the data collection with a specific focus on the comparative transfer lengths and critical strain values in end zone reinforcement between the four specimen designs. The strain values in this chapter are presented in micro-strain units (με).

6.2. Field Observations and Results

The results of the DEMEC transfer length data and the internal strain gauge data captured in the field are presented in this section. A detailed account of the cracking due to prestress transfer is also presented in this section. The processes for capturing the DEMEC transfer length data and the internal strain gauge data are discussed in Chapter 5.

6.2.1. Cracking due to Prestress Transfer

Cracking immediately after prestress transfer was seen in all specimens except Specimen 4 (lower draping and debonding). For all specimens, cracks grew over time, with the majority of the cracking occurring within the first week. The girder end zones were inspected for cracks between three to four times at different girder ages and crack lengths were measured for each specimen. The results of these inspections can be seen in Table 6-1. The cracks were carefully digitized and the total length was approximated through the use of software. Cracks occurring at

"Day 0" were recorded immediately after prestress before the girder was lifted and transported to the storage yard. Day 7, 8, and 15 inspections occurred while the girder was still in storage at the precast plant. Finally, the end zone cracks were inspected once the girder was transported to the LSSL. Since the experimental testing program consisted of testing of girders individually, the ages of the girders during the final inspection were different. The crack lengths and girder ages are presented in Table 6-1. Photographs of the girders one week after prestress release can be seen in Figure 6-2. The cracks have been marked for clarity.

Table 6-1 End Zone Crack Length Growth

Specimen	Day	Crack Length Growth (in.)	Total Length (in.)	Percent Total Length
Specimen 1	0	170	170	57%
	8	101	271	91%
	15	26	297	100%
	51	0	297	100%
Specimen 2	0	113	113	61%
	8	52	165	88%
	15	22	187	100%
	96	0	187	100%
Specimen 3	0	279	279	73%
	7	76	355	92%
	64	29	384	100%
Specimen 4	0	0	0	0%
	7	26	26	54%
	106	23	49	100%

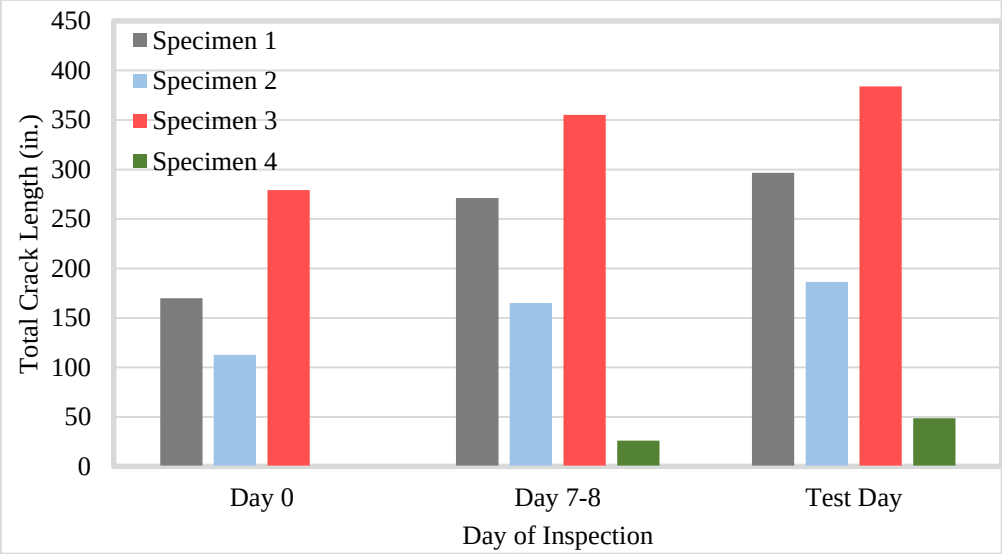

Figure 6-1 End zone crack lengths over time

a) Specimen 1 **b) Specimen 2** **c) Specimen 3** **d) Specimen 4**

Figure 6-2 End zone cracking one week after prestress transfer and lifting

Specimen 1, the control specimen, which contained fully bonded strands and strands at the standard draping angle, produced diagonal cracks in the upper portion of the web, horizontal web

cracks, and cracks at both flange-web interfaces. The diagonal cracks, which extended down at approximately 35 degrees from the top of the web, reached a length of 36 in. The cracks in Specimen 1 reached a total length of approximately 300 in., including the cracks from both sides of the girder and the end face. The specimen showed cracking fairly early, with 57 percent of the cracking occurring immediately after prestress, and 91 percent occurring by day 8. By day 15, the cracks had extended their total length. The diagonal crack extended 39 in. from the girder end, or half-the height of the girder, $h/2$. Specimen 1 contained more longitudinal web cracks than any other specimen as well as more individual cracks overall than any other specimen.

Specimen 2, which contained strands at the standard draping angle and partial debonding, produced diagonal cracks in the upper portion of the web, horizontal web cracks, and cracks at only the top flange-web interface. The diagonal cracks, which propagated from about two inches from the girder end at an angle of roughly 20 degrees, was approximately 36 in. long. The crack lengths for the Specimen 2 end zone totaled to about 185 in, or approximately 37 percent less than the control specimen. Cracks recorded at prestress release accounted for about 61 percent of the total crack length, while cracks recorded on day 8 accounted for 88 percent of the total length. Crack lengths showed no growth between day 15 and day 96. The diagonal cracks extended as far as 35 in. from the girder end, or slightly less than half-the depth of the girder, $h/2$. The cracking pattern for Specimen 2 was similar to that of the control specimen. However, there were significantly fewer cracks and the crack lengths were slightly smaller. The presence of debonding in Specimen 2 is thought to be the cause of the reduction in crack lengths. The absence of cracks at the bottom flange-web interface further supports this notion.

Cracking was noticed earliest in Specimen 3, which contained lower draping and fully bonded strands, when long diagonal cracks appeared in the web immediately after the release of

the first strand cluster (strand rows 1-13). These were by far the longest cracks in any specimen; however, after visual inspection some of the initial cracks were believed to close after the release of the strands in the bottom flange. Both diagonal cracking and horizontal web cracking occurred in this specimen. The diagonal cracks in Specimen 3, which occurred after the release of the first cluster of strands, were two pronged, with the vertex propagating 9 in. from the girder end. The longest of these diagonal cracks extended downward for 58 in. at an angle close to 45 degrees, while the upper of the two diagonal cracks traveled 20 inches at a 45 degrees above the horizontal. The combined crack lengths in Specimen 3 was 384 in. by day 99, or nearly 30% more than the control specimen. The cracks in Specimen 3 had reached 73 percent of their total length by the end of prestress transfer and 92 percent by day 7. The long diagonal crack extended approximately 51 in., or over 0.65*h*. The horizontal web cracks in Specimen 3 were fewer in quantity but longer in length than those within the control specimen.

Specimen 4, which contained both lower draping and debonding, yielded less cracking than any other specimen. Immediately after prestress release, Specimen 4 was investigated and no cracking was noticed. On day 7, horizontal cracks were noticed in the middle of the web, beginning 10 in. from the girder end and extending for 26 in. at a low angle away from the girder end. By day 141, a similar horizontal crack was recorded on the opposite face of the girder, doubling its total crack length. This crack was not noticed during inspection on day 7. The longest crack extended to a distance of 35 in. from the girder end, or nearly *h*/2. The total crack length of Specimen 4 was 49 in., or 84 percent less than the control specimen. The growth of the cracks between investigations can be seen in Figure 6-3 and Figure 6-4.

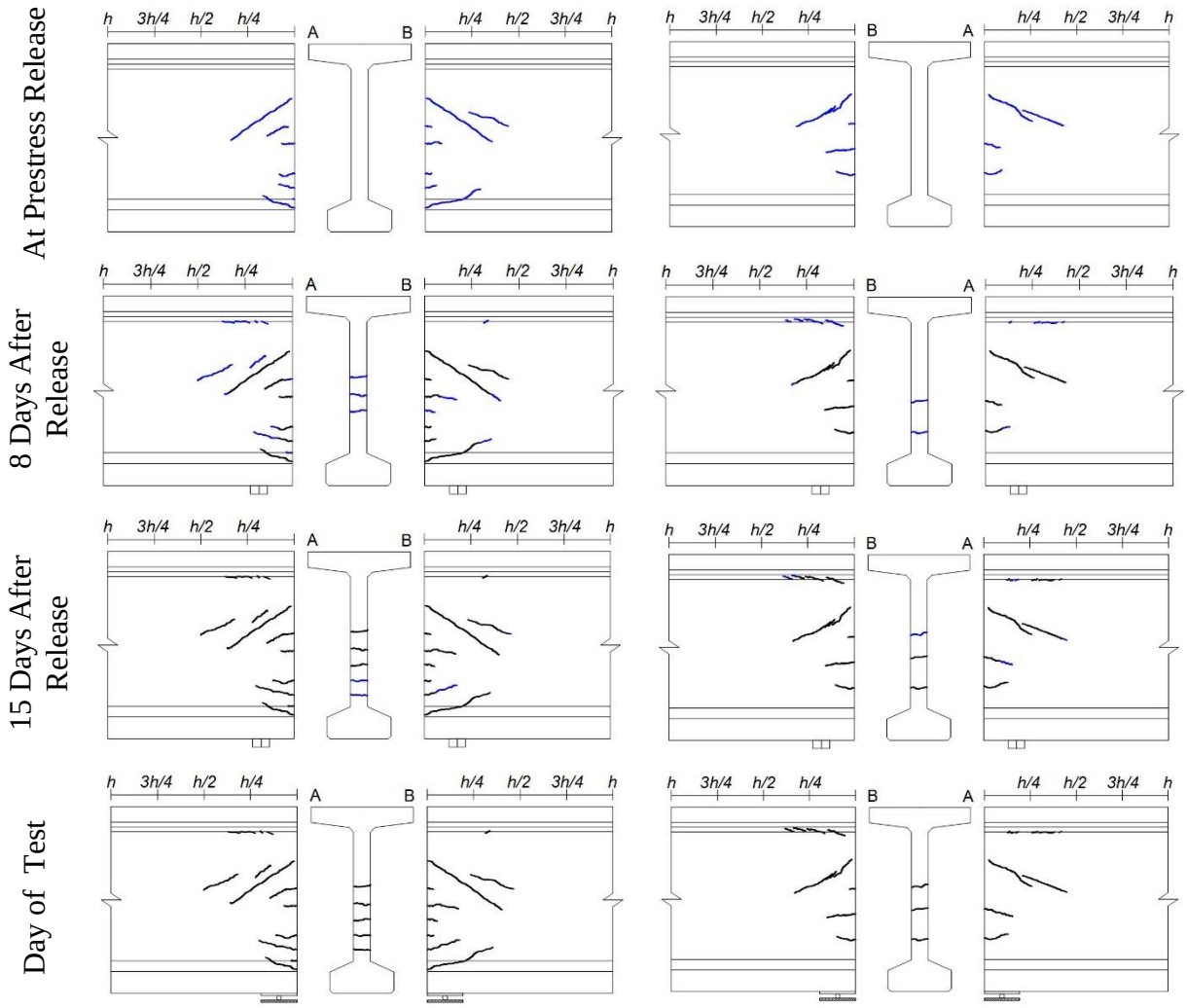

a) Specimen 1 **b) Specimen 2**

Figure 6-3 End Zone Cracking in Specimen 1 and Specimen 2

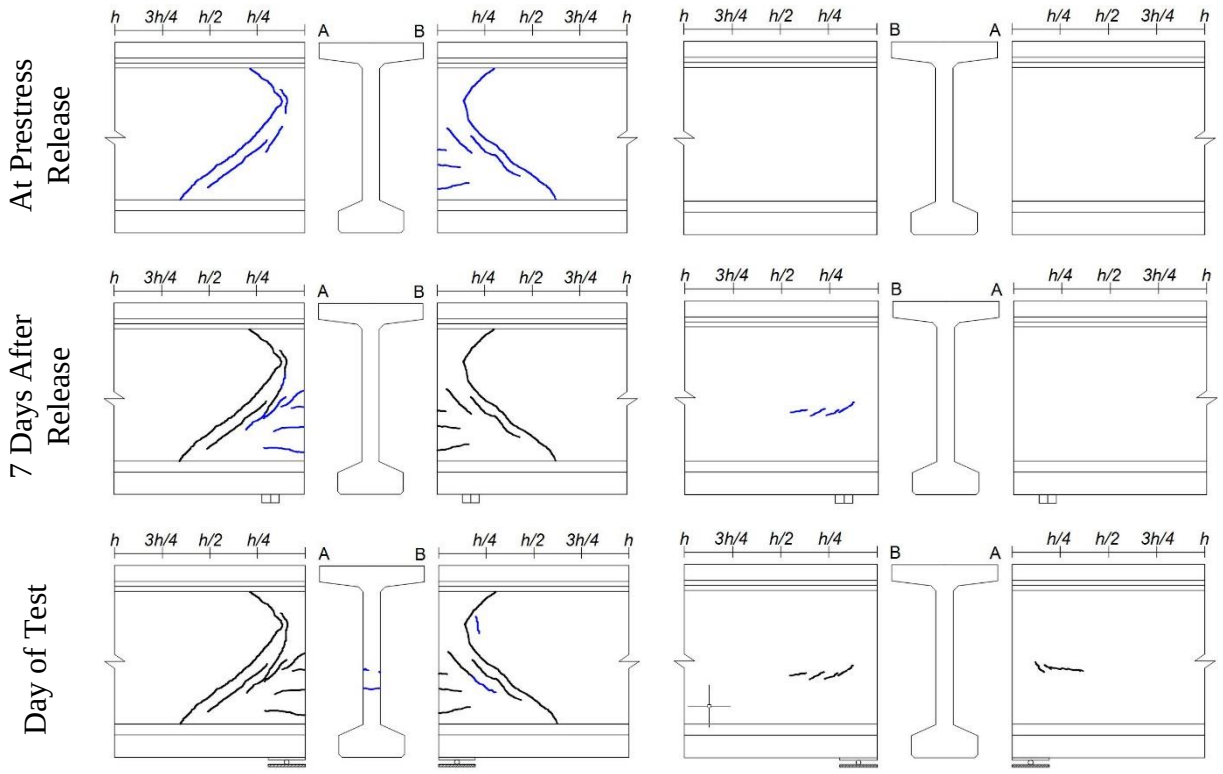

a) Specimen 3 **b) Specimen 4**

Figure 6-4 End Zone Cracking in Specimen 3 and Specimen 4

6.2.2. Strain Gauges

The strain gauges used in the field data collection are shown in this section. For the steel gauges, each figure contains the strain, with respect to time, from the working strain gauges used on a single reinforcement bar. Changes in strain readings correspond with certain phases of detensioning. These phases are represented by A-E in the following figures, and are explained in more detail in Table 6-2. For the concrete gauges, the plots were separated into horizontal gauges and vertical gauges. Data collected from strain gauges which were determined to be damaged was not used in this study. For the steel gauges, the strains were converted into stress by multiplying them with the elastic modulus (29,000 ksi). The field results from the strain gauges confirmed the

cracking behavior of the girders during prestress release. For both the steel and concrete strain gauges, tensile strain is represented as positive and compressive strain is negative. The following figures contain small images relating the strain gauge positions to crack locations. The final positions of the strain gauges within the girder were measured for some, but not all, of the strain gauges, so the plotted locations of the strain gauges should be taken as close approximations.

Table 6-2 Detensioning Phase Descriptions

Phase	Description of Phase
A	Strand rows 1-13 were cut
B	Pause for DEMEC measurement
C	Strand rows 14-15 were cut
D	Pause for DEMEC measurement
E	Strand rows 16-18 were cut

For Specimen 1, the control specimen, a total of 22 gauges out of the 31 steel gauges were functional during detensioning process. The maximum stress recorded by these steel gauges was 22.8 ksi (SG1-2A-3). This was the only working gauge in any girder end zone that recorded a tensile stress in excess of 20 ksi during detensioning. As shown in Figure 6-5, the highest tensile forces occurred immediately after all the strands were cut, which suggests that the cracks occurred while cutting the last strand group. The strains which caused the diagonal cracks in the upper web were captured in strain gauges SG1-2A-2, as well as SG1-1B-5, which can be seen in Figure 6-5 and Figure 6-6, respectively.

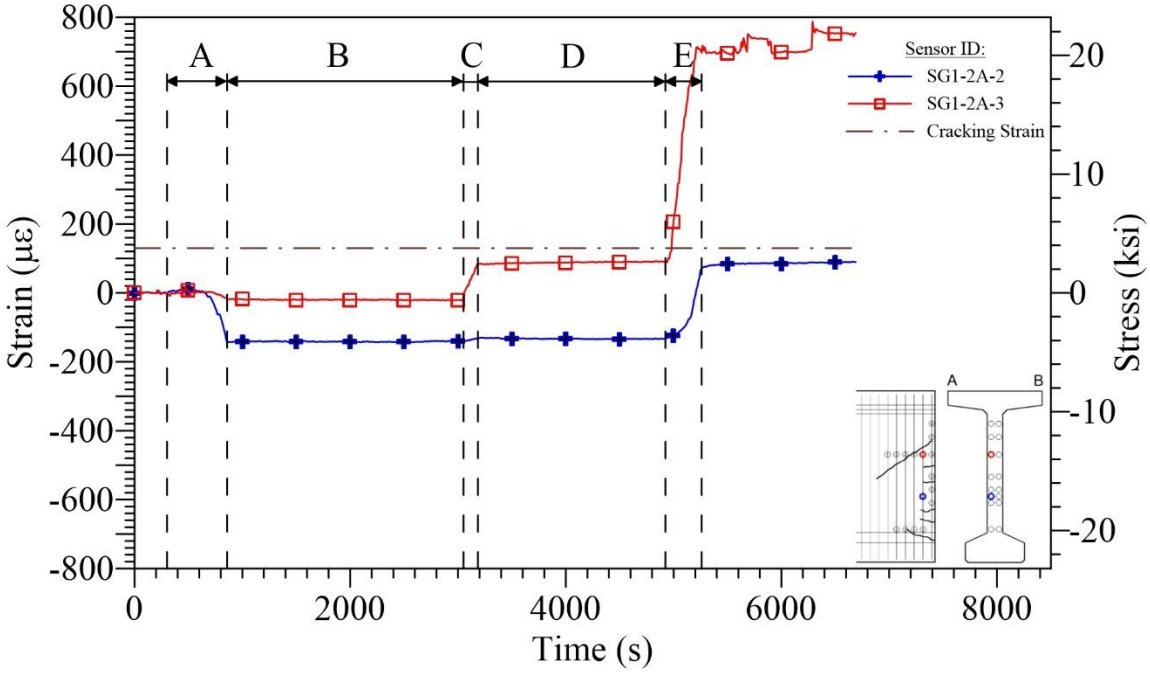

Figure 6-5 Specimen 1, Bar 2A, Steel strain gauges during detensioning

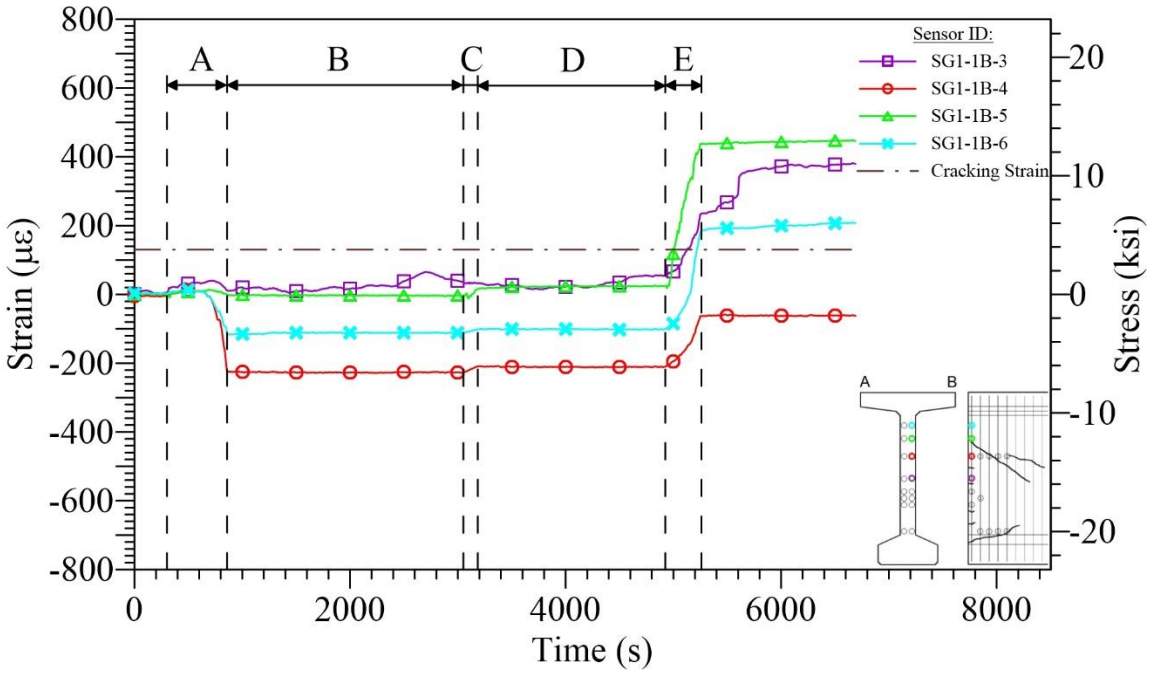

Figure 6-6 Specimen 1, Bar 1B, Steel strain gauges during detensioning

In Specimen 2, a total of 20 gauges out of the 31 steel strain gauges produced useful data during the detensioning process. The maximum stress recorded was 19.7 ksi, and occurred in

SG2-5B-2 after the last strands were cut. The measured strain in SG2-5B-2 over time can be seen in Figure 6-7. The strain in SG2-1B-2 is thought to correlate to a strain of approximately 537 με, or a stress of 15.6 ksi, and the corresponding horizontal web cracks can be seen in Figure 6-8.

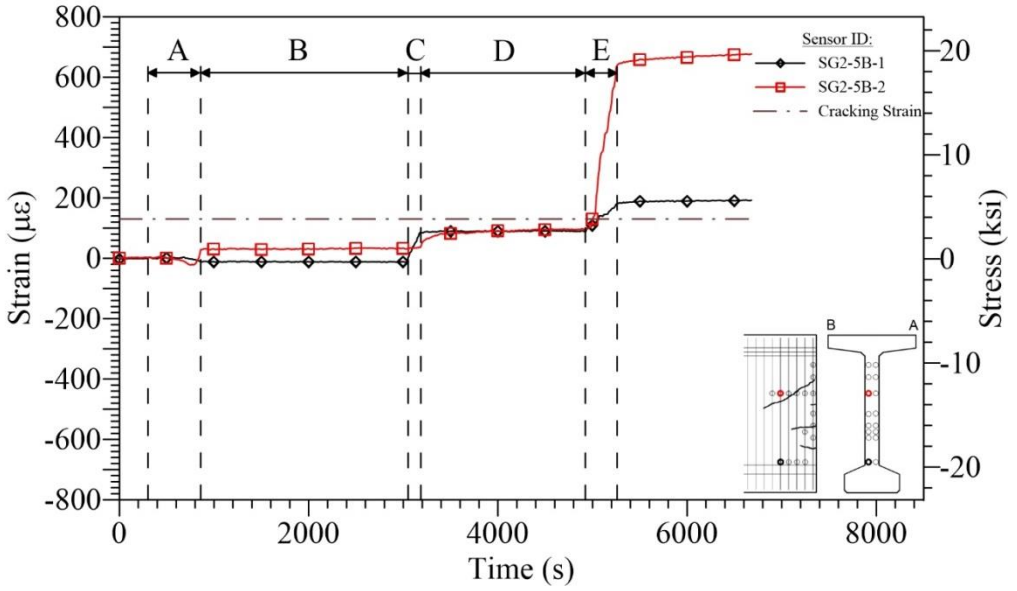

Figure 6-7 Specimen 2, Bar 5B, Steel strain gauges during detensioning

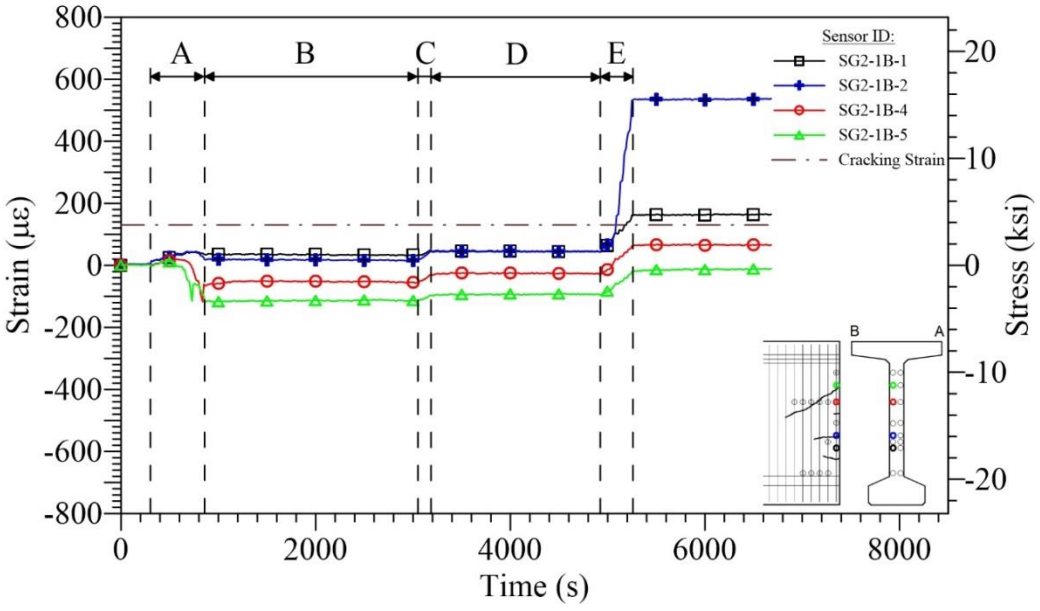

Figure 6-8 Specimen 2, Bar 1B, Steel strain gauges during detensioning

All of the strain gauges in Specimen 3 were functional during detensioning process. The maximum stress measured in Specimen 3 reinforcement was 17.1 ksi, which was estimated from the reading of strain gauge SG3-2A-1. This stress occurred in bar 2A at the bottom flange-web interface after the final strands were cut. A long horizontal crack occurred in this location, as can be seen in Figure 6-9. The strain which caused the massive diagonal cracking in Specimen 3, as discussed in the previous section was, however, captured by the concrete gauges. The peak at the end of Phase A in Figure 6-10 represents a period in which large amounts of cracking occurred. Furthermore, this vertically oriented concrete gauge was located at the vertex of the diagonal cracks, as shown in the lower right portion of Figure 6-10. The peak tensile force in CG10V49 was 504 με.

Finally, in Specimen 4, a total of 18 gauges out of the 31 steel strain gauges produced useful data for the detensioning process. A vast number of gauges were lost during the cleanup process resulting from the form collapse during fabrication. More details of the incident are provided in Chapter 4. Tensile forces in Specimen 4 were the lowest of any specimen. The maximum tensile stress in Specimen 4 was 8.6 ksi at SG4-2B-3, as can be seen in Figure 6-11.

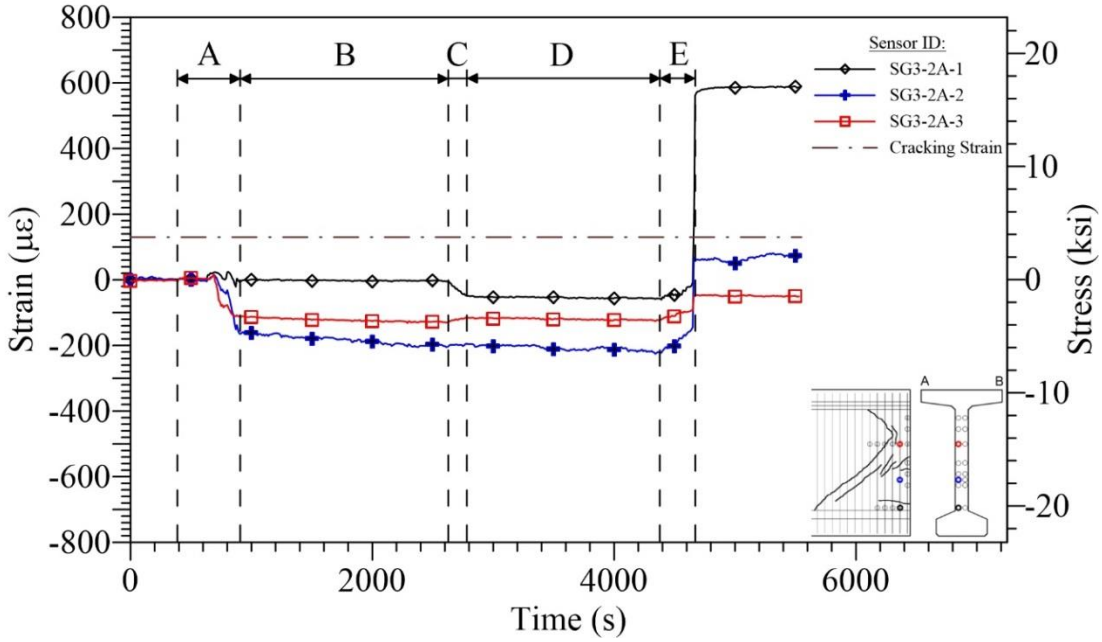

Figure 6-9 Specimen 3, Bar 2A, Steel strain gauges during detensioning

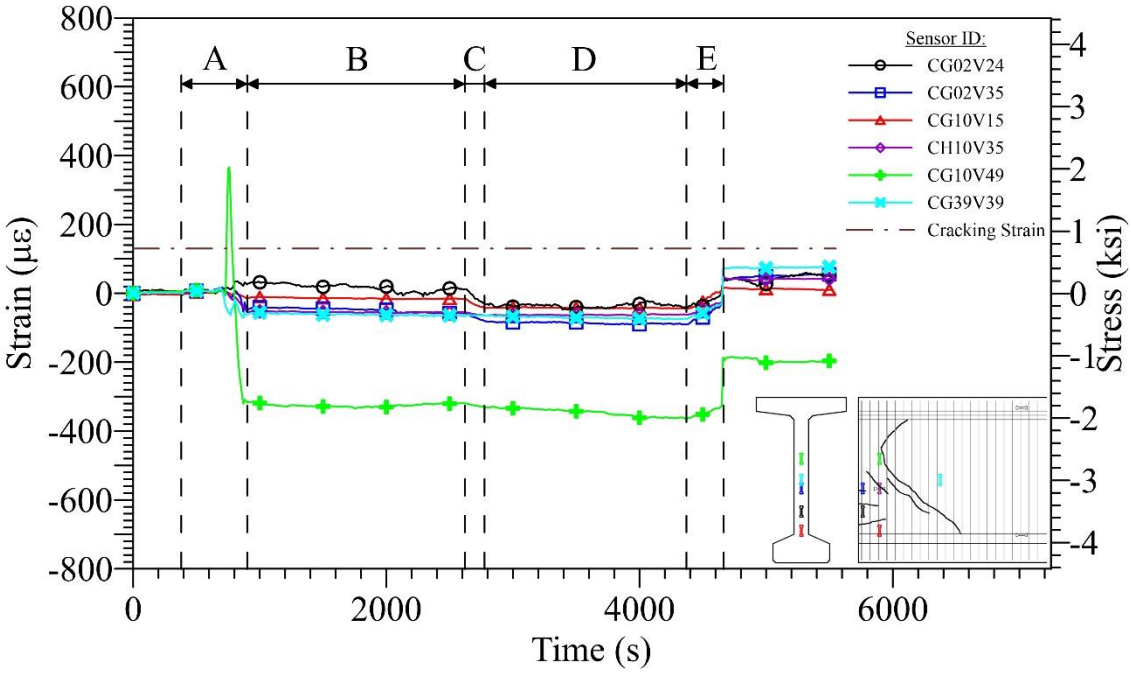

Figure 6-10 Specimen 3 vertical concrete gauges during detensioning

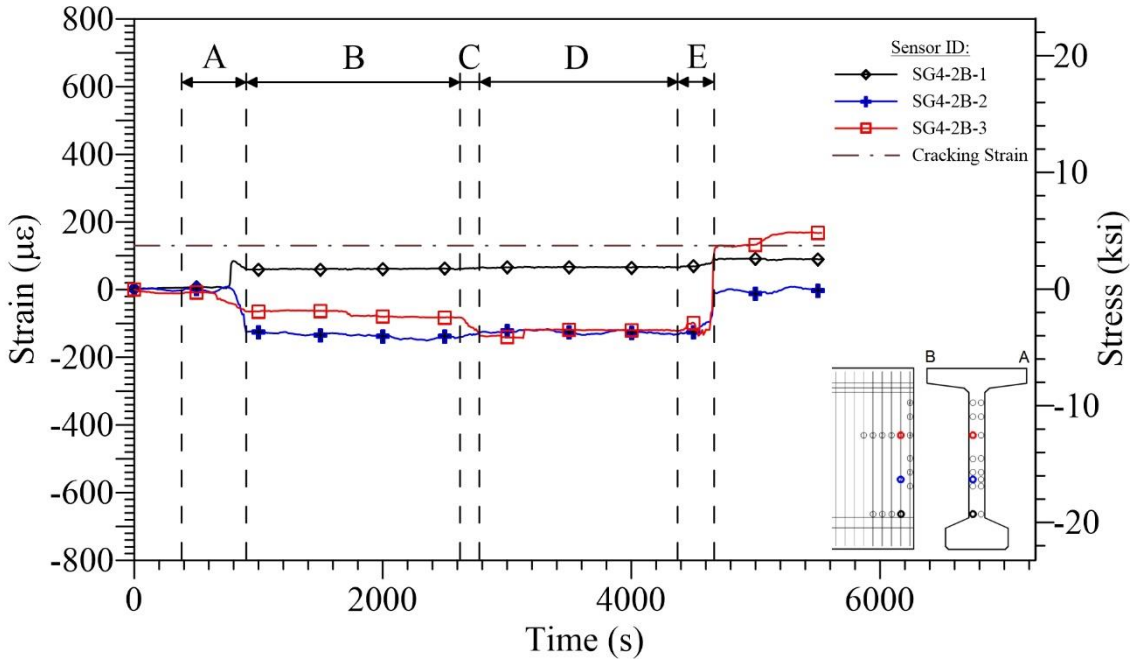

Figure 6-11 Specimen 4, Bar 2B, Steel strain gauges during detensioning

The measured vertical tensile stress in the end zone reinforcement exceeded AASHTO's 20 ksi design limit in only one bar (Specimen 1, Bar 2). Stresses exceeding 88 percent of the 20 ksi design limit were measured in every specimen except Specimen 4. The maximum stress recorded in Specimen 4 reached 7.7 ksi, or only 38 percent of the 20 ksi design limit. The maximum stresses of the instrumented bars during the detensioning process can be seen in Figure 6-12. The distance between the centerline of the bars and the girder end is also shown in the figure. The maximum vertical reinforcement stresses are apparently less proportionate to the distance from the girder end than the stresses measured in the study conducted by Tuan, et al. (2004) as can be seen by comparing Figure 6-12 with Figure 2-2. However, the difference in vertical stress distributions between the Nebraska girders and the BT-78 girders can be attributed to the differences in cross-sectional shape, girder depth, and prestressing force. As shown by the finite element analysis, every girder shape produces concentrated areas of stress of varying sizes and in

different locations. The maximum vertical stress from the BT-78 reinforcement was adequately predicted by the finite element analysis.

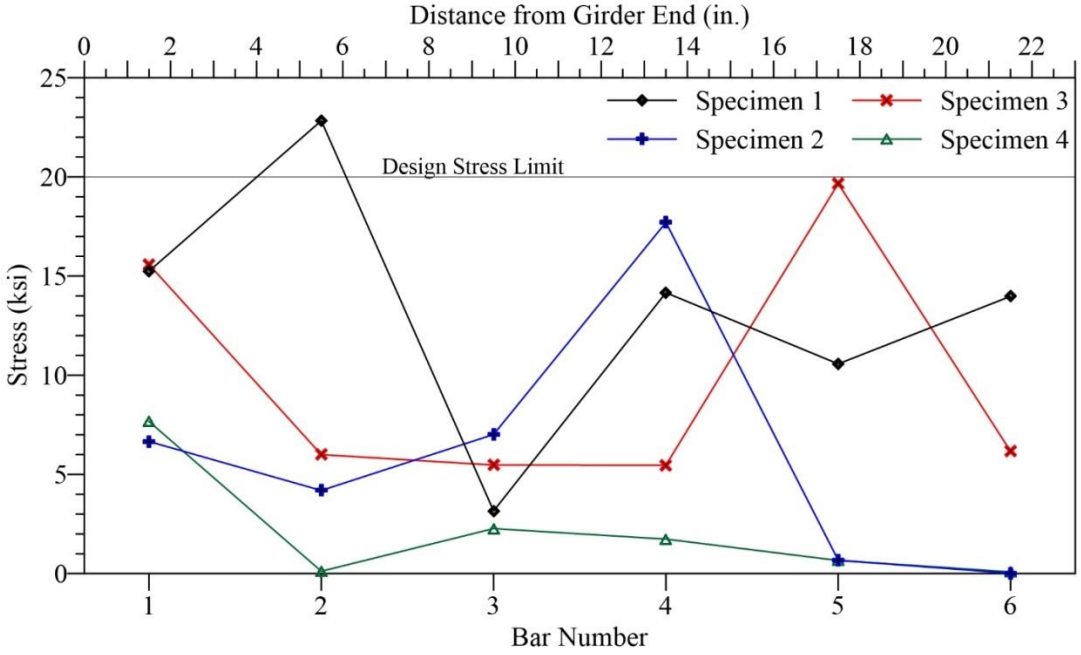

Figure 6-12 Vertical Stress in End Zone Reinforcement

Furthermore, the maximum vertical tensile stress values in the end zone reinforcement of all specimens measured below the AASHTO recommended design splitting force equal to 4 percent of the total prestressing force. The splitting forces were plotted against the prestressing force in Figure 6-13. This figure can be compared to the results of Tuan et al. (2004) as shown in Figure 2-3. The total prestressing force was calculated by multiplying the 66 strands by their recorded initial prestressing force. The four strands in the top flange were not included in this calculation. The total prestresseing force for the debonded specimens (Specimen 2 and Specimen 4) did not include the forces created by the twelve debonded strands. The splitting force values were calculated by multiplying the maximum vertical tensile strains in the end zone reinforcement by the area of a 0.6 in. diameter strand (0.217 in^2). Specimen 4 produced a splitting force equal to

1.5 percent of the total prestressing force in the end zone, well below the design splitting force equal to 4 percent of the total prestressing force in the end zone.

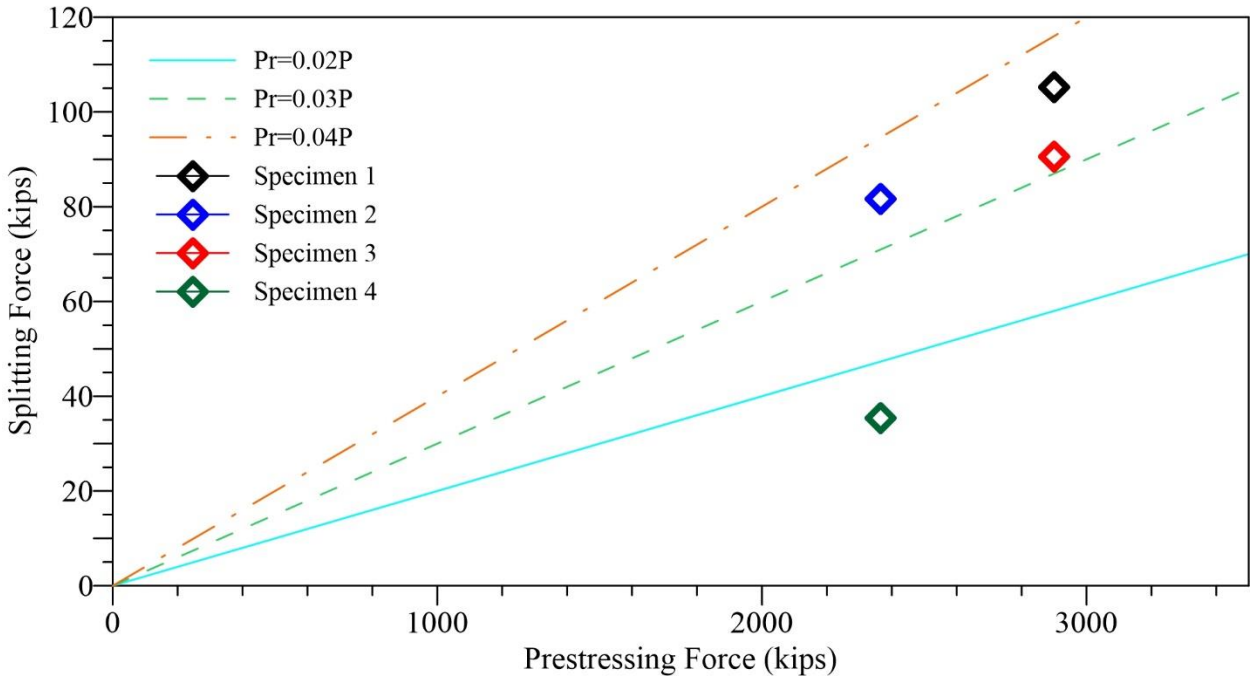

Figure 6-13 Splitting Force vs. Prestressing Force in Test Specimens

6.2.3. DEMEC Transfer Length

A total of eight transfer lengths were captured through the use of the DEMEC strain gauges and target screws. Each transfer length was captured immediately after a specified series of prestressing strands were cut, as well as after the final cut. The strand cutting pattern can be seen in Figure 4-18. In addition, the transfer lengths of Specimens 3 and 4 were captured both 7 days after prestress release and during the week of testing. The process for capturing these transfer lengths is fully described in Chapter 5.

As expected, the measured strains of the specimens containing partial debonding were much lower than the measured strains of the fully bonded specimens. Since the partially debonded

specimens each contained twelve strands which were debonded within the entire 60 inches of the DEMEC transfer length acquisition system, the transfer of force from these strands was not administered to the concrete within the measured area. The measured average maximum strain of the debonded specimens was between 65-85% of the measured average maximum strain of their fully bonded counterparts.

The point at which the onset of the 95% AMS plateau occurred varied for all specimens. In general, the transfer length was lower for the specimens with only fully bonded strands. Furthermore, among specimens with like bonding designs, the specimens which had higher draping produced lower transfer lengths. Specimens 1 and 2, which contained the standard draping angle, had a transfer length of roughly $27d_b$ and $31d_b$, respectively, while Specimens 3 and 4, which contained the lower draping angle, had a transfer length of roughly $45d_b$ and $53d_b$, respectively. Although this trend could be an effect of the lower draping angle, another variable that could have produced the longer transfer lengths is the concrete mix. Specimens 3 and 4 were poured with concrete from the same batch, which produced an unconventional pool of paste that leaked out of the headers of Specimens 3 and 4 and hardened around the bottom strands on either side of both girders. The average concrete strengths at prestress release were 9,205 psi and 8,958 psi for Pour 1 and Pour 2, respectively. Although these compressive strengths are above the required 8,500 psi, the strength of the concrete at the girder ends in the second pour may have had an effect on the lower transfer lengths for Specimens 3 and 4.

The average compressive surface strain profiles of each specimen can be seen in Figure 6-14. These profiles were used to find the transfer lengths. The transfer lengths were found using the 95 percent average maximum strain (AMS) method. The final transfer length for each specimen was determined by averaging the transfer lengths of Side A and Side B for each

specimen. The 31 measured DEMEC strain points are represented in Figure 6-14 by the symbols. Plotted along with the transfer lengths in Figure 6-14 are lines representing the transfer length values calculated using the AASHTO and ACI equations. The average transfer lengths for Specimens 1 and 2 can be seen in Figure 6-15 while the average transfer lengths for Specimens 3 and 4 can be seen in Figure 6-16. In addition to the transfer length, a line representing the 95% AMS is shown in the figures.

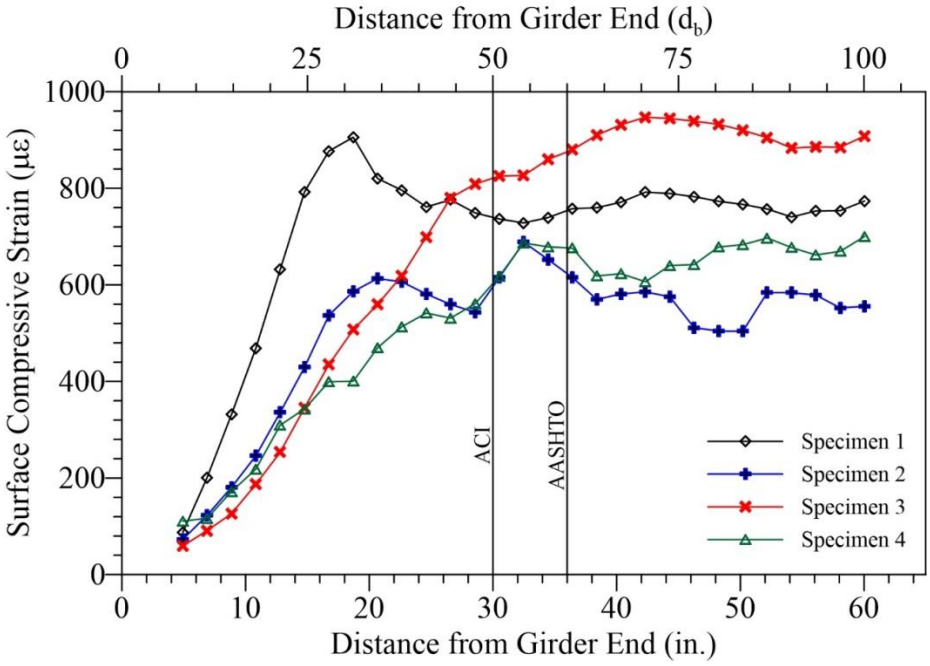

Figure 6-14 Average Surface Strain Comparison of all specimens

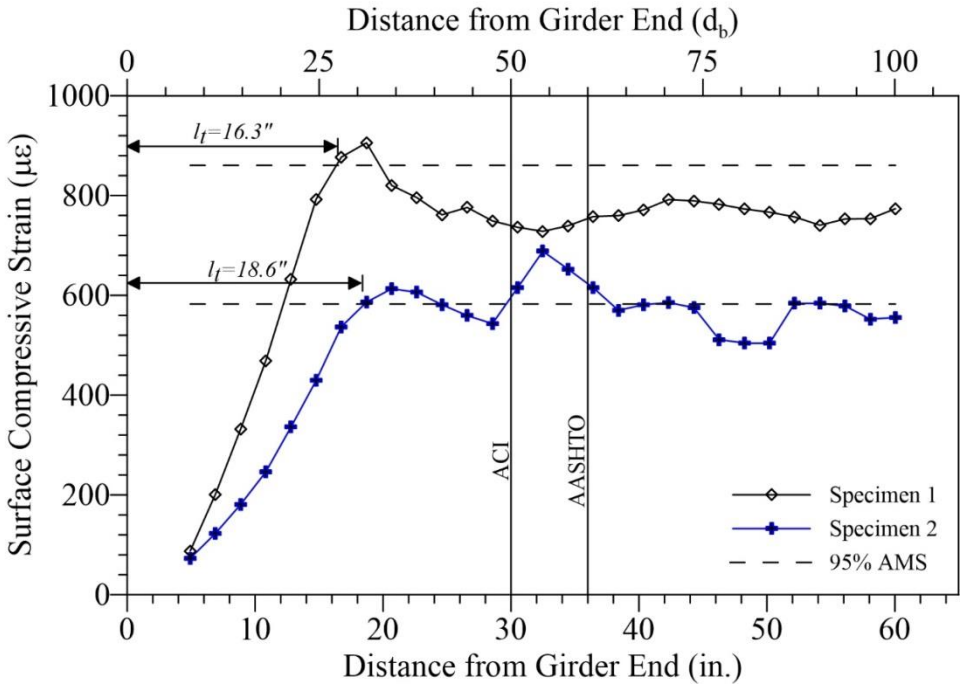

Figure 6-15 Transfer length of Specimen 1 (standard) and Specimen 2 (debonding)

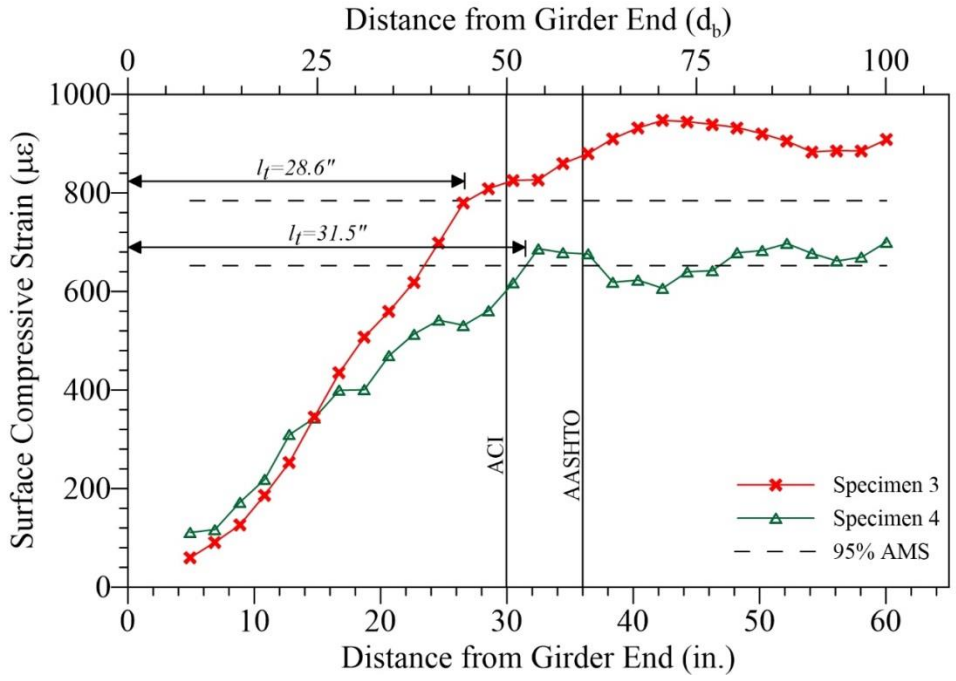

Figure 6-16 Transfer length of Specimen 3 (lower draping) and Specimen 4 (lower draping with debonding)

6.3. Comparison of Measured Transfer Length with Previous Expressions

The literature review found in Chapter 2 contains an abundance of historical expressions for transfer lengths based on research conducted over the last few decades. The following section provides a comparison with the transfer lengths found in this study with the expressions proposed in literature. A compilation of transfer lengths found from some of the landmark transfer length studies are shown in The calculated transfer lengths from the expressions are shown in Figure 6-17 with the transfer length results obtained from the test specimens. Four expressions provided transfer lengths higher than those found in all specimens: AASHTO (2014), Buckner (1995), Russell & Burns (1993), and Martin & Scott (1976).

No expressions gave transfer lengths with lower values than those measured from Specimen 1 and Specimen 2. However, the transfer length of Specimen 3 and Specimen 4 both exceeded the length calculated in three expressions: Mattock (1962), ACI 318 (1962), Ramirez and Russell (2008). Furthermore, the transfer length of Specimen 4 also exceeded the expression given in ACI 318 (2015).

As noted earlier, the concrete consistency of the SCC near the girder end and the unconventional span-to-depth ratio of the test specimens may be the cause of the high variance in the measured transfer lengths between the first two specimens and the second two specimens.

Table 6-3. A list of frequently used variables in these equations is provided in Table 6-4.

These variables were assigned values representative of the BT-78 test specimens, and the theoretical transfer lengths based on these expressions were calculated. The values for both 28-day compressive strength and concrete compressive strength at release were averaged from the cylinder tests from both pours. The calculated effective stress in the strands after losses, f_{se}

differed between specimens with high draping and specimens with low draping. Since the variance of these two values was roughly 2 ksi, the lower value (from the specimens with draped strands) was chosen. The development length of the test spans was not measured in this study.

The calculated transfer lengths from the expressions are shown in Figure 6-17 with the transfer length results obtained from the test specimens. Four expressions provided transfer lengths higher than those found in all specimens: AASHTO (2014), Buckner (1995), Russell & Burns (1993), and Martin & Scott (1976).

No expressions gave transfer lengths with lower values than those measured from Specimen 1 and Specimen 2. However, the transfer length of Specimen 3 and Specimen 4 both exceeded the length calculated in three expressions: Mattock (1962), ACI 318 (1962), Ramirez and Russell (2008). Furthermore, the transfer length of Specimen 4 also exceeded the expression given in ACI 318 (2015).

As noted earlier, the concrete consistency of the SCC near the girder end and the unconventional span-to-depth ratio of the test specimens may be the cause of the high variance in the measured transfer lengths between the first two specimens and the second two specimens.

Table 6-3 Transfer Length Expressions from Previous Research

Study	Transfer length, $\boldsymbol{l_t}$	Calculated Transfer Length, $\boldsymbol{l_t}$, in.
Mattock (1962)	$\frac{1}{3} f_{se} d_b$	27.5
ACI 318 (1963)	$\frac{1}{3} f_{se} d_b$	27.5
Martin and Scott (1976)	$80 d_b$	48
Russell and Burns (1993)	$\frac{1}{2} f_{se} d_b$	41.2

Buckner (1995)	$\frac{1}{3} f_{si} d_b$	40.5
Ramirez and Russell (2008)	$\frac{120 d_b}{\sqrt{f'_{ci}}} \geq 40 d_b$	24
ACI 318 (2014)	$50 d_b$	30
AASHTO (2014)	$60 d_b$	36

Table 6-4 Symbols Used in Transfer Length Expressions

Symbol	Description	Assumed Value
d_b	nominal diameter of the prestressing strand	0.6 in.
f_{se}	effective stress in prestressing strand after losses	137.3 ksi
f_{si}	initial stress in strand before long-term losses	202.5 ksi
f_{su}	ultimate strength of the prestressing strand	270 ksi
f'_c	28-day compressive strength of concrete	11745 psi
f'_{ci}	concrete compressive strength at release	9082 psi

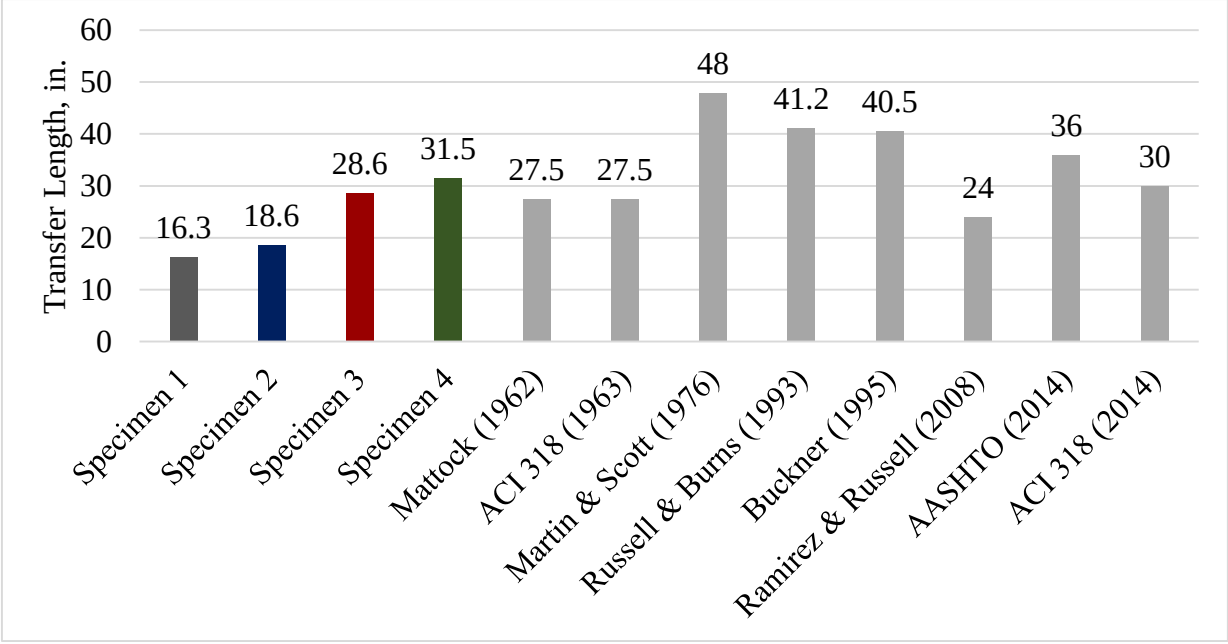

Figure 6-17 Comparison of transfer length values and expressions from previous studies

6.4. Results of Load Testing

Two main objectives of the load tests were to verify that the modified end zone details did not create failure during loading and to determine the effects of loading on end zone crack propagation. Russell and Barnes (1993) found that strand bond failures only occur when cracks propagate in the prestressing strand transfer zone. As a result it was necessary to verify that the four specimens could withstand a shear capacity which surpassed the equivalent design demand of the full-span girder. Furthermore, it was necessary to investigate how end zone cracks change during the loading of the BT-78.

During the testing phase, each specimen was loaded with a manually operated hydraulic pump. Periodical pauses were taken during the load tests. The load-displacement curves for each specimen can be seen in Figure 6-18. The point at which the initial crack occurred is marked in the figure. The displacement shown is representative of the measured displacement at mid-span. Since there were two string potentiometers under the mid-span load for Specimen 1 and 3, the shown displacement is representative of the average between the two readings. Although the load point, was not at mid-span for Specimens 2 and 4, the maximum measured displacement was still at the mid-span string potentiometer; therefore, the shown displacement is the measured displacement at mid-span. The initial cracks occurred between the values of 652 and 804 kips. Table 6-5 shows the initial cracking load for each specimen.

Table 6-5 Load Test Cracking Capacities

Specimen	Initial Cracking Load (kips)
Specimen 1	727
Specimen 2	652
Specimen 3	804
Specimen 4	702

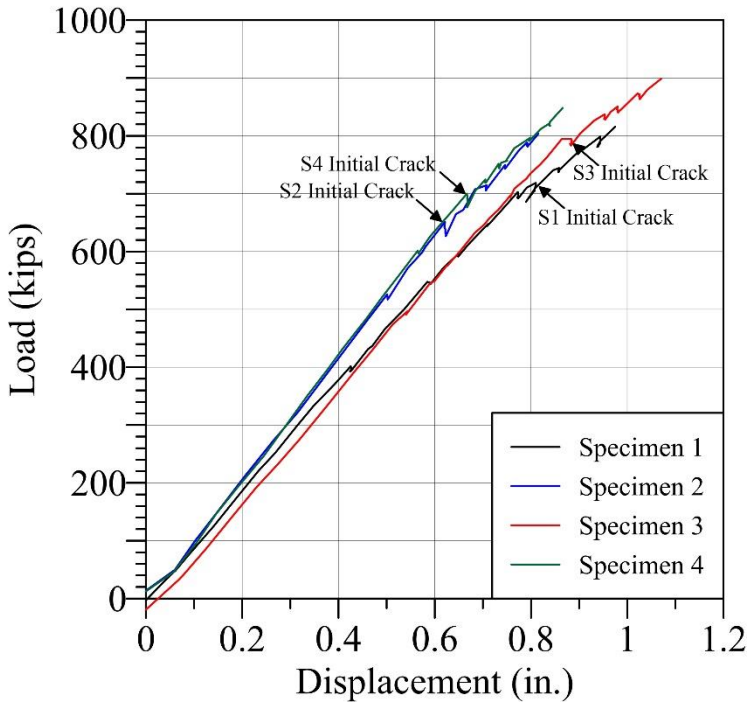

Figure 6-18 Load displacement curves

6.4.1. String Potentiometer Deflection

Throughout the experimental load testing string potentiometers were used to capture the deflection of the specimens. Potentiometers were distributed along the length of the girder and attached to the center of the bottom face. There was also an additional potentiometer on the outer-most edge of the bottom face of the girders. This potentiometer was placed at the load point to measure any undesired rotation caused by loading. For the purposes of the following figures, the ultimate deflection is represented by the average of the two load point potentiometer readings.

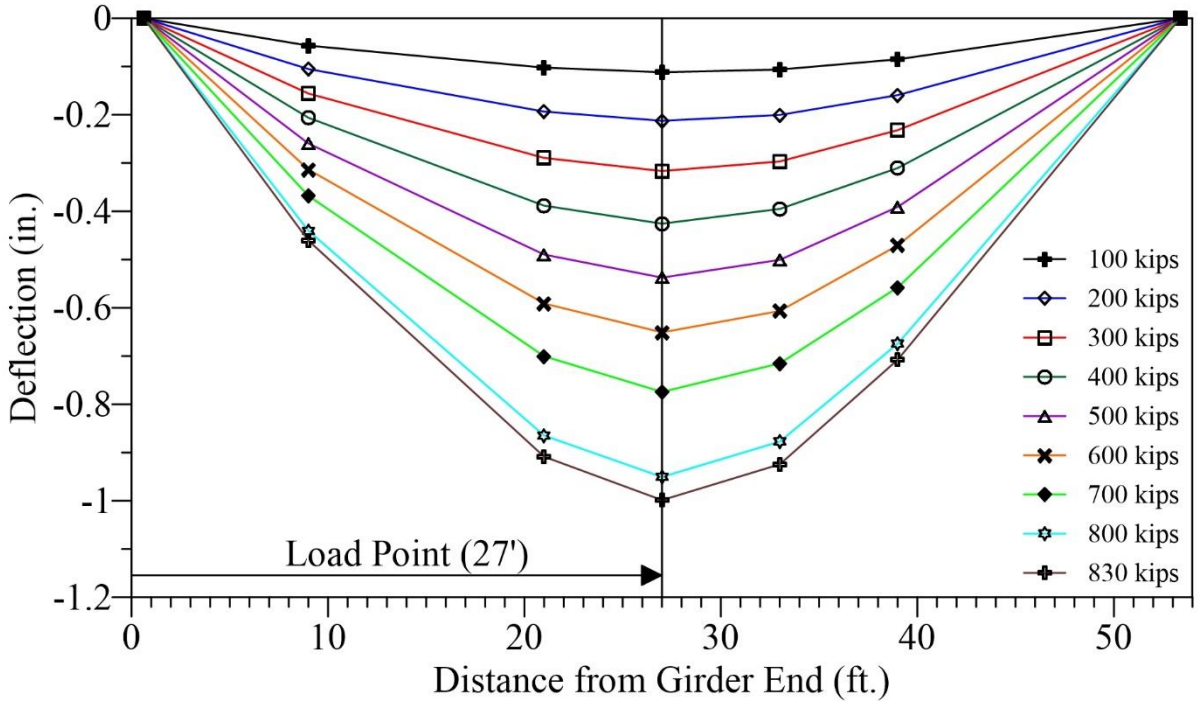

Figure 6-19 Specimen 1 deflection

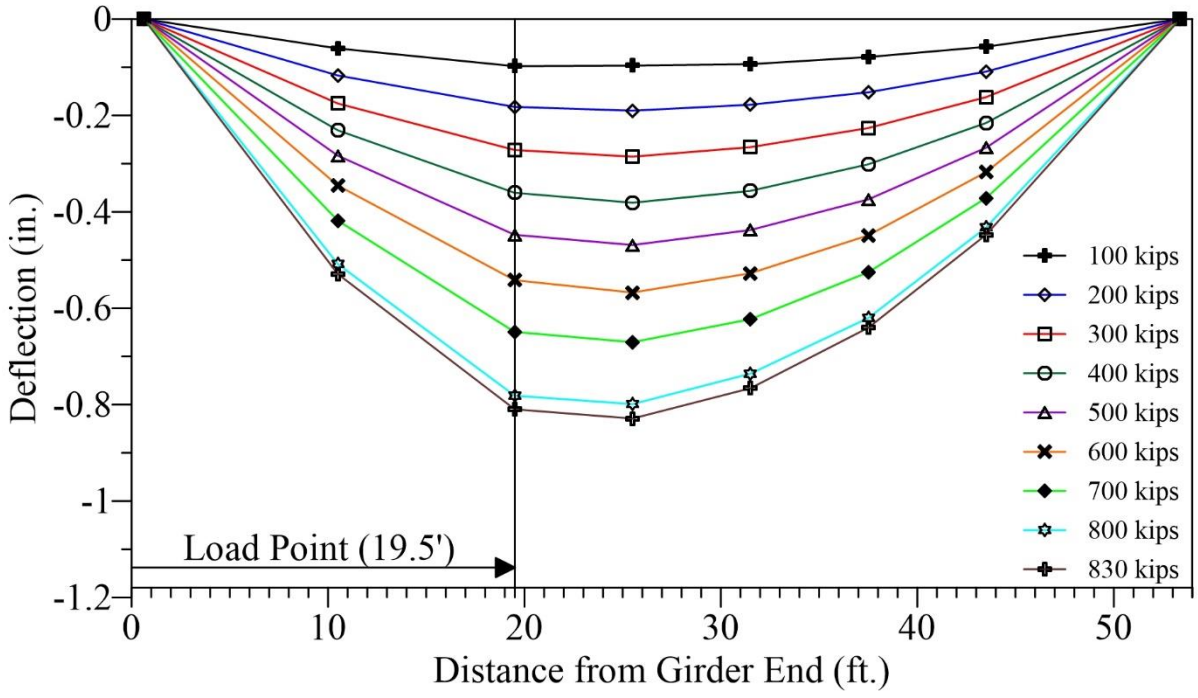

Figure 6-20 Specimen 2 deflection

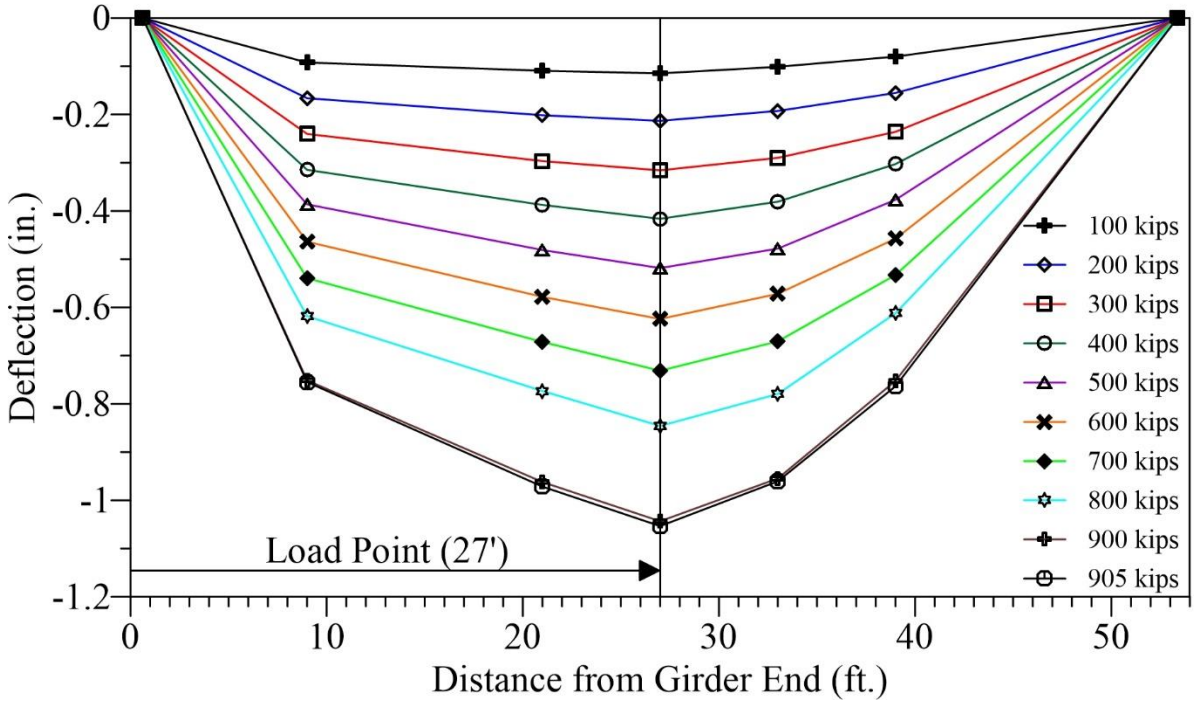

Figure 6-21 Specimen 3 deflection

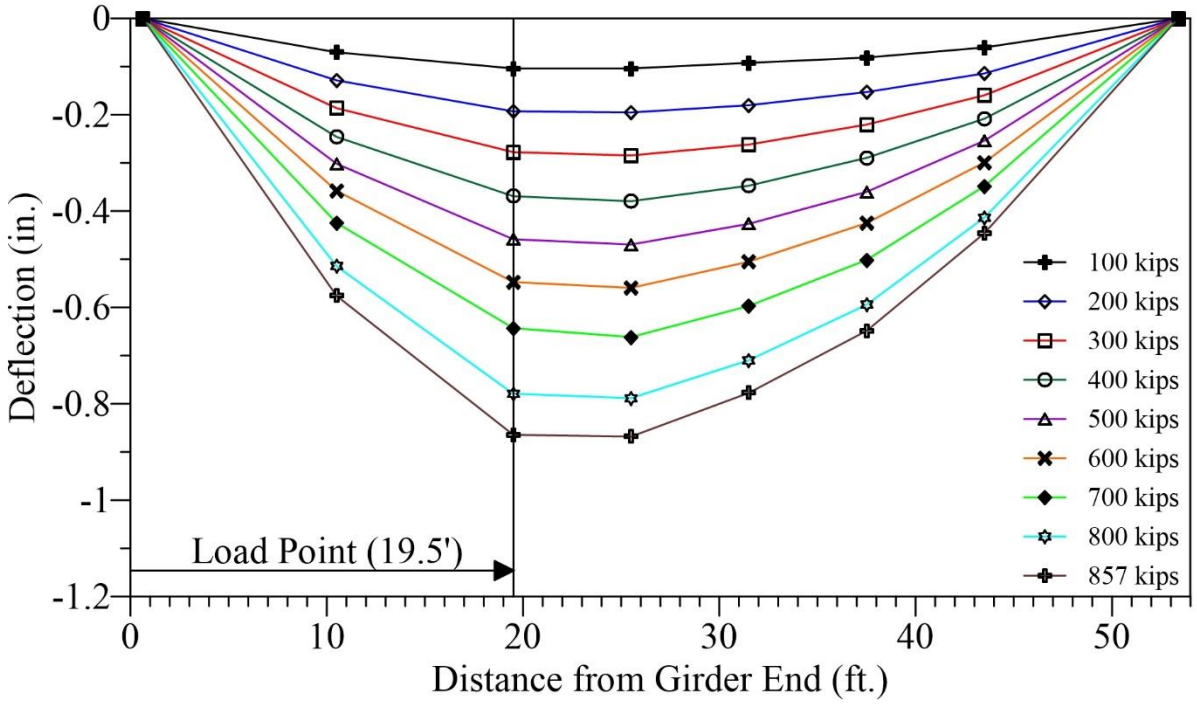

Figure 6-22 Specimen 4 deflection

6.4.2. Load Point DCDT Strain Profile

For all lab tests, eight DCDTs were attached along the depth of the girder and measured the horizontal displacement between points on either side of the line of loading. The displacement was continually measured throughout the loading process, and after loading the displacement readings were converted into strains. A strain profile at the load point for each girder was developed from these DCDTs. Figure 6-23 through Figure 6-26 show the strain profiles from the girders during the load testing. On Specimen 2, two DCDTs (one at -2 in. and the other at 32 in.) were determined to be improperly fastened; therefore, the resulting data from these DCDTs is not included in this study. The strain in these figures represents the incremental strain at each location caused by the applied load only. The actual strains at each location can be easily obtained by adding the strains at each due to prestressing force alone.

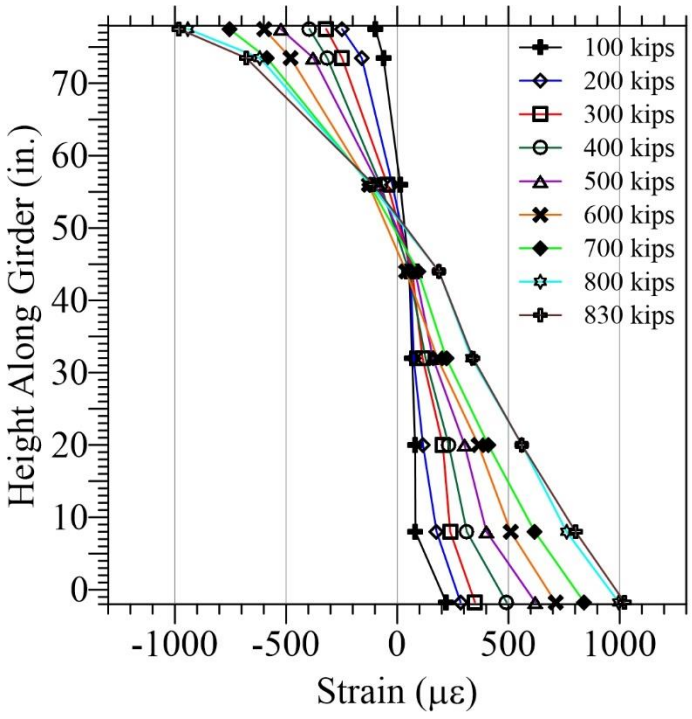

Figure 6-23 Specimen 1 strain profile

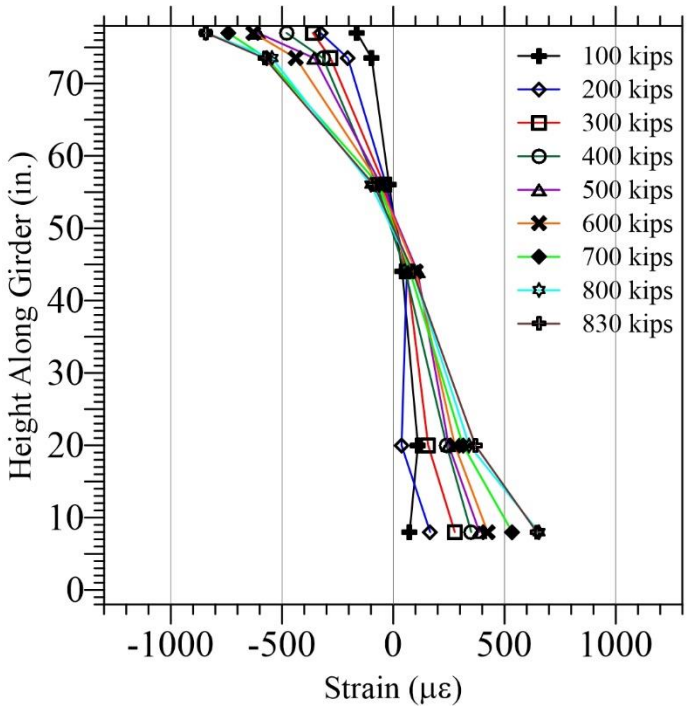

Figure 6-24 Specimen 2 strain profile

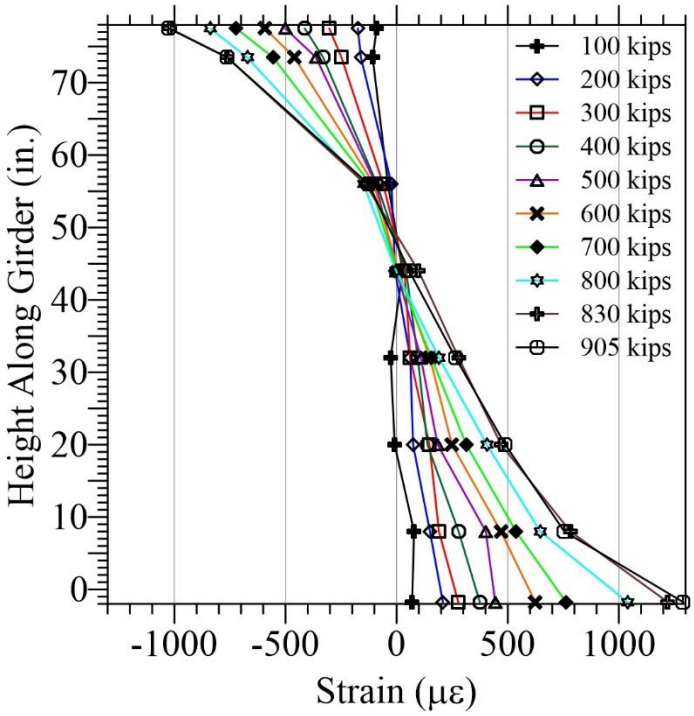

Figure 6-25 Specimen 3 strain profile

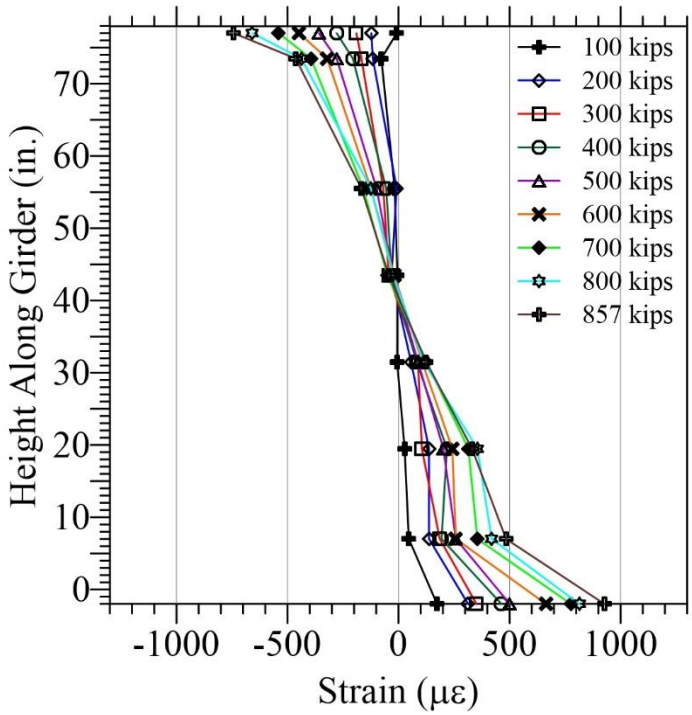

Figure 6-26 Specimen 4 strain profile

6.4.3. Load Test Cracking

As mentioned in Chapter 5, load tests were performed by applying a single point load with the help of a 1500 kip hydraulic jack. During testing, the load was continuously increased in 50 kip increments until 500 kips. After this point, the load was increased in approximately 25 kip increments with brief pauses between to check for cracking. All cracks that occurred during the four load tests were web-shear cracks, except for three small flexural cracks in the bottom flange of Specimen 1. The cracks were recorded with respect to the load at which they initiated. The cracking locations for each specimen with relation to the load at which the cracks were first noticed can be seen in Figure 6-27 though Figure 6-30. In these figures the end representing the full-scale girder end, is pictured on the right hand side. For clarity, the end zone cracks were omitted from the following figures.

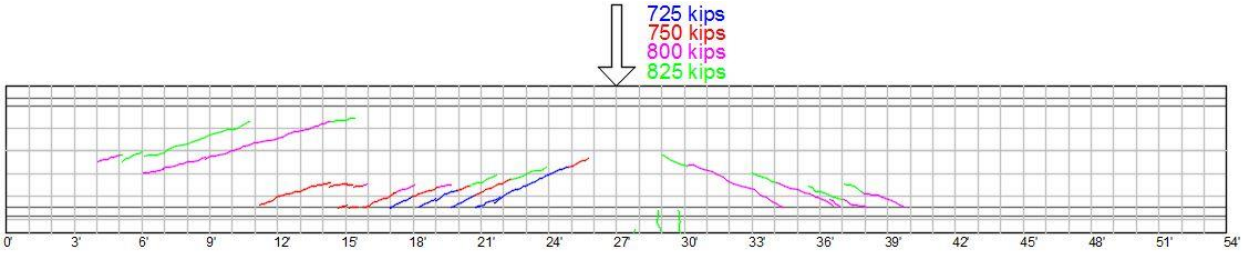

Figure 6-27 Specimen 1 load test cracks, Side A

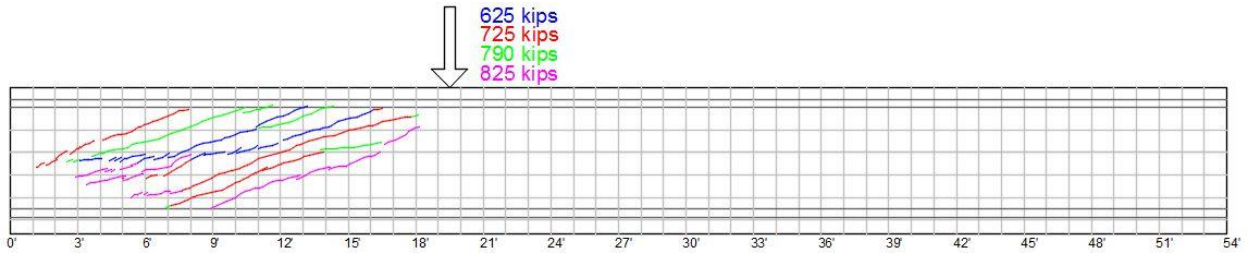

Figure 6-28 Specimen 2 load test cracks, Side B

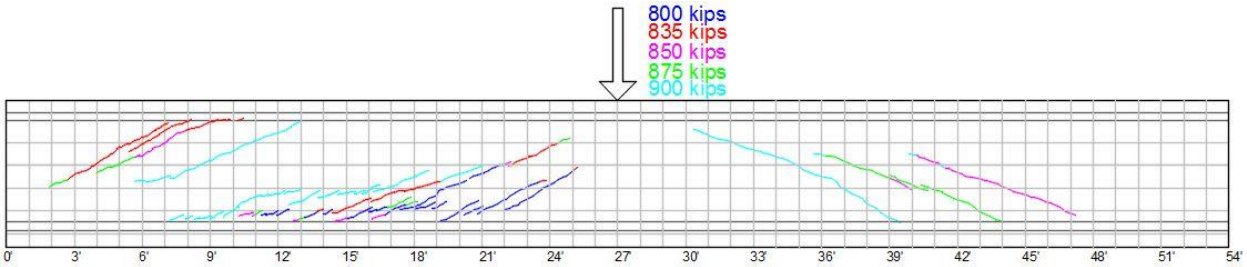

Figure 6-29 Specimen 3 load test cracks, Side A

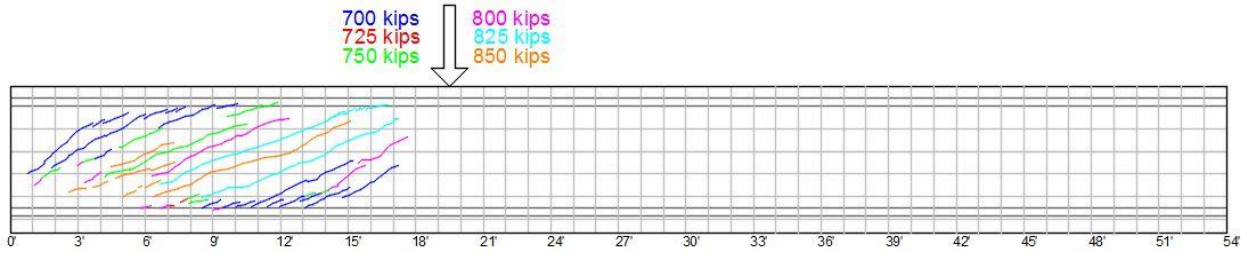

Figure 6-30 Specimen 4 load test cracks, Side B

As expected, the web shear cracks in the specimens with the adjusted loading point were more highly concentrated towards one side. The adjusted loading point was approximately 36% from the girder end, which lowered the shear demand on end zone of Specimen 2 and Specimen 4 by nearly one-third.

A major motivation for the load tests was to evaluate the girders' shear force resisting capacity and compare them to current AASHTO and ACI regulations. A comparison between the applied shear forces at the time of the first crack and the calculated shear capacities at certain points along the girder is shown in Table 6-6. For comparison, the calculated concrete shear capacity, V_c, and the ultimate shear capacity, ϕV_n, are shown in the table. The last column represents the calculated shear demand on the full-scale, 180 ft girder in accordance to standard AASHTO loading with a center-to-center girder spacing of 6 ft and a 7 in. thick deck.

The ultimate shear capacity is included in Table 6-6 for the purpose of comparison with the concrete shear capacity. The ultimate shear capacity is calculated by added the shear capacity of the concrete, $V_{c,}$ with the shear capacity of the shear reinforcement, $V_{s,}$ and multiplying the result by a factor, ϕ, of 0.9 (AASHTO). Vertical steel shear reinforcement bars are located throughout the girder, outside of the end zone, at spacing which vary between 12 and 18 in. Due to the perfect bond assumption of reinforced concrete, the strain in the reinforcing steel must always be equal to the strain in the surrounding concrete. Therefore, the added shear resistance of the vertical steel reinforcement bars only comes into effect after the cracking of the concrete. Hence, the AASHTO and ACI concrete capacity values should be used in comparison with the applied cracking shear force values, rather than the ultimate shear capacities, since the shear resisting force of the steel is not active until after the concrete cracks.

Table 6-6 Comparison of Experimental and Calculated Shear Force Capacities

Specimen	Location	Cracking Shear Force Applied in Tests (kips)	Calculated Concrete Shear Capacity, V_c (kips)		Calculated Ultimate Shear Capacity, $\phi V_s+\phi V_c=\phi V_n$ (kips)		Demand on Full-Scale Girder, V_{demand} (kips)
			AASHTO	ACI	AASHTO	ACI	
Specimen 1	x=0’	364	120	218	939	450	338
	x=*h*		341	456	1077	630	318
	x=27’		338	313	546	428	--
Specimen 2	x=0	417	119	217	939	450	338
	x=*h*		303	434	854	532	318
	x=19.5’		313	411	593	577	--
Specimen 3	x=0	402	119	202	876	414	338
	x=*h*		342	436	859	567	318
	x=27’		345	320	562	385	--
Specimen 4	x=0	449	128	220	1014	458	338
	x=*h*		313	433	911	580	327
	x=19.5’		288	389	477	389	--

As can be seen in Table 6-6, the performance of the girders in comparison to AASHTO standards was successful. For every specimen, the shear force that caused the first was much higher than the shear capacity in the concrete calculated using the AASHTO guidelines at the girder end, at a distance equal to the height *h* from the girder end, and at the loading point. Comparison of these values suggests that the lower draping and debonding of the strands do not decrease the performance of the girders in resisting shear capacity.

The comparison of ACI recommendations with the applied cracking shear capacities presents a non-conservative estimation of the concrete shear cracking capacity within the ACI recommendations, particularly around the distance *h* from the girder end. The calculated ACI values for Specimens 1, 2, and 3 range from 4 to 25 percent higher than the applied shear force. In contrast, Specimen 4 outperformed the calculated ACI concrete capacity by 3 percent.

The cracks were measured using a crack comparator card at the time of the highest applied load. Specimen 1 and Specimen 2 contained web shear crack widths of up to 0.010 in. Specimen 3 crack widths reached as high as 0.020 in. Specimen 4 contained cracks widths up to 0.016 in. Photographs of the cracking after load tests can be seen in Figure 6-31 through Figure 6-34.

Figure 6-31 Specimen 1 web shear cracking after load test

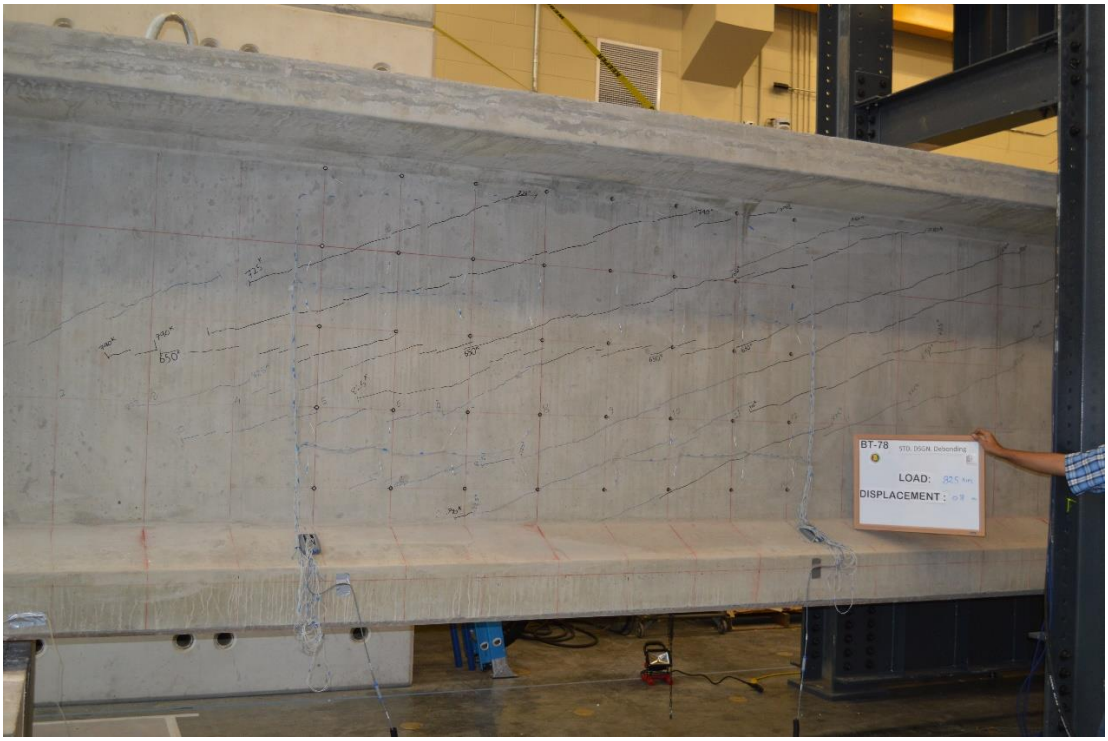

Figure 6-32 Specimen 2 web shear cracking after load test

Figure 6-33 Specimen 3 web shear cracking after load test

Figure 6-34 Specimen 4 web shear cracking after load test (with NDI sensors)

6.5. End Zone Strains during Load Testing

During the load tests, the strains in the end zone region of the specimens were measured by the internal steel and concrete strain gauges mounted during fabrication. The process of installing the strain gauges is described thoroughly in Chapter 4. These strains were measured over the entire extent of the loading process. As expected, the application of the load applied mainly compressive strain to the vertical reinforcement located in the end zone. The strain gauges near the bottom of the section measured higher compressive strains while the strain gauges near the top of the section measured lower compressive strains. An example plot of the load versus the measured strain for vertical gauges on bar 1B in Specimen 1 is shown in Figure 6-35. As in the strain plots shown from detensioning, a negative value represents compression. The strains in the plot represent the vertical strains incurred in bar 1B due to the load test, hence the strain values were calibrated to equal zero at the initiation of the load test. The figure also includes the unloading of the specimen. The high measured compression strains at the bottom of the web are contributed to the proximity of the gauges to the shear strains created by the load path from the applied load to the supports.

The concrete gauges were also employed for capturing the strains during the load tests. The vertical strains in Specimen 2 were measured using concrete gauges, as shown in Figure 6-36. The gauges measured the strain in the girder during the application of the load, however, the unloading is not shown in Figure 6-36.

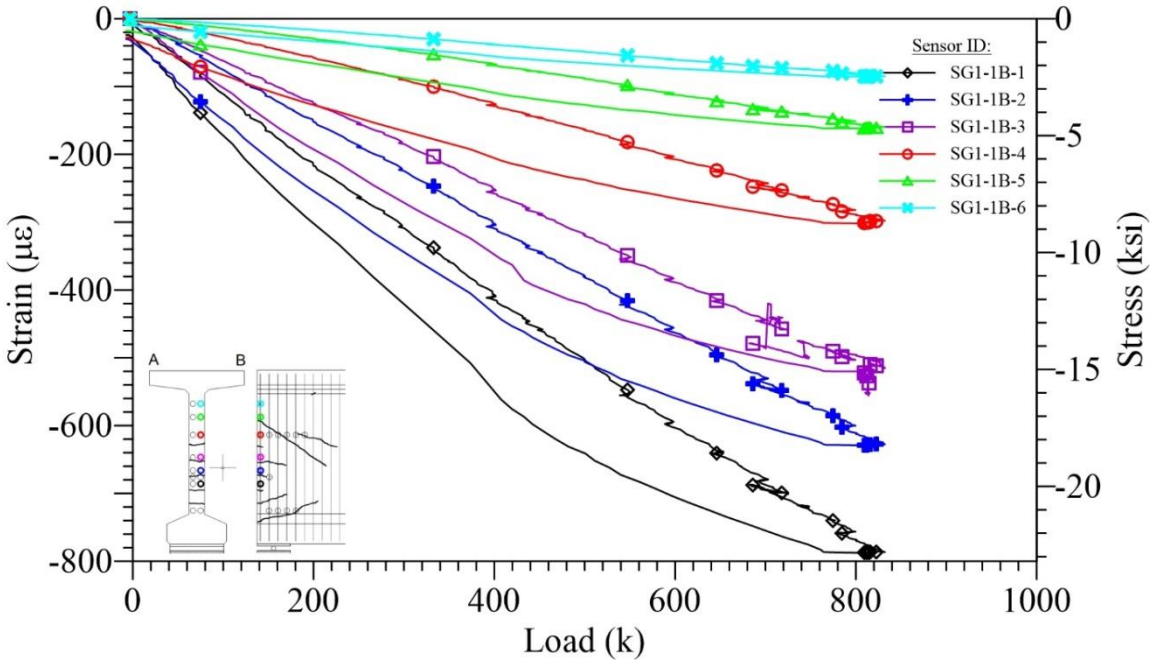

Figure 6-35 Load test strains from vertical steel gauges on Specimen 1, Bar 1B

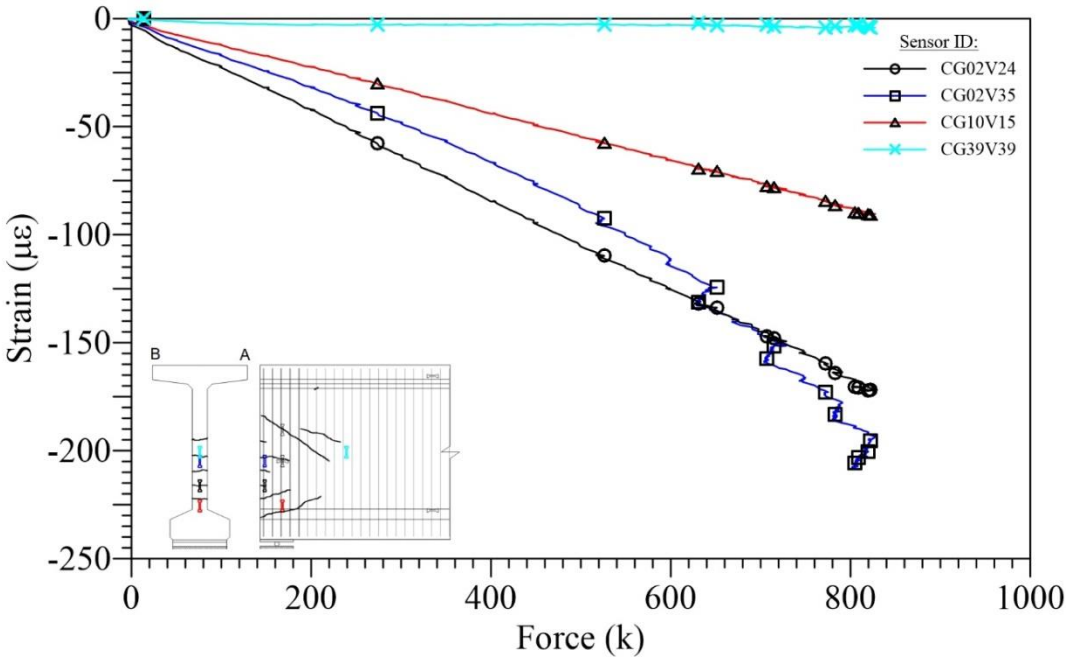

Figure 6-36 Load test strains from vertical concrete gauges on Specimen 2

The results of the strain gauges and visual inspection suggest that the end zone cracking found in these specimens was not worsened upon loading of the girders. Measurements from both the vertical steel gauges and vertical concrete gauges support this claim since the strain in all gauges increased in compression as the load increased. This suggests that after the addition of the 7 in. deck and vehicular loading, the end zone cracks will not propagate further, and will likely close upon loading.

Chapter 7 Conclusions and Recommendations

7.1. Summary

The use of deep prestressed concrete girders for long-span bridges in the United States is becoming increasingly popular. However, in deep, narrow-stemmed girders with high amounts of prestressing, end zone cracking has been frequently observed during the time of prestress transfer. In an effort to develop a girder which can reach spans of up to 180 ft, the Alabama Department of Transportation (ALDOT) sponsored a study to investigate a solution to the end zone cracking problem in 78 in. bulb-tee (BT-78) girders.

A preliminary study was conducted to analyze the effect of different end zone modifications on principle strains in the girder end through the use of finite element modeling. A finite element model was created and calibrated using previously cast girders. As a result of the analysis, four end zone designs of the BT-78 were chosen to be fabricated: 1) a standard design corresponding to the typical specifications currently used by ALDOT, 2) a specimen with twelve strands debonded in the bottom flange, 3) a specimen with a draping angle which was lowered by roughly 1.2 degrees, and 4) a specimen which contained both the lower draping angle and debonded strands.

The four specimens were fabricated in an Alabama precast yard with a full-scale cross section (78 in. deep) and a reduced span of 54 ft. The specimen end zones were each instrumented with thirty-one internal steel strain gauges, nine internal concrete strain gauges, and DEMEC targets on both exterior faces along the transfer length. Internal strains and concrete surface strains were

captured during the detensioning process and recorded for later analysis. The specimens were then brought to the University of Alabama's Large Scale Structures Lab (LSSL) to be tested. Load tests were conducted to compare the shear capacity of the specimens with the equivalent shear demand required of the full-scale 180 ft girder.

As a result of the study, it was found that Specimen 4, which contained both debonding and the lower draping angle, provided the best resistance to end zone cracking during detensioning.

7.2. Conclusions

The following conclusions were reached based on the results of this study:

- Debonding twelve of the forty-four strands in the lower flange reduced the cracking from Specimen 1 to Specimen 2 by 53 percent and from Specimen 3 to Specimen 4 by 87 percent. For the girders studied, debonding strands in the lower flange can significantly reduce the amount of prestressing force transferring to the concrete in the end zone which can result in a reduction in end zone cracking.
- Specimen 4 produced the least amount of cracking from prestress transfer. Lowering the draping angle in combination with debonding strands in the bottom flange reduced the amount of cracking in the end zones by 84 percent, in comparison with the control specimen.
- Cracks grew over time in all cases, however, the majority of growth occurred within the first two weeks. At least 88 percent of the total crack length was developed by day 8 in all girders, excluding Specimen 4 which showed the least amount of cracking.
- As a result of the finite element modeling, it was determined that horizontal reinforcement in the end zone webs has little-to-no effect on the reduction of principle

strains in the end zone which cause splitting. For this reason, these bars were not used in any of the four specimens.

- Debonding and lowering of the draping angle have a positive effect on the shear capacity of the girder. All three modified specimens reached higher shear capacities before initial cracking than the control specimen.
- The measured transfer length for all specimens was conservatively below the recommended AASHTO length of 60 strand diameters, $60d_b$. Specimen 4 had the highest transfer length at 31.5 in., or $52.5d_b$, and was the only specimen with a transfer length greater than the recommended ACI length of 50 strand diameters, or $50d_b$.
- The splitting force observed in the end zones of all four specimens was below 4 percent of the prestressing force. The stresses measured in the end zone reinforcement were also lower than 20 ksi. The current AASHTO prescribed limitations are therefore adequate.

7.3. Recommendations for Future Research

Based on the findings from the research conducted in this study further research of the following subjects are recommended:

- A high variance in transfer lengths measured from the test specimens may be a function of a low-strength paste from the SCC mix settling in near the girder end. This paste leaked out of the formwork after the pouring of Specimens 3 and 4. Future investigations should be conducted considering the potential for irregularities due to paste found at the "bottom of the bucket" for girders poured using SCC.

- Future investigations should also explore the long-term effect of end zone cracking in girders which are in use. This study showed that after the loading of girders end zone cracks are likely to be reduced as the girder is loaded. Still, serviceability issues could be presented in the long-term due to creep, shrinkage, and freeze-thaw. This investigation should also include an aspect for monitoring repaired cracks over long periods.
- The AASHTO splitting resistance requirements should be reevaluated using the end zone modifications presented in this research. The maximum tensile strain in the Specimen 4 end zone reinforcement reached only 38 percent of the 20 ksi design limit and the splitting force was under 2 percent of the total prestressing force. The combination of debonding and lower draping in the end zone greatly reduced the splitting force and end zone cracks. As a result, less stringent requirements for vertical splitting reinforcement should be investigated.

References

AASHTO. (2002). *Standard Specifications for Highway Bridges* (16 ed.). Washington D.C.: American Association of State Highway and Transportation Officials (AASHTO).

AASHTO. (2015). *AASHTO L.R.F.D. Bridge Design Specification* (5 ed.). Washington, D.C.: American Association of State Highway and Transportation Officials.

ACI Committee 318. (2014). *Building Code Requirements for Reinforced Concrete (318-14).* American Concrete Institute (ACI).

Arab, A. A., Badie, S. S., & Manzari, M. T. (2011). A methodological approach for finite element modeling of pretensioned concrete members at the release of pretensioning. *Engineering Structures, 33*(6), 1918-1929.

Arab, A., Badie, S. S., Manzari, M. T., Khaleghi, B., Seguirant, S. J., & Chapman, D. (2014, Spring). Analytical investigation and monitoring of end-zone reinforcement of the Alaskan Way viaduct super girders. *PCI Journal*, 109-128.

Barnes, R. W., Grove, J. W., & Burns, N. H. (2003). Experimental Assesment of Factors Affecting Transfer Length. *ACI Journal*, 740-748.

Buckner, C. D. (1995). A Review of Strand Development Length for Pretensioned Concrete Members. *PCI Journal*, 84-105.

Castrodale, R. W., & White, C. D. (2002). Simplified analysis of web splitting in pretensioned concrete girders. *Proceedings, PCI/FHWA/NCBC Concrete Bridge Conference*, (pp. 6-9). Nashville, TN.

Crispino, E. D. (2007). *Anchorage Zone Design for Pretensioned Bulb-tee Bridge Girders in Virginia.* MS Thesis, Virginia Polytechnic Institute and State University.

Dassault Systèmes Simulia Corporation. (2012). *Abaqus Analysis User's Manual* (Vol. 6). Providence, RI, USA: Dassault Systèmes.

Dunham, E. L. (2011). *Transfer Length in Blub-Tee Girders Constructed with Self-Consolidating Concrete.* MS Thesis, Auburn University.

Gergely, P., & Sozen, M. A. (1967). *Design of anchorage-zone reinforcement in prestressed concrete beams.* University of Illinois.

Hamilton, H. R., Consolazio, G. R., & Ross, B. E. (2013). *End Region Detailing of Pretensioned Concrete Bridge Girders.* University of Florida Civil and Coastal Engineering.

Hanson, N. W., & Kaar, P. H. (1959). Flexural Bond Tests of Pretensioned Prestressed Beams. *ACI Journal*, 783-802.

Marshall, W. T., & Mattock, A. H. (1962, October). Control of Horizontal Cracking in the Ends of Pretensioned Prestressed Concrete Girders. *PCI Journal, 7*(5), 56-74.

Martin, L. D., & Scott, N. L. (1976). Development of Prestressing Strand in Pretensioned Members. *Journal of the American Concrete Institute*, 453.

Oliva, M. G., & Okumus, P. (2011). *Finite Element Analysis of Deep Wide-flanged Pre-stressed Girders to Understand and Control End Cracking.* University of Wisconsin-Madison, Civil and Environmental Engineering. Wisconsin Highway Research Program.

Ramirez, J. A., & Russell, B. W. (2008). *NCHRP Report 603: Transfer, Development, and Splice Length for Strand/Reinforcement in High-Strength Concrete.* Washington, D.C.: Transportation Research Board.

Russell, B. W., & Burns, N. H. (1993). *Design Guidelines for Transfer, Development and Debonding of Large Diameter Seven Wire Strands in Pretensioned Concrete Girders.* Austin, TX: The University of Texas at Austin.

Shahawy, M. A., & Issa, M. (1992). Effect of Pile Embedment on the Development Length of Prestressing Strands. *PCI Journal*, 44-59.

Tuan, C. Y., Yehia, S. A., Jongpitaksseel, N., & Tadros, M. K. (2004, April). End zone reinforcement for pretensioned concrete girders. *PCI Journal, 49*(3), 68-82.

Appendix A: Configuration of Instrumentation during Load Tests

Table A-1 Midspan DCDT Configuration

Specimen ID	DCDT #	h_{top} (in.)	x_{span} (in.)	Stroke Length (mm)
Specimen 1	1	0.5	14.5	50
	2	4.5	14.5	50
	3	22	14.5	50
	4	34	14.5	75
	5	46	14.5	75
	6	58	14.5	100
	7	70	14.25	75
	8	79.75	15	150
Specimen 2	1	1	13	50
	2	4.5	13.25	50
	3	22	14	50
	4	34	14.25	75
	5	46	14	75
	6	58	14	100
	7	70	14	100
	8	80	15.5	150
Specimen 3	1	0.5	14	50
	2	4.5	14	50
	3	22	13.75	50
	4	33.5	13.75	75
	5	46	14.25	75
	6	58	14	100
	7	71.5	14.25	75
	8	79.75	14	150
Specimen 4	1	1	--	50
	2	4.5	--	50
	3	22.5	--	50
	4	34.5	--	75
	5	46.5	--	75
	6	58.5	--	100
	7	71	--	100
	8	80	--	150

Where h_{top}= the distance of the DCDT rod from the top surface of the girder

x_{span} = the horizontal distance between the center of the two DCDT blocks

Table A-2 String Potentiometer Configuration

Specimen ID	String Pot. #	$X_{Mark\ End}$ (in.)	$Y_{DCDT\ End}$ (in.)
Specimen 1	1	45	13.5
	2	39	14
	3	33	14.5
	4	27	14.5
	5	27	4
	6	21	15
	7	15	14.5
Specimen 2	1	10.5	14.5
	2	16.5	14.5
	3	22.5	13.75
	4	28.5	13.5
	5	34.5	13.5
	6	34.5	19
	7	43.5	14.25
Specimen 3	1	15	13.5
	2	21	14.25
	3	27	4.75
	4	27	14.25
	5	33	13.5
	6	36	13.5
Specimen 4	1	39	13.5
	2	33	19.5
	3	33	13
	4	27	12.75
	5	21	12.75
	6	15	12.75
	7	9	12.75

Where $X_{Mark\ End}$ = distance from the "Mark End" of the girder, or "Crane East" in the LSSL

$Y_{DCDT\ Side}$ = distance from the side of the girder containing the DCDTs, or LSSL "Crane South"

Appendix B: Concrete Cylinder Strengths

Table B-1 Pour 1 Concrete Strengths

Pour 1: Specimen 1 and 2				
Day	Cylinder 1	Cylinder 2	Cylinder 3	**Avg.**
0.72	9395	9015	--	**9205**
1	9480	9485	--	**9483**
5	10320	10337	--	**10329**
8	10400	10497	11137	**10678**
14	10992	10620.9	11005.8	**10873**
21	11226.4	11080.4	11598.2	**11302**
28	11729.3	11551.1	11637.1	**11639**

Table B-2 Pour 2 Concrete Strengths

Pour 2: Specimen 3 and 4				
Day	Cylinder 1	Cylinder 2	Cylinder 3	**Avg.**
0.67	9180	8735	--	**8985**
1	8874	9068	9580	**9174**
3	9834	10042	9650	**9842**
5	9879	10080	9924	**9961**
14	10862	11315	10928	**11035**
21	11713	12000	11520	**11744**
28	11470	12341	11739	**11850**